AEDC-TR-79-1

copy 14

Store Separation Testing Techniques at the Arnold Engineering Development Center

Volume III
Description and Validation of
Captive Trajectory Store Separation Testing in
the Von Karman Facility

J. P. Billingsley, R. H. Burt, and J. T. Best
ARO, Inc.

March 1979

Final Report for Period October 1, 1977 — May 25, 1978

ARNOLD ENGINEERING DEVELOPMENT CENTER
ARNOLD AIR FORCE STATION, TENNESSEE
AIR FORCE SYSTEMS COMMAND
UNITED STATES AIR FORCE

NOTICES

When U. S. Government drawings, specifications, or other data are used for any purpose other than a definitely related Government procurement operation, the Government thereby incurs no responsibility nor any obligation whatsoever, and the fact that the Government may have formulated, furnished, or in any way supplied the said drawings, specifications, or other data, is not to be regarded by implication or otherwise, or in any manner licensing the holder or any other person or corporation, or conveying any rights or permission to manufacture, use, or sell any patented invention that may in any way be related thereto.

Qualified users may obtain copies of this report from the Defense Technical Information Center.

References to named commerical products in this report are not to be considered in any sense as an indorsement of the product by the United States Air Force or the Government.

This report has been reviewed by the Office of Public Affairs (PA) and is releasable to the National Technical Information Service (NTIS). At NTIS, it will be available to the general public, including foreign nations.

APPROVAL STATEMENT

This report has been reviewed and approved.

Alexander F. Money

ALEXANDER F. MONEY
Project Manager, Research Division
Directorate of Technology

Approved for publication:

FOR THE COMMANDER

Robert W. Crossley

ROBERT W. CROSSLEY, Lt Colonel, USAF
Acting Director of Test Engineering
Deputy for Operations

REPORT DOCUMENTATION PAGE

READ INSTRUCTIONS BEFORE COMPLETING FORM

1. REPORT NUMBER: AEDC-TR-79-1	2. GOVT ACCESSION NO.
3. RECIPIENT'S CATALOG NUMBER	
4. TITLE (and Subtitle): STORE SEPARATION TESTING TECHNIQUES AT THE ARNOLD ENGINEERING DEVELOPMENT CENTER, VOLUME III, DESCRIPTION AND VALIDATION OF CAPTIVE TRAJECTORY STORE SEPARATION TESTING IN THE VON KÁRMÁN FACILITY	5. TYPE OF REPORT & PERIOD COVERED: Final Report - October 1, 1977 - May 25, 1978
	6. PERFORMING ORG. REPORT NUMBER
7. AUTHOR(s): J. P. Billingsley, R. H. Burt, and J. T. Best, ARO, Inc., a Sverdrup Corporation Company	8. CONTRACT OR GRANT NUMBER(s)
9. PERFORMING ORGANIZATION NAME AND ADDRESS: Arnold Engineering Development Center/DOT Air Force Systems Command Arnold Air Force Station, Tennessee 37389	10. PROGRAM ELEMENT, PROJECT, TASK AREA & WORK UNIT NUMBERS: Program Element 65807F
11. CONTROLLING OFFICE NAME AND ADDRESS: Arnold Engineering Development Center/OIS Arnold Air Force Station, Tennessee 37389	12. REPORT DATE: March 1979
	13. NUMBER OF PAGES: 90
14. MONITORING AGENCY NAME & ADDRESS (if different from Controlling Office)	15. SECURITY CLASS. (of this report): UNCLASSIFIED
	15a. DECLASSIFICATION/DOWNGRADING SCHEDULE: N/A

16. DISTRIBUTION STATEMENT (of this Report)

Approved for public release; distribution unlimited.

17. DISTRIBUTION STATEMENT (of the abstract entered in Block 20, if different from Report)

18. SUPPLEMENTARY NOTES

Available in DDC

19. KEY WORDS (Continue on reverse side if necessary and identify by block number)

documents	trajectories
validation	store model
von Kármán Gas Dynamics Facility	Mach number
captive tests	Reynolds numbers

20. ABSTRACT (Continue on reverse side if necessary and identify by block number)

Tests were conducted on a four-finned, ogive-cylinder store model which was mounted on the von Kármán Gas Dynamics Facility (VKF) Captive Trajectory System (CTS) in the Arnold Engineering Development Center (AEDC) Supersonic Wind Tunnel A. The purpose of these tests was to provide information necessary for an independent check on the VKF CTS trajectory mode results. Grid and trajectory data were obtained for the store, both in the free

DD FORM 1 JAN 73 1473 EDITION OF 1 NOV 65 IS OBSOLETE

20. ABSTRACT (Continued)

stream and in the interference flow field of a generalized parent-aircraft model. The Mach number was 1.63, with Reynolds numbers per foot of 5.0 and 3.8 million. Grid data from these tests were used in conjunction with the Air Force Flight Dynamics Laboratory (AFFDL) Six-Degree-of-Freedom Computer Program (SDFCP) to simulate the trajectories obtained by the VKF CTS. These SDFCP simulations compared favorably with the CTS trajectories, providing an important independent verification of the VKF CTS trajectory mode results. This report documents this validation effort and provides a general description of the VKF CTS as well as guidelines for potential users of this system.

PREFACE

The work reported herein was conducted by the Arnold Engineering Development Center (AEDC), Air Force Systems Command (AFSC). One test was conducted at the request of the Air Force Flight Dynamics Laboratory (AFFDL), Wright-Patterson Air Force Base, Ohio, for Nielsen Engineering and Research, Inc. (NEAR), Mountain View, California. Cal Dyer was the AFFDL/FGC project manager for this test. The other test was conducted at the request of the AEDC/DOT and J. M. Rampy was the AEDC/DOTA project manager for this test. The results of both tests were obtained by ARO, Inc., AEDC Division (a Sverdrup Corporation Company), operating contractor for the AEDC, AFSC, Arnold Air Force Station, Tennessee. The ARO Project No. for the AFFDL/Nielsen Test was V41A-M9A, and the data reduction was completed on April 19, 1977. The AEDC/DOT Test was conducted under ARO Project No. V41A-U5A, and the data reduction was completed on December 6, 1977. This report was written under ARO Project No. V32A-P7A, and the manuscript was submitted for publication May 31, 1978. The project manager for this project was A. F. Money, AEDC/DOTR.

CONTENTS

Page

1.0 INTRODUCTION
1.1 General Remarks 7
1.2 Purpose and Scope of Report 7
2.0 VKF CAPTIVE TRAJECTORY SYSTEM
2.1 General Description 8
2.2 Operational Modes 10
2.3 User Guidelines 14
3.0 VKF CTS STORE SEPARATION WIND TUNNEL TESTS
3.1 General Description 20
3.2 Apparatus 21
3.3 Procedures 24
3.4 Data Reduction 27
3.5 Test Results 28
4.0 AFFDL TRAJECTORY PROGRAM
4.1 General Remarks 28
4.2 Addenda for CTS Simulation 28
5.0 CTS AND SDFCP TRAJECTORY COMPARISONS
5.1 Tunnel Active (Air On) 30
5.2 Tunnel Passive (Air Off) 32
6.0 SUMMARY OF RESULTS
6.1 Basic Conclusions 32
REFERENCES 33

ILLUSTRATIONS

Figure

1. VKF Captive Trajectory System
a. Installed in Tunnel A 35
b. Installed in Tunnels B and C 36
2. VKF CTS Sting Mechanism 37
3. VKF CTS Sting Angles and Rotation Arms 38
4. Store-Parent Schematic, Fuselage Centerline Launch Point
a. Initial Position, t = 0 39
b. Position at t ≠ 0 39

Figure Page

5. Store-Parent Schematic, Wing-Mounted Pylon Launch Point
   a. Side View (along +Y, Initial Position, t = 0) . . . 40
   b. Rear View (along +X, Initial Position, t = 0) . . . 41
   c. Top view (along +Z, Position of Store at t ≠ 0) . . . 42
6. Ejector Force and Thrust Simulation Constant Definitions
   a. Ejector Force . . . 43
   b. Thrust . . . 44
7. Tunnel A . . . 45
8. N1-B2-W Details and Dimensions . . . 46
9. Pylon Locations on Parent Aircraft . . . 47
10. Details and Dimensions of the Swept Pylon (P3) and Double-Wedge Pylon (P2)
   a. Swept Pylon (P3) . . . 48
   b. Double-Wedge Pylon (P2) . . . 49
11. Store Model . . . 50
12. Tunnel Installation
   a. Sketch . . . 51
   b. Photograph . . . 52
13. Coordinate Systems Showing Positive Vector Directions for Wind Tunnel Test Data . . . 53
14. Simulated Ejector Force Curve . . . 54
15. Free-Stream Trajectory Motion Comparison, Pitch Oscillation, Data Groups No. 918 and 481
   a. θ versus t . . . 55
   b. ψ versus t . . . 55
   c. X versus t . . . 56
   d. Y versus t . . . 56
   e. Z versus t . . . 56
16. Free-Stream Trajectory Motion Comparison, Yaw Oscillation, Data Group 919 and 480
   a. θ versus t . . . 57
   b. ψ versus t . . . 57
   c. X versus t . . . 57
   d. Y versus t . . . 58
   e. Z versus t . . . 58

Figure Page

17. Centerline Trajectory Motion Comparison, Data Group 649
a. θ versus t 59
b. ψ versus t 59
c. X versus t 59
d. Y versus t 60
e. Z versus t 60
18. Centerline Trajectory Motion Comparison, Data Group 651
a. θ versus t 61
b. ψ versus t 61
c. X versus t 61
d. Y versus t 62
e. Z versus t 62
19. Wing Pylon Launch Point Trajectory Motion Comparison, Data Group 743
a. θ versus t 63
b. ψ versus t 64
c. X versus t 64
d. Y versus t 65
e. Z versus t 65
20. Wing Pylon Launch Point Trajectory Motion Comparison, Data Group 912
a. θ versus t 66
b. ψ versus t 67
c. X versus t 67
d. Y versus t 68
e. Z versus t 68
21. Asymmetric Store Trajectory, Data Group 277
a. θ versus t 69
b. ψ versus t 70
c. ϕ versus t 70
d. X versus t 71
e. Y versus t 71
f. Z versus t 72

TABLES

1. VKF CTS Motion Capabilities 73
2. VKF CTS Drive System Accuracies 74

Page

3. VKF CTS Load Capacity 75
4. AFFDL/Nielsen Test Summaries 76
5. AEDC/DOT Test Summaries 79
6. Launch Point and Ejection Characteristics for Active CTS Trajectories 80
7. Full-Scale Store Characteristics for Active CTS Trajectories 81
8. Initial Conditions for Active CTS Trajectories 82
9. Store Characteristics, Aerodynamic Input, and Initial Conditions for Passive CTS Trajectory 83

NOMENCLATURE 84

MODEL NOMENCLATURE 89

1.0 INTRODUCTION

1.1 GENERAL REMARKS

The Captive Trajectory System (CTS) concept was first developed and employed by the David Taylor Model Basin, Washington, D.C., in 1960 (Ref. 1). The motivation for such a system was the difficulty in predicting aircraft store trajectories of bombs, missiles, fuel tanks, etc. in the immediate vicinity of the parent aircraft where aerodynamic interference is prevalent.

CTS testing at the Arnold Engineering Development Center (AEDC) was first accomplished in 1968 at the Propulsion Wind Tunnel Facility (PWT) Aerodynamic Wind Tunnel (4T) with a mechanism developed specifically for that purpose (Ref. 2). This system has been employed in numerous tests.

In order to provide AEDC CTS testing capability in the supersonic-hypersonic flight regime, a CTS mechamism has been developed for the von Kármán Gas Dynamics Facility (VKF) Supersonic Wind Tunnel (A) and Hypersonic Wind Tunnels (B) and (C), hereinafter referred to as Tunnels A, B, and C. The VKF CTS has been employed in the "grid mode" since 1973. A considerable amount of grid mode data has been acquired for vehicle staging (primarily the space shuttle), store separation, flow-field mapping, and tunnel calibration. In 1977, the "trajectory mode" of operation was added to the system. Because of the complexity of the trajectory mode of operation, it was essential that this system be checked as thoroughly as possible before routine test utilization. Consequently, an independent trajectory program was employed to simulate certain VKF CTS trajectories. The good agreement between the CTS trajectories and the independently predicted trajectories provides considerable verification and validation for VKF CTS test results.

1.2 PURPOSE AND SCOPE OF REPORT

This report is Volume III of a four-volume series covering store separation testing at AEDC. Volume I covers the various store separation testing techniques, Volume II covers captive trajectory system testing in the Propulsion Wind Tunnel Facility Tunnel 4T, and Volume IV addresses dynamic store separation testing.

This volume documents the independent trajectory analysis validation of VKF CTS trajectories and contains a general description of the VKF CTS components and operational modes along with certain test results. Also included are guidelines for prospective users of the VKF CTS unit.

2.0 VKF CAPTIVE TRAJECTORY SYSTEM

2.1. GENERAL DESCRIPTION

The VKF CTS may be installed in either Tunnel A or Tunnels B and C which provides a Mach No. range from 1.5 to 10.0 (1.5 to 5.5 in Tunnel A, 6.0 and 8.0 in Tunnel B, and 10.0 in Tunnel C, see Ref. 3). As shown in Fig. 1, the CTS mechanism is installed from the top of the tunnel. It may be transferred from one tunnel to another with a minimum of disassembly. The unit is operated from a centralized control console located in the VKF Tunnel A Control Room.

The basic CTS components are described in the following sections.

2.1.1 Hardware

The model support system employs electromechanical drives that can continuously vary the translational position (X,Y,Z) and angular orientation (ψ, θ, ϕ) of the CTS store model within the tunnel test section providing a full six-degree-of-freedom (6-DOF) motion capability.

The axial (X_c) and vertical (Z_c) translational motions are achieved by linear ball screw drives which are driven by printed circuit motors through gear drives equipped with electromechanical brakes. A loss of power locks the brakes to keep the system from falling or moving downstream because of aerodynamic drag.

Lateral motion (Y) is achieved by rotating the vertical model support shaft (η_c) which in turn rotates the various radius arms of the model support sting (see Figs. 2 and 3). Then the model is directly translated laterally (Y) through the arc of the radius arms. The resulting yaw angle is compensated for by another yaw rotation (ψ_c). That is, the total yaw angle (ψ) is the sum of both η_c and ψ_c since both angles are in the same horizontal plane.

Tunnels B and C operational requirements dictated that the VKF CTS mechanism be water cooled via flexible tubing. This critical design requirement was easier to accomplish with indirect lateral translation (via the yaw angles and radius arms) rather than direct translation.

The pitch angle (a_c) is achieved through a knuckle joint which is just forward of the second yaw axis (ψ_c). Roll motion (ϕ_{cB}) occurs forward of the pitch and yaw axis. Roll, like pitch and yaw, is driven via a flexible shaft by a printed circuit motor located outside the tunnel test section. The employment of printed circuit motors makes the system highly responsive.

The CTS translational positions and angular orientations are monitored via potentiometers which are read by a multiplexed analog-to-digital converter. Table 1 lists the range of motion capabilities for the VKF CTS in all the tunnels. Also shown in Table 1 are the maximum rates of travel. Table 2 lists the position accuracies of the individual mechanical drives. Section 3.3.3.3 gives the model attitude and position uncertainties for a typical installation.

In addition to the transient angles mentioned above, three additional fixed or constant angles can be incorporated, if necessary. There are two pitch angles (α_{P_C} and θ_C) and one roll angle (ϕ_{CA}) which can be preset forward of the transient angle hinge locations (Figs. 2 and 3). Certain test requirements (interference, large pitch angle, etc.) occasionally require that a fixed, preset angle be employed.

The tunnel standard model support system is commonly employed to support the parent model during interference testing. The standard support system is used in the "short inject" mode, whereas it is not completely injected vertically into the test section (see Section 3.2.3). This reduces the possibility of tunnel blockage and also provides for more maneuverability of the CTS by reducing mechanical interference. The parent model may be instrumented by conventional methods for force and moment, heat transfer, or pressure distribution information.

The CTS model may be attached to a balance or instrumented for pressure. It has also been a pressure probe and employed in flow-field surveys. When using the trajectory mode of operation, the model must be attached to a balance.

2.1.2 Software

The CTS computer program directs the mechanism (described above) that positions the store model. The store model position may be a preselected input (grid mode) or a computed result (trajectory mode). In either mode, the model positioning generally requires X_C-Z_C translation of the entire sting plus successive rotations of the various sting radius arms through the appropriate angles (Figs. 2 and 3). These rather complex relationships have been placed in matrix form and are solved numerically by the program which is operational on the VKF DEC System 10 Computer.

In the grid mode of operation, the desired grid matrix is input to the grid mode program. The program then automatically controls the model positioning and data acquisition.

For the trajectory mode of operation, the computed position is based on a solution of the 6-DOF equations of motion for a full-scale store vehicle with the measured (from

the balance) and then scaled aerodynamic forces and moments as a primary forcing function. Other important forces and moments can be numerically simulated in the program (gravity, thrust, ejector, etc.) so that a realistic trajectory is "flown" by the captive (restrained) store model. The computed full-scale translation distances are then appropriately scaled to the CTS store and/or tunnel test section dimensions.

The trajectory generation program can be divided into three primary parts as follows:

1. CTS model position-orientation equations. These relate the full-scale vehicle position to the model position in the tunnel.

2. Six-degree-of-freedom equations of motion for the full-scale store and their numerical solution. An option to eliminate the roll degree of freedom is available.

3. Applied forces and moments. These are primary forcing functions for the equations of motion. Static aerodynamic forces and moments are measured by the CTS store balance at points along the trajectory. The other forces and moments (thrust, ejector, etc.) must be numerically simulated.

The CTS trajectory mode equations of motion are essentially the same as those given in Refs. 1 and 2. Additional details of the VKF CTS computer program are contained in Section 2.2.

2.2 OPERATIONAL MODES

Since the VKF CTS can be operated in either of two distinctly different and independent modes, these operational options (trajectory mode and grid mode) will be described in detail in this section.

2.2.1 Grid Mode

For the grid mode, the desired grid matrix is selected and loaded into the computer and the positioning of the CTS model is controlled by the computer which automatically records all the data inputs at each grid point location. A grid matrix may be as large as 6 by 40, (each of the 6-DOF may have as many as 40 values) but need not be symmetrical. A subgrid system is employed within the grid to combine the various grid values into the required combinations.

Two procedures are available in the grid mode for correction of model sting-balance deflections. The CTS is under computer control at all times, and, if the tunnel sector were under computer control, it would be a simple matter to adjust the settings of both support systems as they deflected to maintain constant values throughout the grid. Unfortunately, however, the sector is not under computer control, and it would be too time consuming to manually adjust the sector for each point on a grid or trajectory. Furthermore, the sector has no remote yaw control available. Therefore, the following procedures and options are used: (1) Both the parent and CTS models linear displacements are calculated for each nominal point on the grid. The CTS is then automatically moved an amount equal to the sum of the deflections of the two models. (2) The parent-model angular attitude is nominally set to the specified position air on but will slightly deflect from that position (see Section 3.2.4). The parent angle is not corrected for this deflection, but when mounted on a balance the true angular attitude is determined and tabulated. (3) The tunnel user must now specify one of the two following options: (a) that the CTS model attitude be corrected, or (b) that the difference between the parent and CTS models attitudes be corrected. An iteration process is used for all of these corrections, and the linear and angular positions are iterated until they are within specified tolerances (normally ±0.050 in. and ±0.1 deg, respectively) of the specified values. The time required to position the model, iterate the deflections, verify the position, read the instrumentation, and perform all data reduction is only a few seconds per point.

To emphasize the fact that the grid mode and trajectory mode are entirely different, it should be noted that a CTS unit is not absolutely necessary for grid data acquisition. The conventional tunnel model support system can be manually modified (sting component changes, etc.) to position a model or probe at any location in the test section. However, the CTS can position a model much faster and more accurately than this procedure. As such, the CTS has been employed in numerous tunnel calibration and flow-field mapping tests. Motion boundaries or travel limits are always established to ensure that the CTS model does not hit the tunnel wall.

In the grid mode, the aerodynamic forces and moments on the CTS (store) model, including aerodynamic interference of an adjacent parent model, can be measured as a function of the relative position and orientation of the two models. This type of aerodynamic grid data, when properly processed, may be employed for store trajectory computation via any suitable trajectory program (Ref. 1). This scheme has been employed in one phase of the present validation analysis to check the VKF CTS trajectory mode results.

Three different sets of grid data were acquired for validation purposes during the wind tunnel tests described in Section 3.0. These data were systematically taken in three regions: (1) around a pylon (or launch rack) located underneath the fuselage in the aircraft plane of symmetry (referred to herein as the centerline pylon), (2) around a pylon located underneath the left wing of a generalized aircraft at 1/3 of the semispan outboard of the fuselage centerline (herein referred to as the wing pylon), and (3) in the free stream. None of these sets of grid data included a roll position variation. That is, ϕ was zero for all points.

2.2.2 Trajectory Mode

This is the most complex operational mode of the CTS. Basically, in the trajectory mode the CTS model position (scaled to tunnel coordinates) is continuously computed from the appropriate motion-position equations for the full scale vehicle.

Generation or simulation of a store vehicle flight path in the interference flow field of an adjacent parent aircraft is an important and unique testing capability of the CTS trajectory mode. A description of the operational procedures for such a test follows.

For a trajectory starting from the launch position (say a wing-mounted pylon), the CTS store model is moved to the launch position via manual inputs to the CTS control console. This launch position is normally the reference point from which store model movement with respect to the parent model is measured. To begin a trajectory at other than the launch point (a postlaunch), it is necessary to specify first, the coordinates of the new starting point relative to the launch or zero reference point; second, the store velocity components at this point; third, the attitude of the store model at this point; and finally the time offset at the point.

It is always necessary to specify the initial values of the full-scale store angular rate components and the translational velocity (which may be different from the tunnel flow velocity because of altitude simulation).

Static aerodynamic force and moment measurements are taken at the initial point. These six component measurements are converted to standard aerodynamic coefficients using the tunnel dynamic pressure and model scale reference lengths and area. Full-scale aerodynamic forces and moments are computed from these coefficients in conjunction with the appropriate full-scale dynamic pressure, reference lengths, and reference area. These scaled aerodynamic loads and the simulated thrust and ejector loads, in conjunction with the specified initial velocities, are employed by the program to compute the next point on the trajectory. Aerodynamic coefficients (based on the measured data) are also predicted for the new point - a linear extrapolation forward in time.

If the computed point is within the CTS travel limitation boundaries (and will not hit the tunnel wall or exceed an individual drive limit), then the CTS moves the model to the computed position taking into account the anticipated deflections and displacements of the CTS model. No parent deflections or displacements are used. If, in the process of driving to the new position, a collision of the CTS model and parent model or their support systems occur the trajectory is terminated. The CTS mechanism is electrically isolated from the tunnel, and an electrical circuit uses this to control stopping the CTS whenever contact with the tunnel or parent model is made.

If a solid boundary is not contacted, then the predicted position is obtained and the static aerodynamic forces and moments are measured. These forces and moments are then converted to coefficient form and compared to the predicted coefficients. If the measured aerodynamic coefficients are within the specified tolerances (C_{N_T}, C_{m_T}, C_{Y_T}, C_{n_T}, C_{ℓ_T} and C_{A_T}) relative to the predicted values, then the computed point is considered a valid point on the trajectory and computation begins to determine the next point. If the measured coefficients are not within tolerance, the CTS retreats to the last valid point and computation begins anew which will yield a smaller motion interval than was previously computed. The checking sequence is repeated until the prediction interval is equal to twice the integration interval, at which point the data is accepted and computation continues.

On the other hand, if a specified number (nominally six) of successive valid trajectory points are predicted, the program doubles the prediction interval, thus a consequent reduction in tunnel test time. The maximum size of the prediction interval is limited in the program. The aerodynamic coefficient prediction-checking procedure provides a method of adjusting the motion increment between valid trajectory points. Small steps are required in regions where the aerodynamic forces on the store are abruptly changing, and larger steps are made in regions where the forces are well behaved. The prediction--checking procedure described above is continued until the trajectory is terminated. A trajectory can be terminated in various ways: (1) model contact or exceeding a boundary limit as described previously, (2) exceeding a balance limit, or (3) manual termination at any time.

Four different sets of trajectory data were acquired for validation purposes during the wind tunnel tests described in Section 3.0. The trajectories were obtained in the same three regions as the grid data (see Section 2.2.1) along with a fourth set of trajectory data which consisted of air-off trajectories in which the motion was determined by the input of constant aerodynamic coefficients into the program.

2.3 USER GUIDELINES

2.3.1 CTS Capabilities

The general data acquisition capabilities of the VKF CTS are described in Sections 2.1 and 2.2. The basic physical capabilities of the system are given in Sections 2.1.1 and 3.3.3.3 and are listed in Tables 1, 2, and 3.

The VKF CTS load-carrying capacities given in Table 3 are larger than similar systems designed just for aircraft store separation. This design capability was based on anticipated uses of the system in space vehicle staging applications.

Along with the basic capabilities of the CTS system, additional systems have been provided to further advance the capabilities of the VKF CTS. These additional systems are described in the following comments.

Jet and rocket plume simulation has been available for the sector-mounted model. This simulation is also available for the CTS model because a high-pressure gas line is provided in the CTS strut. It is sized for flowing gas at a maximum of 2 lbm/sec at 450°F at a supply pressure of 1,500 psia. The line terminates in the test section at the end of the vertical strut. A flexible line then carries the gas to the model.

For tests in which the CTS model will be used for obtaining pressure data, the capability of using one of three different pressure instrumentation packages is available. They are described as follows:

1. One package consists of twenty 15-psid transducers mounted on top of the tunnel. The capability of measuring 19 pressures is available (one transducer is for measuring a variable reference pressure which, when applied to the other transducers, allows pressures up to 30 psia to be measured). The accuracy of each of these transducers is within ±0.0075 psi or ±0.25 percent of the measured pressure, whichever is greater. To use this package, approximately 20 ft of pressure tubing is required which requires a relatively long stabilization time.

2. A second package consists of eight fast-response, 15-psid transducers referenced to a vacuum and mounted on the CTS vertical strut. The accuracy of these transducers is within ±0.012 psi or ±0.25 percent of the measured pressure, whichever is greater. Approximately 50 in. of pressure tubing is required when using this package thus reducing pressure stabilization times. This package is commonly used for base pressure measurements on static force and moment tests and flow-field probing

tests using only one or two probes. Accessibility to the package is very limited during tunnel operation since the package is located inside the tunnel.

3. A third package is made up of one fast-response, 15-psid transducer connected to a 48-port S type Scanivalve®. The accuracy of this transducer is the same as that given in 2 above. The Scanivalve-transducer combination is mounted in the model sting forward of the CTS roll mechanism and requires approximately 16 in. of pressure tubing. This package is used in tests where a CTS pressure model is required to roll, since the number of instrumentation leads (tubing, wires, etc) routed through the yaw-pitch-roll head of the CTS is greatly reduced. Accessibility is the same as noted for 2 above.

Another capability which exists for trajectory tests applies to interference-free trajectory simulation. This capability is that the physical translation of the CTS store model can be deleted and thus avoid the problem of exceeding drive limits. To do this the full-scale store translation positions from the solution of the equations of motion are computed and recorded, but when scaling them to CTS coordinates they are set to zero. Therefore, translational motion of the CTS is deleted, but angular motion is handled normally. This capability also allows free-stream data on the CTS model to be obtained in favorable locations in the test sections (regions of best flow uniformity).

Experience with CTS testing in VKF has yielded the following test data productivity values:

Grid Mode

Flow-field survey measurements - up to 200 points/hour

Pressure distribution measurements - up to 250 points/hour

Static force and moment measurements - up to 500 points/hour

Trajectory Mode

Trajectories - up to six 0.5-sec trajectories per hour

2.3.2 CTS Limitations

CTS units are inherently subject to certain limitations and compromises in relation to the simulation of actual trajectories. Two of these limitations, and their influence on trajectory simulation, are described in this section.

A simulation compromise, common to all CTS store separation trajectories, involves the different flight path angles of the store and the parent aircraft. A CTS test anomally exists since both flight path angles cannot be simultaneously simulated. Fortunately, this anomalous situation is of minor importance in most applications but its existence is noteworthy (see Ref. 4). A simple example of this particular CTS testing compromise is noted below.

Consider a parent aircraft with its attached store which are both flying straight and level as illustrated in Figure 4a. The velocity vectors of both configurations with respect to the horizontal are $\gamma_c = \gamma_s = 0$. After store separation, this situation is changed as illustrated in Fig. 4b. The parent aircraft is still flying straight and level ($\gamma_c = 0$) with the same velocity magnitude (U_A). The orientation (γ_s) and magnitude (U_R) of the store velocity vector has changed because of gravity, aerodynamic forces, thrust, and ejector forces. The wind tunnel cannot simulate both flow directions ($\gamma_c = 0$ and $\gamma_s \neq 0$) simultaneously. Consequently, the VKF CTS trajectory program contains the following options:

1. Do not align the store velocity vector (U_R) with the tunnel velocity vector V_∞. Then the total angle of attack of the store is $\theta = \alpha_s + \gamma_s$ (see Fig. 4b). Even though the interference loads from the parent or the store may be correct, the store aerodynamic loads measured by the balance may be incorrect because the store angle of attack is θ instead of α_s.

2. Align the store total velocity vector (U_R) so that it is parallel to the tunnel velocity vector (V_∞). Then the angle of attack of the store is α_s which it should be. However, the store has been rotated through γ_s so that the angle between the store and the parent is also α_s instead of $\theta = \alpha_s + \gamma_s$. Even though the store angle of attack is correct, its aerodynamic loads may still be somewhat in error. This depends on the magnitude of aerodynamic interference error caused by the incorrect angular orientation of the store with respect to the parent model.

The above options also apply to the yaw plane when $\sigma_s \neq 0$ (see Fig. 5c). In the above example, if the store flight path angle (γ_s) is large (say a few degrees) or large relative to α_s or θ, then CTS trajectory results from either option (1 or 2) may be spurious. The store flight path angle (γ_s) is generally small (less than one degree) in the interference region where a CTS trajectory is practical. Consequently, the inevitable test compromise exerts only a minor influence on the results. All the example CTS trajectories presented herein (Section 5.0) employed option (2) as described above.

The CTS rates of positioning the model are generally not equal to the full-scale trajectory translational and angular velocities because of physical system limitations (Table 1). These rates are different by orders of magnitude. This is a basic limitation for any CTS unit. Thus, CTS trajectory time (or full-scale trajectory time) and tunnel test time (during a CTS trajectory run) are not equal. It requires several minutes of tunnel time to run a CTS trajectory lasting only a second (see Section 2.3.1). Elimination of the present VKF CTS trajectory point corroboration scheme (a stop-and-go procedure described in Section 2.2.2) would lower the tunnel test time but would not materially help the rate simulation. A CTS trajectory is a somewhat restrained or quasi-steady trajectory compared to an actual free flight, so any transient, unsteady, or rate-dependent aerodynamic loads are not measured during a CTS trajectory. However, provision is made in the present program to numerically simulate conventional aerodynamic damping ($C\ell_p$, C_{m_q}, and C_{n_r}). These damping coefficients are normally user supplied. Other transient, unsteady, or rate-dependent aerodynamic loads may be numerically simulated if their mathematical model is known from theory or experiment. This information must also be supplied by the user. Special programming will be required to input these effects.

It must also be emphasized that the trajectories or flight path of most practical store configurations are controlled by the steady or static aerodynamic loads. It is, of course, realized that unsteady aerodynamic loads may be a dominant feature of certain configurations. However, the magnitude and rather large variation with relative position of steady aerodynamic interference loads will normally overpower the influence of conventional aerodynamic damping (angular rate-dependent) loads. Aerodynamic damping requires enough time for several angular oscillation cycles to occur before its influence on angular magnitude is evident. By this time, the store will normally be clear of the parent-aircraft interference flow field and further CTS simulation is unnecessary.

The above remarks concerning the minimum influence of the limitations are substantiated by the good agreement between actual full-scale flight test store separation trajectories and CTS trajectories from the PWT Aerodynamic Wind Tunnel (4T). Consequently, regardless of the limitations discussed above, it is concluded that the aerodynamic flow field and store vehicle trajectories within the flow field can be properly simulated by CTS tests for most configurations of practical importance.

2.3.3 Required Input for CTS Tests

Certain basic information is required from users who wish to employ the VKF CTS test capabilities. This required information is categorized and listed in this section to aid the users in planning their tests.

2.3.3.1 Grid Mode

Parent and Store Model Scaled Properties

Coefficient reference area, A_m, in.^{2}

Coefficient reference lengths, ℓ_{1_m}, ℓ_{2_m}, ℓ_{3_m}, in.

Length to be used in length Reynolds number, ℓ_{4_m}, in.

Model base area, A_b, in.^{2}

Model length for computing center-of-pressure location, ℓ_m, in.

Distance from model nose to moment reference point (MRP). This point coincides with the full-scale center of gravity, in.

Grid Matrix Information

Location of reference point on store model for positioning within the grid.

Definition of positive directions in grid axes.

Definition of grid axis reference point.

Definition of all grid points at which data will be obtained.

2.3.3.2 Trajectory Mode

Parent and Store Model Scaled Properties

Coefficient reference area, A_m, in.^{2}

Coefficient reference lengths, ℓ_{1_m}, ℓ_{2_m}, ℓ_{3_m}, in.

Length to be used in length Reynolds number, ℓ_{4_m}, in.

Model base area, A_b, in.^{2}

Model length for computing center-of-pressure location, ℓ_m, in.

Distance from model nose to MRP. This point coincides with the full-scale center of gravity, in.

Launch Position Information

Definition of the position of the store model with respect to the parent model when at the launch position (position where t, X, Y, Z and all store velocities are equal to zero).

Parent Vehicle Full-Scale Properties

Parent-vehicle simulated accelerations along the tunnel axes, a_x, a_y, a_z, ft/sec^2

Parent-vehicle climb angle, γ_c, deg

Parent-vehicle roll angle, ϕ_{AC} deg

Parent-vehicle Mach No. (tunnel free-stream Mach number), M_∞

Initial altitude of parent vehicle, ft

Store Vehicle Full-Scale Properties

Store vehicle mass, $\overline{m}$, slugs

Store vehicle coefficient reference area, A, ft^2

Store vehicle coefficient reference lengths, ℓ_1, ℓ_2, ℓ_3, ft

Store vehicle mass moments of inertia, I_{xx}, I_{yy}, I_{zz}, slug-ft^2

Store vehicle products of inertia, I_{xz}, I_{yz}, I_{xy}, slug-ft^2

Store vehicle damping derivatives in roll, pitch, and yaw, respectively, $C\ell_p$, C_{m_q}, C_{n_r}, rad^{-1}

Store vehicle arbitrary incremental coefficients, C_{N_o}, C_{m_o}, C_{Y_o}, C_{n_o}, $C\ell_o$, C_{A_o}

Postlaunch Information

Time at start of postlaunch trajectory, t_o, sec

Store vehicle angular velocities at postlaunch, p_o, q_o, r_o, rad/sec

Store vehicle linear velocities at postlaunch, u_o, v_o, w_o, ft/sec

Store vehicle coordinates from launch position at postlaunch, X_{I_o}, Y_{I_o}, Z_{I_o}, ft

Store vehicle attitude at postlaunch, ν_{I_o}, η_{I_o}, ω_{I_o}, deg

Ejector Force Simulation Constants

Ejector force vector angle (see Fig. 5), ω_m, deg

Forward and aft ejector locations (see Fig.5) respectively, X_1, X_2, ft

Definition of ejector force as a function of either time of stroke or length of stroke (see Fig. 6a)

Thrust Simulation Constants

Store vehicle jet damping derivatives (see Refs. 5, pp. 221-223 and Ref. 6, Appendix 1), $K\ell_p$, K_{m_q}, K_{n_r}, ft-lbf-sec/rad

Definition of the thrust force utilizing the following sequence of events: store reaches end of lanyard after falling a distance Z_L or time t_L and initiates ignition; at Z_L or t_L thrust buildup begins TD seconds later where $t_t = 0$; definition of the thrust force as a function of t_t until the thrust is terminated at T3 seconds (see Fig. 6b).

The above information is necessary to start a CTS trajectory. Additional simulation features such as thrust vector control or aerodynamic control can be simulated if the appropriate formulation is user supplied. This information must be incorporated in a special subroutine. Enough lead time must be provided for the programming and checkout of these special subroutines.

3.0 VKF CTS STORE SEPARATION WIND TUNNEL TESTS

3.1 GENERAL DESCRIPTION

Two wind tunnel tests, each conducted in the VKF Tunnel A, provided the data employed for the validation and verification effort presented in this report. A detailed description of these tests is given in this section.

3.1.1 AFFDL/Nielsen Test

This investigation was conducted in the VKF Tunnel A. It was one of a series of tests to aid Nielsen Engineering and Research, Inc. in the development of a generalized theoretical method for predicting separation characteristics of stores from high-speed, fighter-bomber aircraft. To aid in the effort to validate the VKF CTS, AFFDL provided time within the test to obtain data specifically for that purpose. Four types of data were obtained during this program at Mach numbers 1.5, 1.6, and 2.0 in the vicinity of a generalized aircraft shape (and in the free stream), but only the force and moment grid data and trajectory data at Mach No. 1.6 apply to this report.

3.1.2 AEDC/DOT Test

This investigation was also conducted in the VKF in Tunnel A. It was a continuation of efforts by AEDC to validate the VKF CTS. This test had two major purposes: (1) to provide trajectory data which should match previously obtained trajectories in the PWT Aerodynamic Wind Tunnel (4T) and (2) to provide data for a repeatability check of grid and trajectory data between two VKF Tunnel A test entries. Similar force and moment grid data and trajectory data were obtained at Mach No. 1.6 using the same models used in the AFFDL/Nielsen Test.

3.2 APPARATUS

3.2.1 Wind Tunnel

Tunnel A is a continuous, closed-circuit, variable density wind tunnel with an automatically driven flexible-plate-type nozzle and a 40- by 40-in. test section. The tunnel can be operated at Mach numbers from 1.5 to 6.0 at maximum stagnation pressures from 29 to 200 psia, respectively, and stagnation temperatures up to 750°R (M_∞ = 6). Minimum operating pressures range from about one-tenth to one-twentieth of the maximum at each Mach number. The tunnel is equipped with a model injection system which allows removal of the model from the test section while the tunnel remains in operation. A description of the tunnel and airflow calibration information may be found in Ref. 3. Figure 7 shows the wind tunnel and model injection system.

3.2.2 Models

The generalized aircraft model was provided by Nielsen Engineering and Research, Inc. Additional parts were fabricated by VKF (SCOC and P3). One parent-model configuration was tested with two pylon attachments, the N1-B2-W configuration. It consisted of an ogive-cylinder-boattail fuselage with a swept wing (NACA 65A006 Airfoil Section), see Fig. 8.

The parent-aircraft model had provisions for mounting pylons on the fuselage centerline, left wing 1/3 semispan, or 2/3 semispan locations. Figure 9 shows these positions. The vertical centerlines of the wing pylons were located on the 40-percent wing chord.

Two different pylon configurations were tested (see Fig. 10). The swept pylon (P3) was tested at the 1/3 semispan position, and the double-wedge pylon (P2) was tested at the fuselage centerline. The 2/3 semispan pylon location was not utilized for these tests.

The store model is shown in Fig. 11. It was an ogive-cylinder with four fins. Provisions were made for testing the model at fin orientation angles, ϕ_{FIN}, of zero or 45 deg, but only the 45-deg position was tested.

3.2.3 Model Support Systems

The store model was supported by the VKF CTS. The parent model was inverted in the test section and supported by an offset sting and strut assembly attached to the main model support system (see Fig. 12). Note that the short inject mode was used. Although the parent model had several possible adjustments, only the 0- and 5-deg parent angles of attack were tested. The data from the 0-deg position was employed in the present analysis.

3.2.4 Instrumentation and Measurement Accuracy

Tunnel A stilling chamber pressure is measured with a 15-, 60-, 150-, or a 300-psid transducer referenced to a near vacuum. Based on periodic comparisons with secondary standards, the accuracy (a bandwidth which includes 95 percent of the residuals, i.e., 2σ deviation) of these transducers is estimated to be within ±0.2 percent of the measured pressure or ±0.015 psia, whichever is greater. Stilling chamber temperature is measured with a copper-constantan thermocouple having an accuracy of ±0.5 percent of the measured temperature based on repeat calibrations (2σ deviation).

The accuracies of the 6-DOF motions of the CTS are based on periodic calibrations of the drives and are presented in Table 2.

A "Gravity Sensing Electrolytic Transducer", closely resembling a bubble level, was used as a null device to zero-out the parent-model pitch deflections. The transducer used was capable of measuring deflections in the ±3-deg range. The accuracy of this instrument, when used as a null device, is estimated to be ±0.05 deg. This technique was used to compensate only for the basic aerodynamic loading on the parent model and its

support system; the small deflections caused by interference loading from the store model were neglected.

Model forces and moments were measured with a six-component, moment-type, strain-gage balance supplied by the AEDC PWT (Balance No. 6-.4-.020-.4M"C") and calibrated by VKF. Before the test, static loads in each plane and combined static loads were applied to the balance to simulate the range of loads and center-of-pressure locations anticipated during the test. The following accuracies represent the bands of 95 percent (2σ deviation) of the measured residuals, based on differences between the applied loads and the corresponding values calculated from the balance calibration equations included in the final data reduction. The range of static loads applied and the measurement accuracies follow.

Component	Balance Design Loads	Calibration Load Range	Range of Static Loads	Measurement Accuracy
Normal force, lb	20.0	20.0	±10.0	±0.05
Pitching moment,* in.-lb	40.0	40.0	±10.0	±0.10
Side force, lb	20.0	20.0	± 5.0	±0.05
Yawing moment,* in.-lb	40.0	40.0	± 5.0	±0.10
Rolling moment, in.-lb	6.0	6.0	± 0.5	±0.02
Axial force, lb	6.0	6.0	0 - 5.0	±0.06

*About balance forward pitching moment bridge

The transfer distance from the balance forward moment bridge to the model moment reference location was -0.862 in. along the longitudinal axis and was measured with an estimated precision of ±0.005 in.

The model base pressure was measured while in the grid mode with a 15-psid transducer. The transducer had a 1.0-psia reference pressure which was also measured by a 15-psid transducer. The accuracy of each of the transducers is within ±0.0075 psia or ±0.25 percent of the measured pressure, whichever is greater.

3.3 PROCEDURES

3.3.1 Test Conditions

The tests were conducted at nominal Mach numbers of 1.51, 1.63, and 2.00. Since only the Mach No. 1.63 data are employed in this report, a summary of these test conditions is given below.

M_∞	p_t, psia	T_t, °R	q_∞, psia	p_∞, psia	$Re_\infty \times 10^{-6}$
1.63	18.9	580	7.92	4.26	5.0
1.63	14.2	580	5.96	3.20	3.8

3.3.2 Test Procedure

Before the tests, trajectories were run with no flow in the tunnel. This is a standard procedure to assure that the program is working correctly before each test entry. Constant aerodynamics were input into the program to provide the desired motions. Four kinds of trajectories were run air off: (1) 3-DOF motion (axial, vertical, and pitch), (2) 5-DOF motion (all but roll), (3) 6-DOF motion with zero cross products of inertia, and (4) 6-DOF motion with nonzero cross products of inertia.

During the tests, before the start of each grid or trajectory, the CTS was manually driven to a reference position. When this reference position was a point relative to the parent aircraft, as opposed to a point in the free stream, certain procedures had to be followed. Using a "Gravity Sensing Electrolytic Transducer" (dangleometer) as a null device, which was attached to the parent-aircraft support mechanism, the angle of the parent under air load was corrected to the desired angle (0 deg) by pitching the entire support system (see Section 3.2.4). The maximum correction during the tests was approximately 0.5 deg. The CTS model was then moved in for optical alignment of its axial, vertical, and pitch positions using a precision optical level. The yaw and lateral position of the CTS model relative to the parent aircraft was precisely set before the tunnel was started but could not be checked after the air was flowing.

The store model positions were referenced to its position when attached to the pylon (carriage position) being tested. The X, Y, and Z of the store from its carriage position were variables (see Fig. 13). The grid data consisted primarily of Z translations. The X, Y, and Z in the trajectories were also measured from the store carriage position in the parent axes.

During both tests, schlieren photographs were obtained. Direct color motion pictures were also obtained on selected trajectory runs.

3.3.3 Data Uncertainty

The accuracy of the basic measurements (p_t and T_t) was discussed in Section 3.2.4. In that section, these errors were found to be

$$\frac{\Delta p_t}{p_t} = 0.002 = 0.2\%, \quad \frac{\Delta T_t}{T_t} = 0.005 = 0.5\%$$

Uncertainties in the tunnel free-stream parameters, the model aerodynamic coefficients, and model attitude and position were estimated using the Taylor series method of error propagation, Eq. (1),

$$(\Delta F)^2 = \left(\frac{\partial F}{\partial X_1}\Delta X_1\right)^2 + \left(\frac{\partial F}{\partial X_2}\Delta X_2\right)^2 + \left(\frac{\partial F}{\partial X_3}\Delta X_3\right)^2 \ldots + \left(\frac{\partial F}{\partial X_n}\Delta X_n\right)^2 \quad (1)$$

where ΔF is the absolute uncertainty in the dependent parameter $F = F(X_1, X_2, X_3 \ldots X_n)$ and X_n is the independent parameter (or basic measurement). ΔX_n is the uncertainty (error) in the independent measurement (or variable).

3.3.3.1 Test Conditions

The accuracy (based on 2σ deviation) of the basic tunnel parameters, p_t and T_t, (see Section 3.2.4) and the 2σ deviation in Mach number determined from test section flow calibrations were used to estimate uncertainties in the other free-stream properties using Eq. (1). The computed uncertainties in the tunnel free-stream conditions are summarized below.

Uncertainty, (±) percent of actual value			
M_∞	p_∞	q_∞	Re_∞
1.0	3.0	0.6	0.9

3.3.3.2 Model Aerodynamic Coefficients

The uncertainties of the model aerodynamic coefficients are presented below. These were established at the maximum aerodynamic loading condition using the Taylor series method of error propagation (Eq. 1) with the independent variables being the accuracy of the six-component balance (listed in Section 3.2.4), the accuracy of the base pressure

transducer (Section 3.2.4), and the uncertainties in the tunnel parameters (p_∞, q_∞) listed above.

	Maximum Coefficient Uncertainty, (± percent)					
M_∞	C_N	C_m	C_Y	C_n	C_A	C_{A_t}
1.63	0.70	1.17	0.70	1.17	2.56	4.48

The uncertainty in C_ℓ is not included since its maximum measured value is near zero and the balance repeatability result given below is more applicable for this coefficient.

The basic precision of the aerodynamic coefficients was also computed using only the balance and base pressure accuracies listed in Section 3.2.4 along with the nominal test conditions, using the assumption that the free-stream flow nonuniformity is a bias type of uncertainty which is constant for all test runs. These values therefore represent the data repeatability expected.

		Repeatability (±) Measured Coefficient Value						
M_∞	p_t	C_N	C_m	C_Y	C_n	C_ℓ	C_{A_t}	C_A
1.63	18.9	0.015	0.052	0.015	0.052	0.008	0.017	0.018
1.63	14.2	0.019	0.070	0.019	0.070	0.010	0.023	0.024

Note that the uncertainties and repeatability values presented here do not include any contribution caused by the positioning uncertainty.

3.3.3.3 Model Attitude and Position

The uncertainties of the model attitude and position are presented in the following tabulation. These were established for a typical installation at nominal drive positions using the Taylor series method of error propagation (Eq. 1). The independent variables were the accuracy of the drive systems (listed in Table 2), the accuracy of the balance deflection calculations, the accuracy of the docking procedure, and the accuracy of the model support dimensions. The uncertainty in the model roll attitude is not given since it was not varied during the tests.

Model Attitude and Position Uncertainties

Motion	Model Attitude and Position Uncertainty
X	±0.050 in.
Y	±0.080 in.
Z	±0.060 in.
α_s	±0.10 deg
β_s	±0.10 deg

3.4 DATA REDUCTION

The forces and moments were transferred to the model MRP (see Fig. 11) and reduced to coefficient form in the body-axis system. The coefficient reference lengths (ℓ_{1_m}, ℓ_{2_m}, and ℓ_{3_m}) were the store diameter (0.75 in.), and the coefficient reference area, A_m was the store cross-section area (0.4418 in.^{2}).

In the trajectory program the coefficient tolerances used in the AFFDL/Nielsen and AEDC/DOT Tests were C_{N_T}: 0.10 and 0.04; C_{m_T}: 0.10 and 0.10; C_{Y_T}: 0.10 and 0.04; C_{n_T}: 0.10 and 0.10; $C\ell_T$: 0.10 and 0.015; and C_{A_T}: 0.10 and 0.02; respectively. The integration interval, Δt, was 0.002 sec, and the initial prediction interval, ΔT_p, was 0.01 sec. The maximum prediction interval was limited to 0.04 sec while the minimum was limited to twice Δt (0.004 sec).

It should be noted that the total axial-force coefficient (C_{A_t}) was used in the full-scale motion equations. Since the base pressure level was similar to those expected in flight, the balance measured value of axial force (C_{A_t}) was felt to be more realistic than the forebody value (C_A).

The trajectories that were obtained were simulating a store having masses of 40.0 or 30.0 slugs at a nominal altitude of 40,000 ft. The moments of inertia I_{xx}, I_{yy}, I_{zz}, I_{xz}, I_{yz}, and I_{xy} were varied between trajectories. The store full-scale coefficient reference length and reference area were 1.25 ft and 1.228 ft^2, respectively. Also in the simulation, it was assumed that the parent aircraft was in level, constant velocity flight. Figure 14 shows the history of the ejector force that was simulated in the trajectories.

For some of the trajectories, the store rolling motion was neglected. Although the balance was measuring the rolling moment on the store, this moment was neglected in the equations of motion.

3.5 TEST RESULTS

As explained in Section 3.1.1, four types of data were obtained during the AFFDL/Nielsen Test. Since only the force and moment grid data and trajectory data were used in this report, the test summaries of those data are presented in Table 4. Table 5 contains test summaries of the data obtained during the AEDC/DOT Test.

4.0 AFFDL TRAJECTORY PROGRAM

4.1 GENERAL REMARKS

The AFFDL Six-Degree-of-Freedom Computer Program (SDFCP) is documented in Refs. 6 and 7. The latest version of this program is currently operational on the AEDC IBM 370/165 Computer. Current SDFCP output has been corroborated by comparison with results from sample problems and other independent trajectory programs.

The AFFDL SDFCP has several flight and aerodynamic input options which make it very versatile. One of these options is 6-DOF flight over a flat planet (SDF-2). This option is ideal for the short-range trajectories simulated by CTS units. One aerodynamic option (SAC-3) provides for tabular input of the static aerodynamic coefficients (C_{A_t}, C_Y, C_N, C_ℓ, C_m, C_n) as a function of six independent variables. Aerodynamic coefficients must be input in a specified systematic form so that a linear interpolation routine may be employed. This feature is ideal for interpolation of aerodynamic interference grid data which is a function of store position (X, Y, Z, a_s, β_s, ϕ_s) with respect to the parent aircraft.

To obtain full simulation of CTS trajectories, certain addenda were incorporated into the program. These additions are briefly described in the following section.

4.2 ADDENDA FOR CTS SIMULATION

The SDFCP computes x, y, z of a vehicle relative to an earth-fixed axis. The CTS computes X, Y, Z relative to an axis moving with the parent model. When the parent model is flying straight and level at a velocity (U_A) at an altitude (-H), two interpolation variables for X and Z distances between the store and parent vehicles have to be computed as follows:

$$X = U_A\, t - x$$

$$Z = z - H$$

In all cases, the parent model did not deviate from the Y = 0 position so y itself could be employed as an interpolation variable. The flight path angle of the parent model was zero (γ_c = 0), consequently, no additional angular interpolation variables had to be computed.

CTS online trajectories can be run with zero roll ($\dot{p} = p = \phi = 0$); therefore, this had to be programmed as an option in the SDFCP. However, the CTS is not run in this mode even if ΣM_x is zero (or arbitrarily set equal to zero) unless:

$$I_{yy} = I_{zz}$$

$$I_{xy} = I_{zx} = I_{yz} = 0$$

ΣM_x is the sum of aerodynamic rolling moments plus any other exterior source that causes a roll torque. If the above conditions are not satisfied, a physical $\dot{p}$ can occur because of inertia coupled terms in the expression for the roll rate so that $\dot{p}$ is not equal to zero.

The store ejector force subroutine for the CTS program was copied and put in the SDFCP program. The additional terms required in the force and moment equations were added along with the appropriate input storage table requirements for the ejector force curve fit coefficients. Thus, the exact CTS simulation of ejector forces and moments is assured in the SDFCP also.

All of the aforementioned additions were required for SDFCP simulation of the CTS trajectories used in the validation effort. Additional features or modifications will be included in the SDFCP as required for future CTS trajectory simulation requirements.

5.0 CTS AND SDFCP TRAJECTORY COMPARISONS

Basically, three different types of CTS air-on trajectories were run during the store separation tests described in Section 3.0. All trajectories were flown at Mach No. 1.63 at a simulated altitude of nominally 40,000 ft. These trajectories differed primarily in the location of the launch position and were as follows:

1. Free stream (no parent aircraft, no interference),
2. Fuselage centerline pylon (symmetrical interference), and
3. Wing-mounted pylon (asymmetrical interference).

Representative CTS examples for each case and their SDFCP simulation are described and compared in Section 5.1.

Before each CTS test entry, it is a VKF standard procedure to run CTS trajectories in the tunnel before air flow is initiated, as a preliminary system checkout. SDFCP simulations are available and are used for comparison. The results of some of these comparisons are described in Section 5.2.

5.1 TUNNEL ACTIVE (AIR ON)

5.1.1 Free Stream

Data group 918 (AFFDL/Nielsen Test) and data group 481 (AEDC/DOT Test) were CTS free-stream trajectories which were run with the same initial conditions and store characteristics (Tables 6, 7, and 8). A transient ejector force (Fig. 14) and its associated pitching moment (via the moment arm X_1) provided the impulse necessary for angular oscillatory pitching motion. The orientation angle (ω_m) for the ejector force was zero. The angular and translational CTS motion and its corresponding SDFCP prediction are illustrated in Fig. 15. The moments of inertia were selected to yield two or three pitch oscillations with minimum influence from the yaw plane.

Data group 919 (AFFDL/Nielsen Test) and data group 480 (AEDC/DOT Test) were CTS free-stream trajectories with the ejector force angle (ω_m) equal to 90 deg. This provided an impulse in the yaw plane. The moments of inertia were selected to yield oscillations in the yaw plane with minimum influence from the pitch plane. Figure 16 illustrates the CTS and SDFCP results for these trajectories.

For all of these free-stream trajectories, the capability of deleting the translation of the CTS model in the tunnel was employed (see Section 2.3.1). The trajectory repeatability (as observed in Figs. 15 and 16) between these separate test entries is good.

The SDFCP simulations employed sets of interference-free aerodynamic grid data for the store model obtained during the tests. The translational motion predictions exhibit very good agreement. The angular oscillation frequency comparison is excellent. The yaw amplitude comparison for data group 919 is excellent also; however, there is a slight discrepancy in maximum pitch amplitude for data groups 918 and 481 (Fig. 15a). Even so, the overall agreement is considered good.

5.1.2 Centerline Pylon Launch Point

During the initial store separation tests (AFFDL/Nielsen), CTS trajectories were run where the store was launched from a pylon mounted beneath the parent fuselage as illustrated schematically in Figure 4. The pylon was located in the X-Z plane of symmetry of the parent model (see Fig. 9). Consequently, the initial store motion is

influenced by flow-field interference which is symmetric with respect to the X-Z plane of the parent aircraft.

CTS/SDFCP motion comparisons for two centerline launch trajectories (data groups 649 and 651) are contained in Figs. 17 and 18. Tables 6, 7, and 8 list the full-scale store characteristics and initial conditions for these trajectories. Both trajectories were restricted to zero roll ($\dot{p} = p = \phi = 0$). Their primary difference was the magnitude of the ejector force moment arm ($X_1 = 0$ for trajectory 649 and $X_1 = +0.2$ ft for trajectory 651).

The basic input to the SDFCP was a set of grid data (from the AFFDL/ Nielsen Test) for the store in the fuselage centerline flow field. Three coefficients (C_{A_t}, C_N, and C_m) were employed with X, Z, and a_s as the position variables. Thus, the SDFCP trajectories were essentially restricted to motion in the X-Z plane (3 DOF). However, this was sufficient to yield a very good corroboration of the CTS store trajectories.

5.1.3 Wing-Mounted Pylon Launch Point

Data groups 743 and 912 (AFFDL/Nielsen Test) are representative of several CTS trajectories where the launch point was from a pylon or launch rack located underneath the wing of a parent vehicle. This location was 1/3 of the wing semispan measured from the fuselage centerline (see Fig. 9). Tables 6, 7, and 8 list the initial conditions and full-scale store characteristics which were employed for these particular trajectories. Note that trajectories 743 and 912 differed primarily in the magnitude of the ejector force moment arm (X_1 and the orientation of the ejector force (ω_m). ω_m was 0 for trajectory 743 (no yaw component) and was 20 deg for trajectory 912 (both pitch and yaw components). The CTS and SDFCP trajectories were restricted to zero roll ($\dot{p} = p = \phi = 0$).

The basic input to the SDFCP for simulation of these trajectories was a rather extensive table of experimental static aerodynamic coefficient data taken for the CTS store model at specified systematic locations in proximity to the store model launch point (near the pylon under the parent-model wing). This data was acquired via the CTS grid mode during the AFFDL/Nielsen Test.

Figures 19 and 20 illustrate the CTS/SDFCP results for the position variables of trajectories 743 and 912, respectively. In general, the CTS and SDFCP results compare favorably, both in trend and magnitude, particularly for X, Y, and Z locations. For trajectory 743, the pitch angle (θ) agrees rather well except at large amplitudes where there is a small discrepancy. The yaw angle comparison for trajectory 743 is very good.

For trajectory 912, the pitch angle comparison is very favorable, considering the final amplitudes reached. However, there are differences in the yaw angle for trajectory 912 which amount to approximately 0.50 deg near maximum amplitudes of -2.0 deg.

Some of the discrepancies between the CTS and SDFCP angular motions may be caused by one or both of the following reasons. Grid data employed in the SDFCP had pitch and yaw limits of ±2.0 deg and 0 to -15.0 deg, respectively. When the SDFCP trajectory exceeded these limts, the data extrapolation option was necessary and may have been erroneous if the variations in these areas are not linear. The other reason may be the magnitude of the CTS drive accuracies when the store model is positioned in a high-gradient flow field. This problem was evident when the aerodynamic forces and moments measured by the balance were different (outside the balance repeatability) each time the store was placed at the launch point.

5.2 TUNNEL PASSIVE (AIR OFF)

Four different air-off CTS/SDFCP comparison trajectories have been run. The CTS was mounted in VKF Tunnel A and the mechanism then positioned the store model under the influence of constant simulated aerodynamic forces and moments. These were input to the CTS via a constant aerodynamic coefficient input option. This option supplements the CTS air-on trajectory simulation capability and has proved very valuable for air-off checking purposes as well.

5.2.1 Asymmetric Configuration

Figure 21 illustrates CTS/SDFCP air-off results for a store configuration with nonzero products of inertia (data group 277). Table 9 lists the pertinent initial conditions and the store full-scale characteristics. This trajectory has full 6-DOF motion. The aerodynamic rolling-moment coefficient was zero, but roll occurred because of inertial coupling. The CTS/SDFCP comparison is essentially a one-to-one identity. Similar agreement was exhibited by the other three air-off examples. Consequently it is concluded that the present version of the CTS trajectory program is correct.

6.0 SUMMARY OF RESULTS

6.1 BASIC CONCLUSIONS

A CTS is now fully operational in the VKF Continuous Tunnels (A, B, and C). The availability of this electromechanical system and its associated software greatly enhances AEDC CTS testing capability by extending it into the high supersonic and hypersonic

regimes. The overall good agreement of the CTS trajectories and the independent AFFDL SDFCP predicted trajectories corroborates and validates VKF CTS test results.

The VKF CTS is both verbally and pictorially described herein and its capabilities and limitations explicitly delineated. Information and guidelines specifically for potential CTS users are included. This includes an explicit tabulation of the information required from the user in order to run a CTS trajectory test.

The VKF CTS trajectory simulation with the independent AFFDL SDFCP has provided considerable insight into CTS testing techniques for both the trajectory and grid modes. The SDFCP simulations have corroborated VKF CTS trajectories to such a remarkable degree that considerable credence is established for future test results.

REFERENCES

1. Bamber, M. J. "Two Methods of Obtaining Aircraft Store Trajectories from Wind Tunnel Investigations." Aero Report 970 (AD233198), David Taylor Model Basin, Washington, D.C., January 1960.

2. Christopher, J. P. and Carleton, W. E. "Captive Trajectory Store Separation System of the AEDC-PWT 4-Foot Transonic Tunnel." AEDC-TR-68-200 (AD83974B), September 1968.

3. Test Facilities Handbook (Tenth Edition). "Von Kármán Gas Dynamics Facility, Vol. 3." Arnold Engineering Development Center, May 1974.

4. Goodwin, F. K., Nielsen, J. N., and Dillenius, M. F. E. "A Method for Predicting Three-Degree-of-Freedom Store Separation Trajectories at Speeds Up to the Critical Speed." AFFDL-TR-71-81, November 1974.

5. Thomson, W. T. Introduction to Space Dynamics. John Wiley and Sons, New York, 1961.

6. Brown, R. C., Brulle, R. B., Combs, A. E., and Griffin, G. D. "Six-Degree-of-Freedom Flight Path Study Generalized Computer Program." Part I, Problem Formulation, FDL-TDR-64-1 Part I, Volume 1, October 1961.

7. Young, Fay O. "Six-Degree-of-Freedom Flight Path Study Generalized Computer Program (SDFCP)." Users Manual, AFFDL TR-75-1, July 1975.

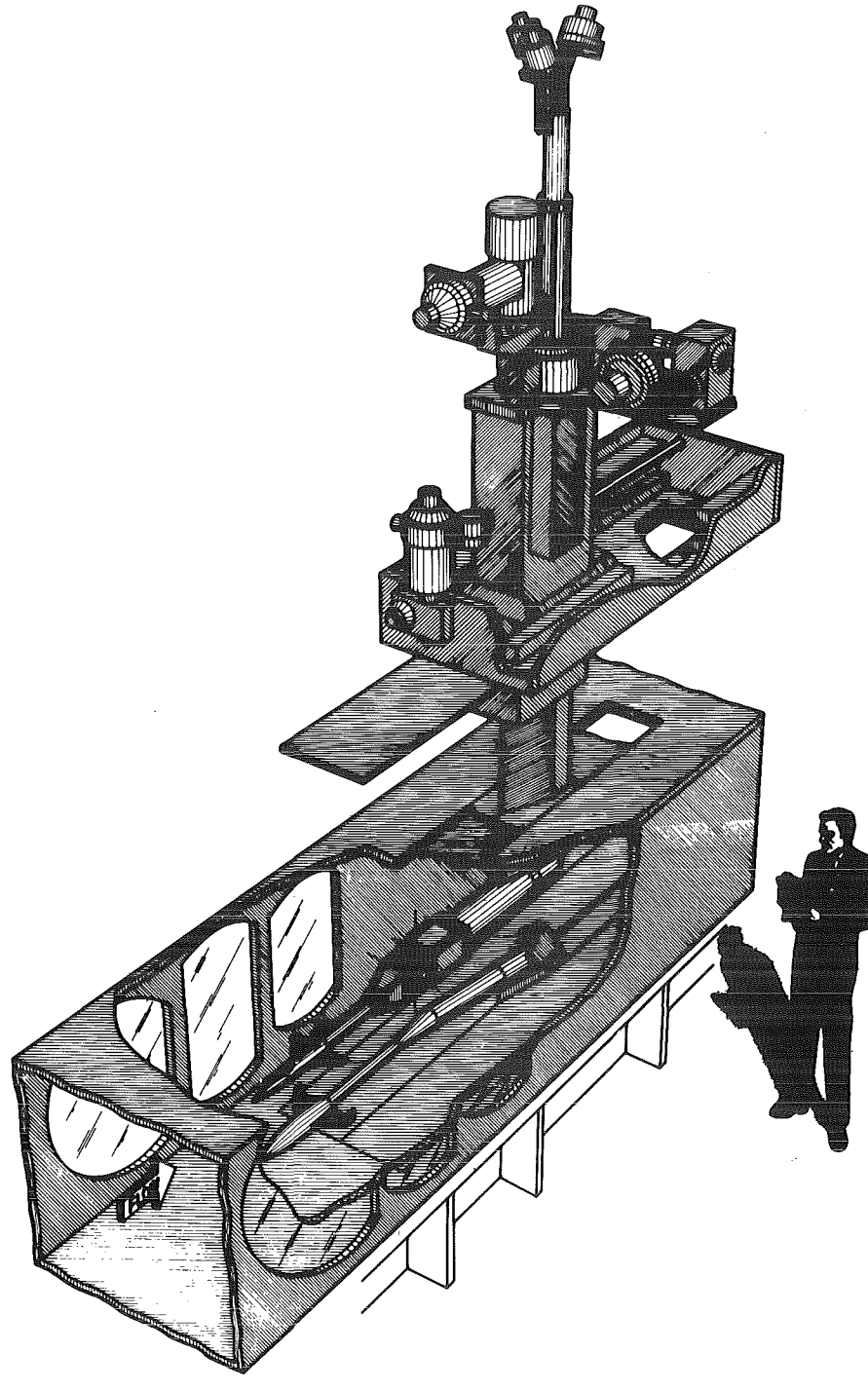

a. Installed in Tunnel A

Figure 1. VKF captive trajectory system.

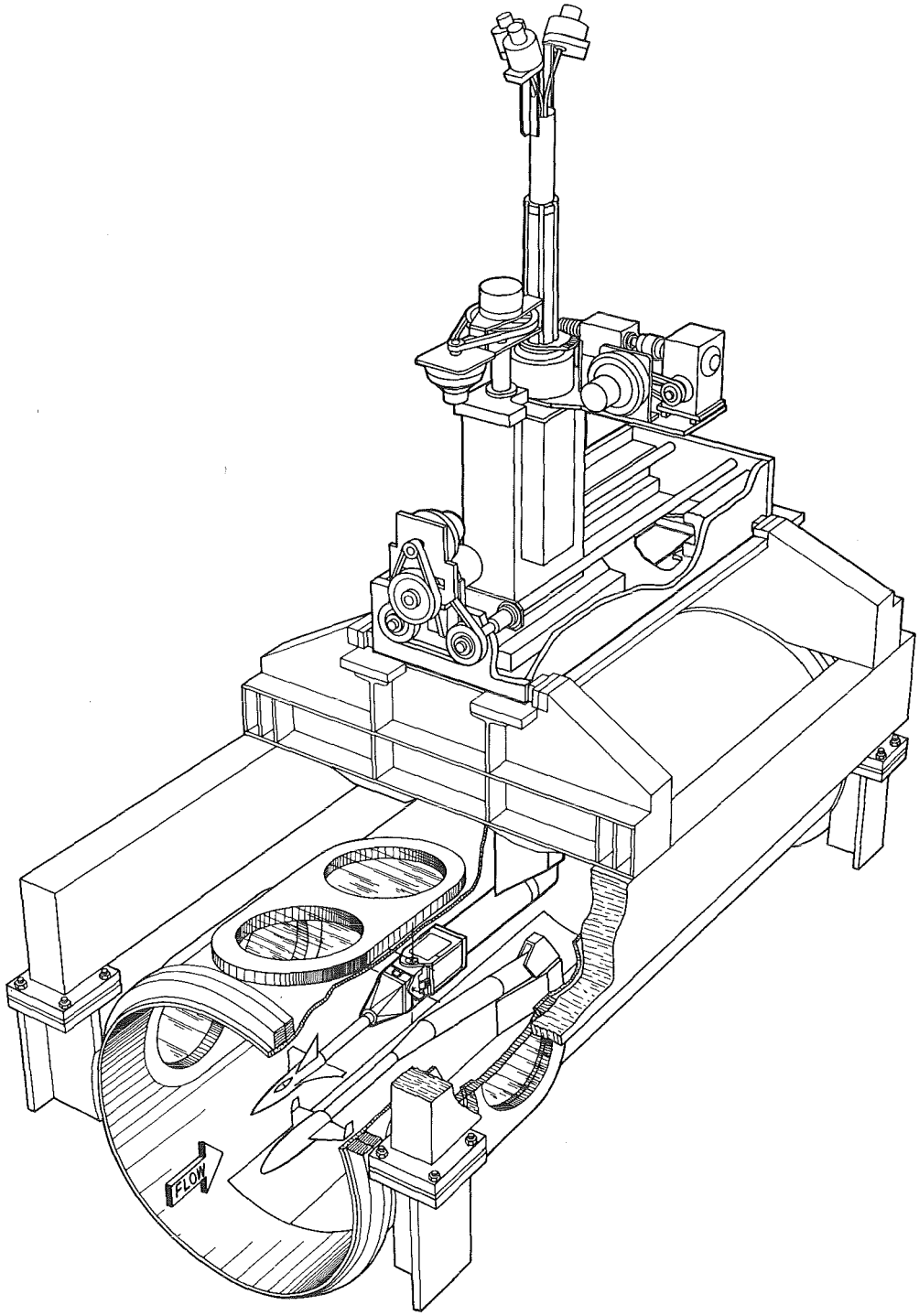

b. Installed in Tunnels B and C
Figure 1. Concluded.

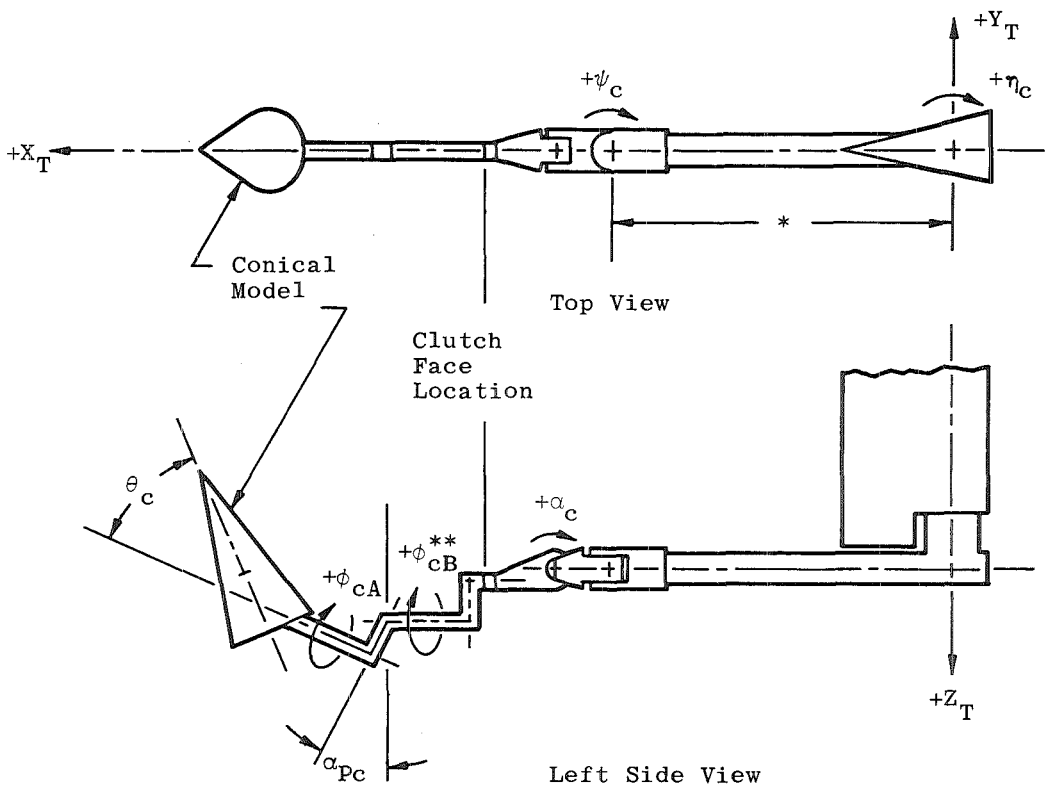

*This arm is interchangeable. Depending upon the test requirements, the 36.007-in. or 21.9995-in. length can be used.

**The roll, ϕ_{cB}, is limited to an offset from the pitch center of 2.0 in. with the present system.

Figure 2. VKF CTS sting mechanism.

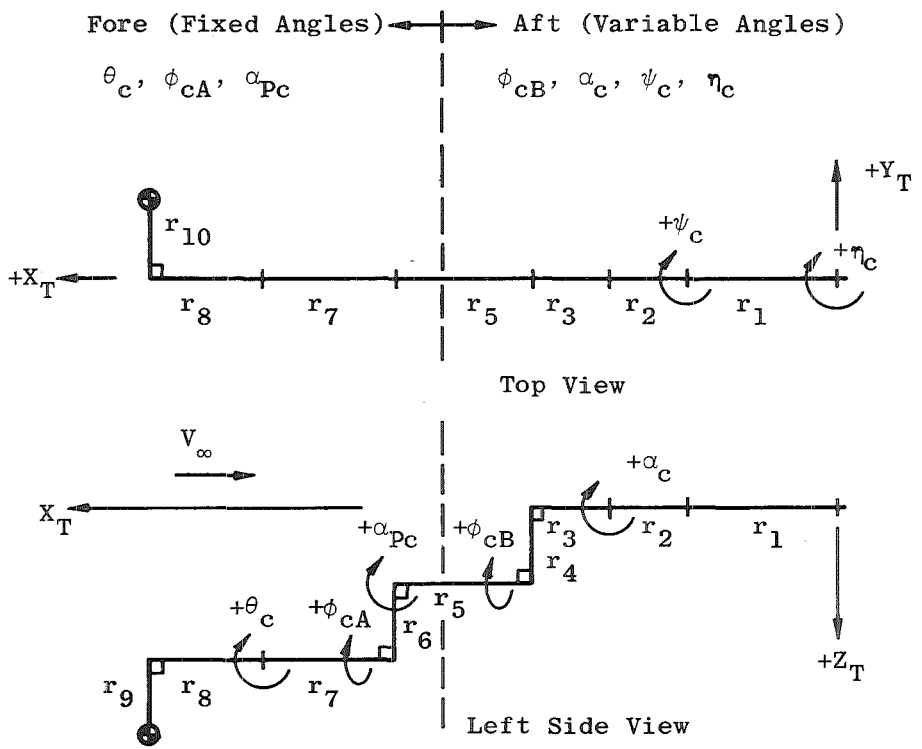

Notes:

1. If cg of Model Is on Balance Axis; $r_9 = r_{10} = 0$
2. If $\theta_c = 0$; $r_8 = 0$, $r_7 = r_7 + r_8$
3. If $\alpha_{Pc} = 0$; $r_6 = 0$, $r_5 = r_5 + r_7$
4. If $\theta_c = \alpha_{Pc} = 0$; $r_6 = 0$, $r_5 = r_5 + r_7 + r_8$

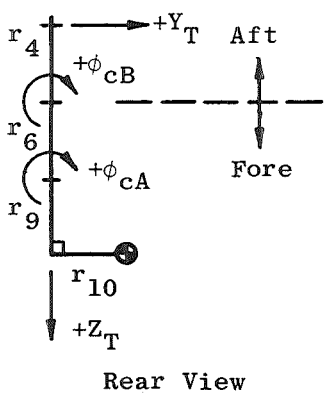

Figure 3. VKF CTS sting angles and rotation arms.

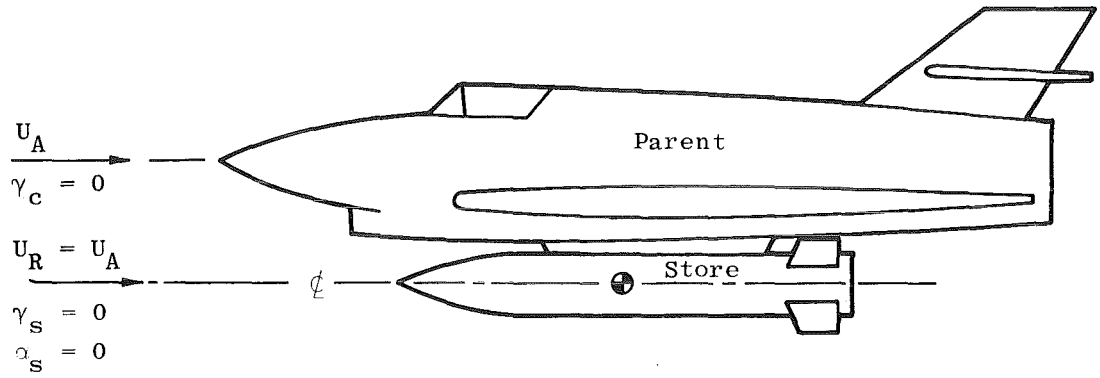

a. Initial position, t = 0

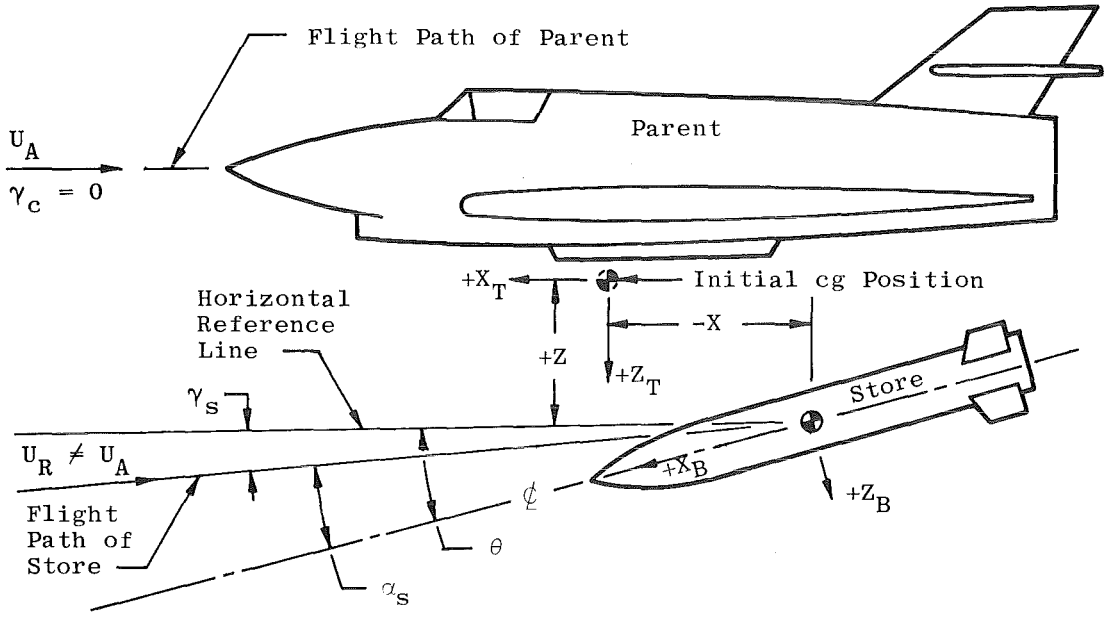

b. Position at t ≠ 0

Figure 4. Store-parent schematic, fuselage centerline launch point.

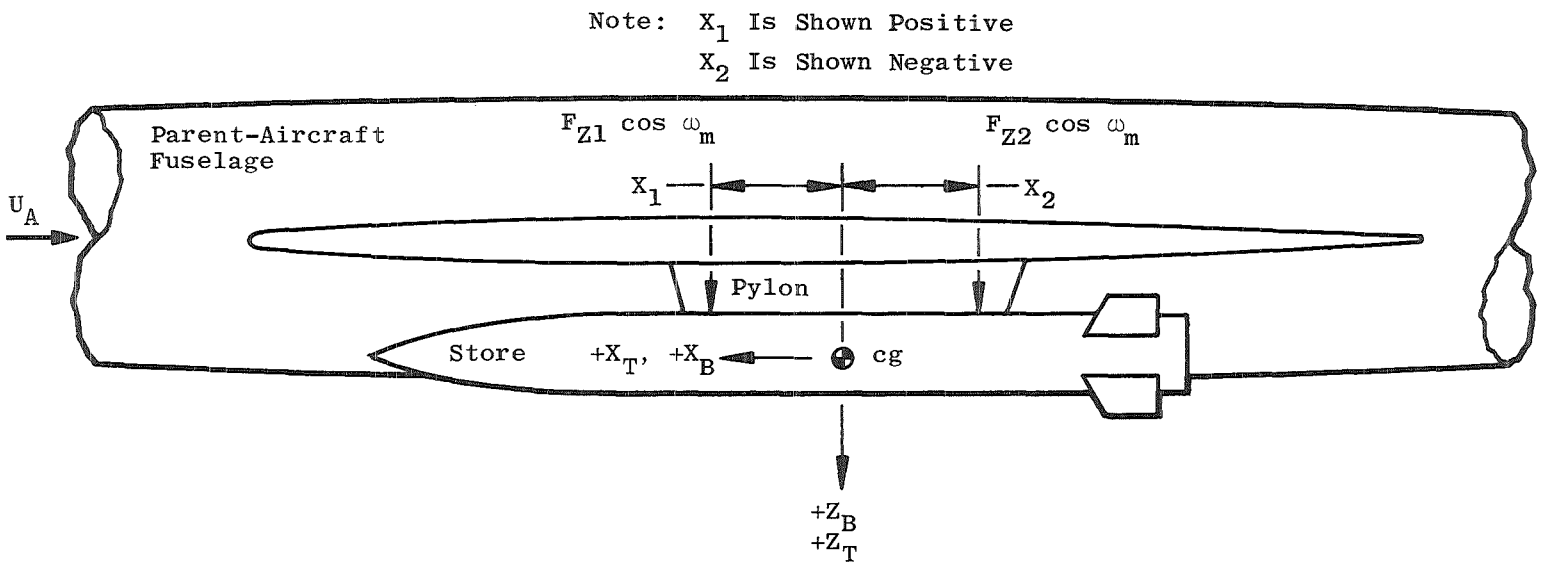

a. Side view (along +Y, initial position, t = 0)

Figure 5. Store-parent schematic, wing-mounted pylon launch point.

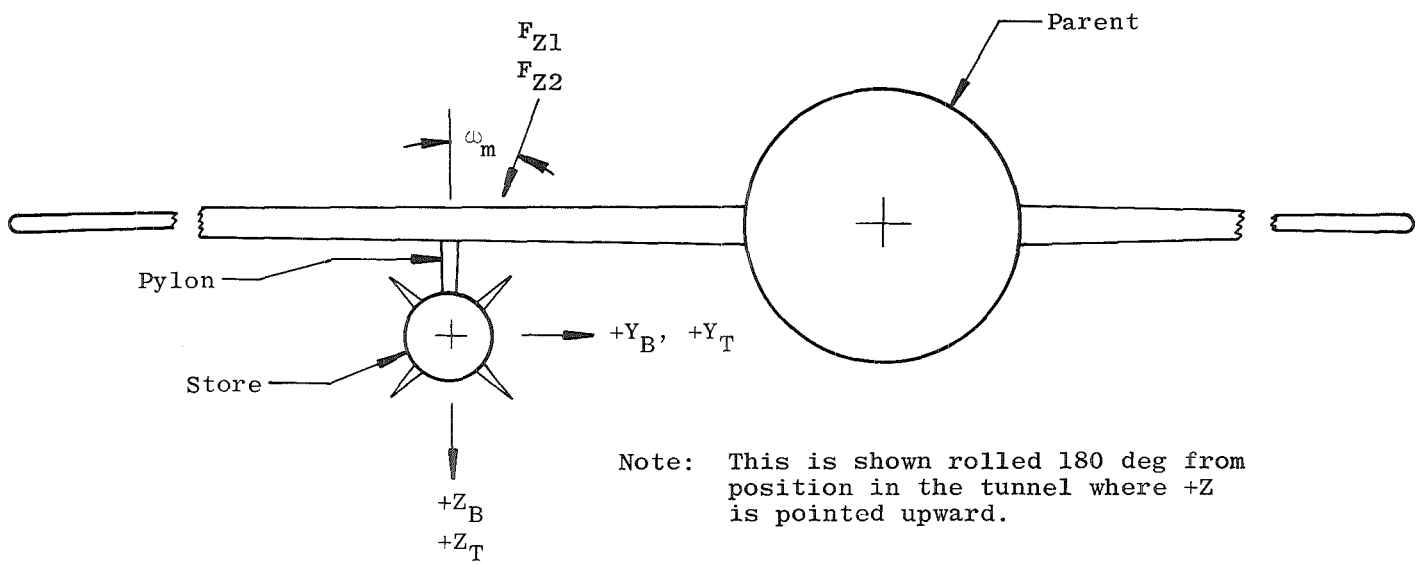

b. Rear view (along +X, initial position, t = 0)
Figure 5. Continued.

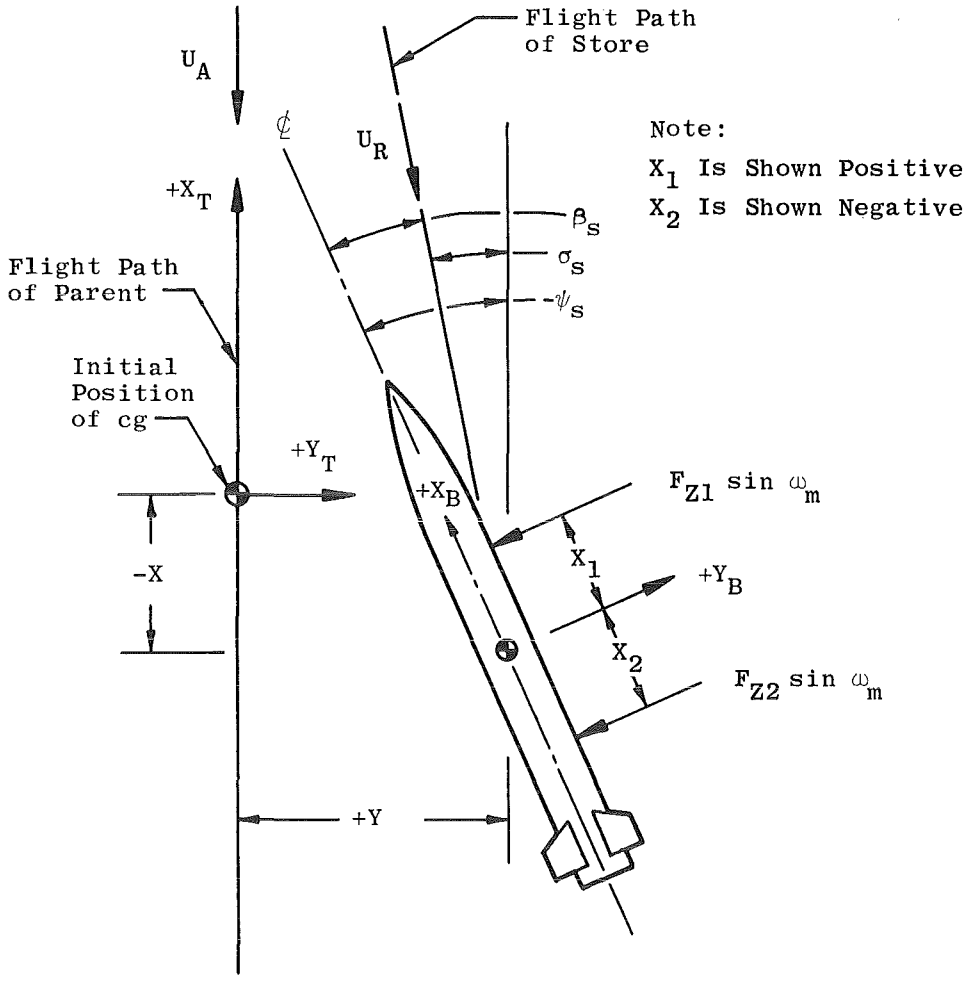

c. Top view (along +Z, position of store at $t \neq 0$)

Figure 5. Concluded.

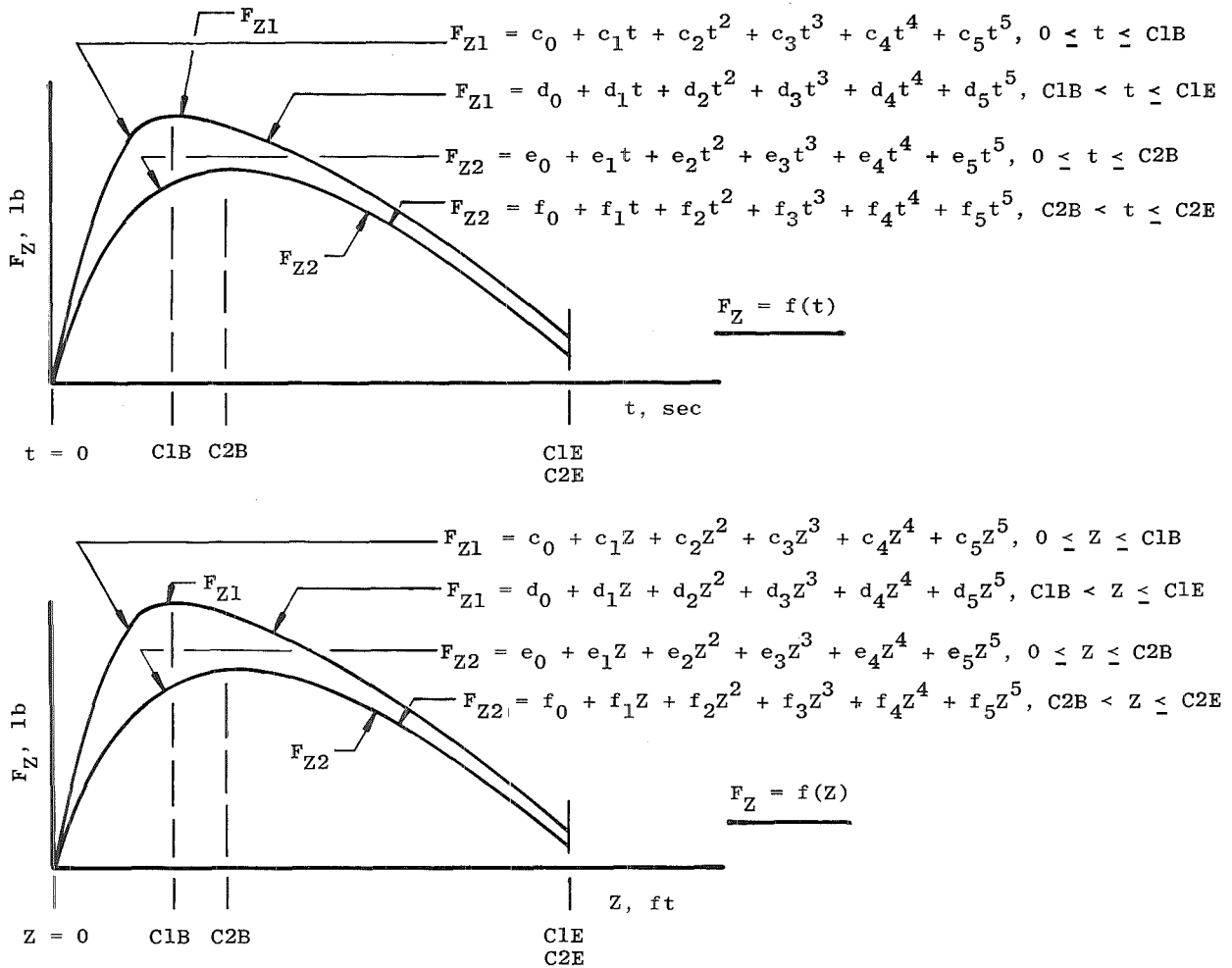

a. Ejector force

Figure 6. Ejector force and thrust simulation constant definitions.

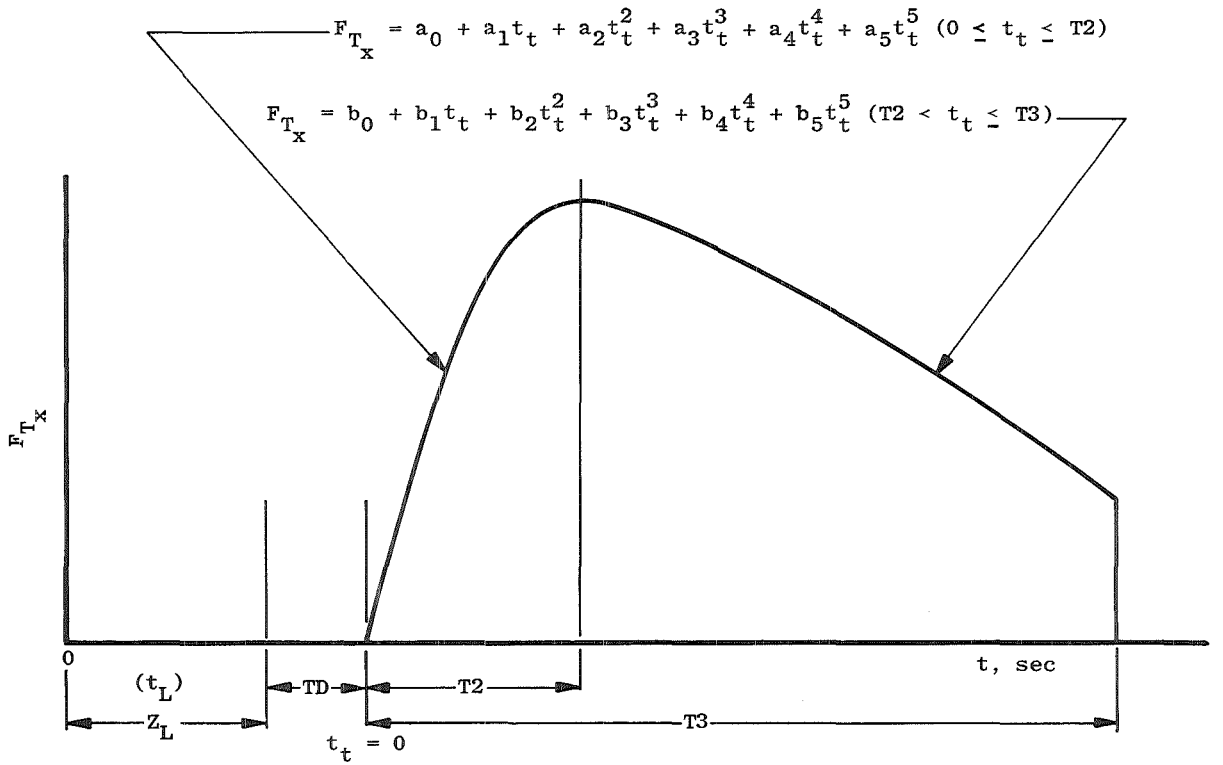

b. Thrust

Figure 6. Concluded.

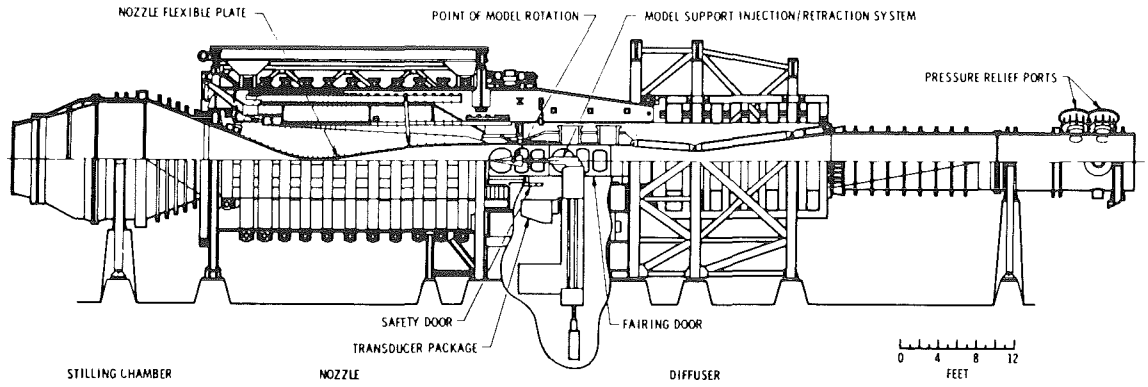

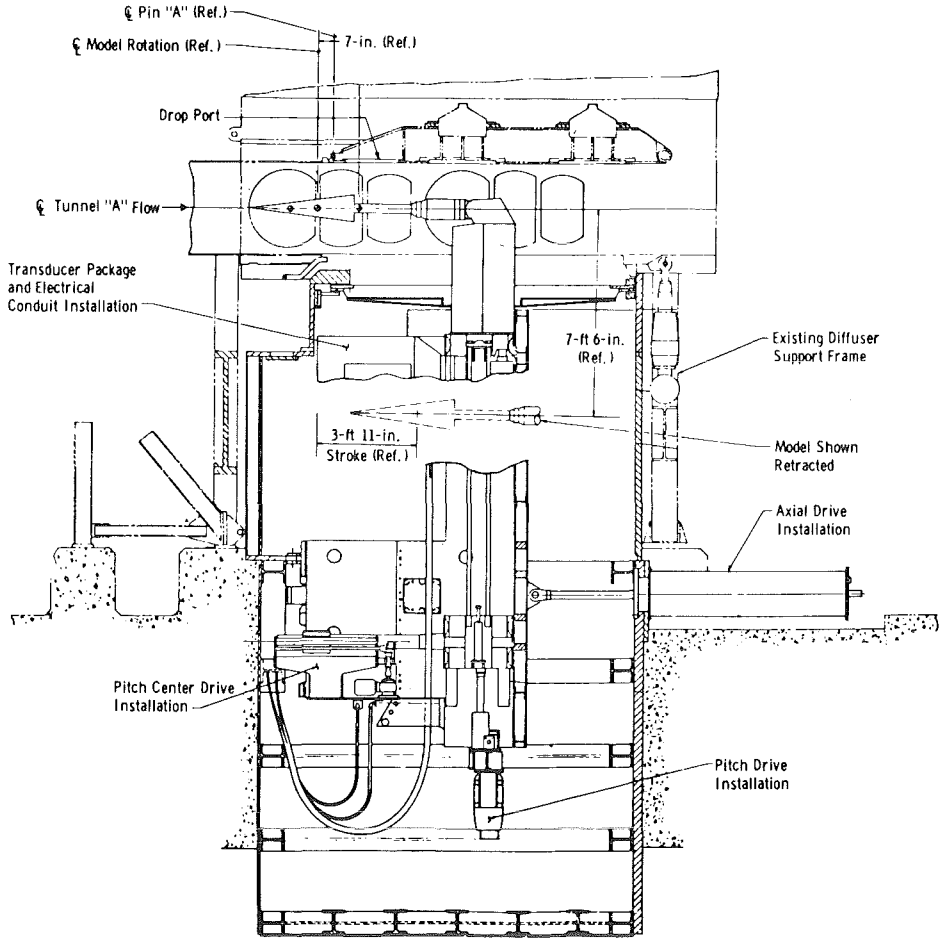

Figure 7. Tunnel A.

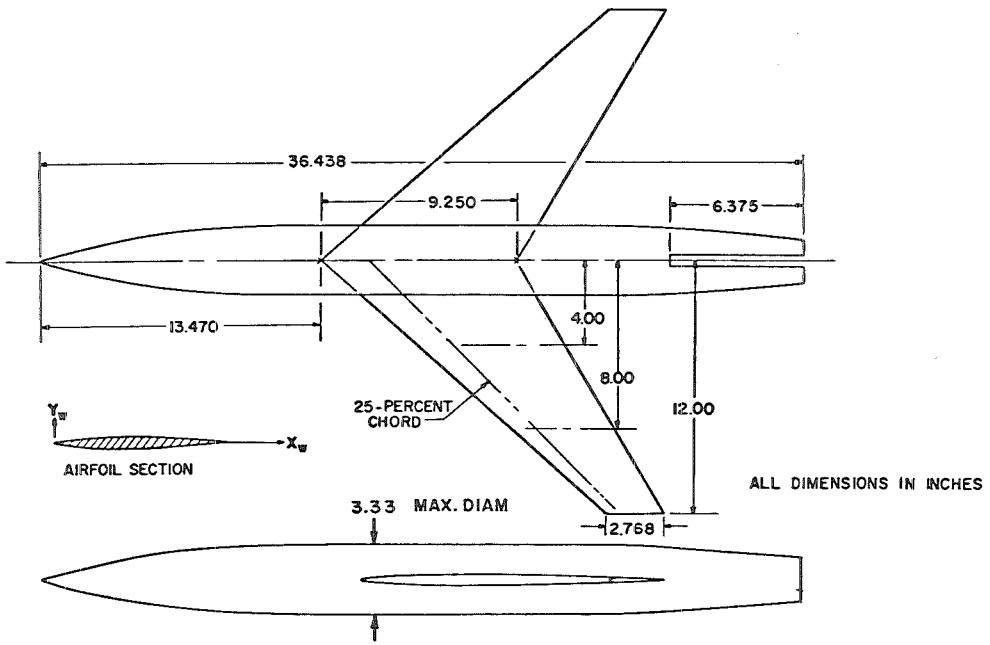

BODY COORDINATES

STATION PERCENT LENGTH	RADIUS PERCENT LENGTH
0.00	0.00
3.28	0.91
6.57	1.71
9.86	2.41
13.15	3.00
16.43	3.50
19.72	3.90
23.01	4.21
26.29	4.43
29.58	4.53
32.00	4.57
75.34	4.57
76.69	4.54
79.98	4.38
83.26	4.18
86.55	3.95
89.84	3.72
93.13	3.49
96.41	3.26
100.00	3.02

AIRFOIL COORDINATES

X_w,% CHORD SEE SEC.	Y_w% CHORD SEE SEC.
0.00	0.000
0.50	0.464
0.75	0.563
1.25	0.718
2.50	0.981
5.00	1.313
7.50	1.591
10.00	1.824
15.00	2.194
20.00	2.474
25.00	2.687
30.00	2.842
35.00	2.945
40.00	2.996
45.00	2.992
50.00	2.925
55.00	2.793
60.00	2.602
65.00	2.364
70.00	2.087
75.00	1.775
80.00	1.437
85.00	1.083
90.00	0.727
95.00	0.370
100.00	0.013
L.E. RADIUS 0.229% CHD.	
T.E. RADIUS 0.014% CHD.	

Figure 8. N1-B2-W details and dimensions.

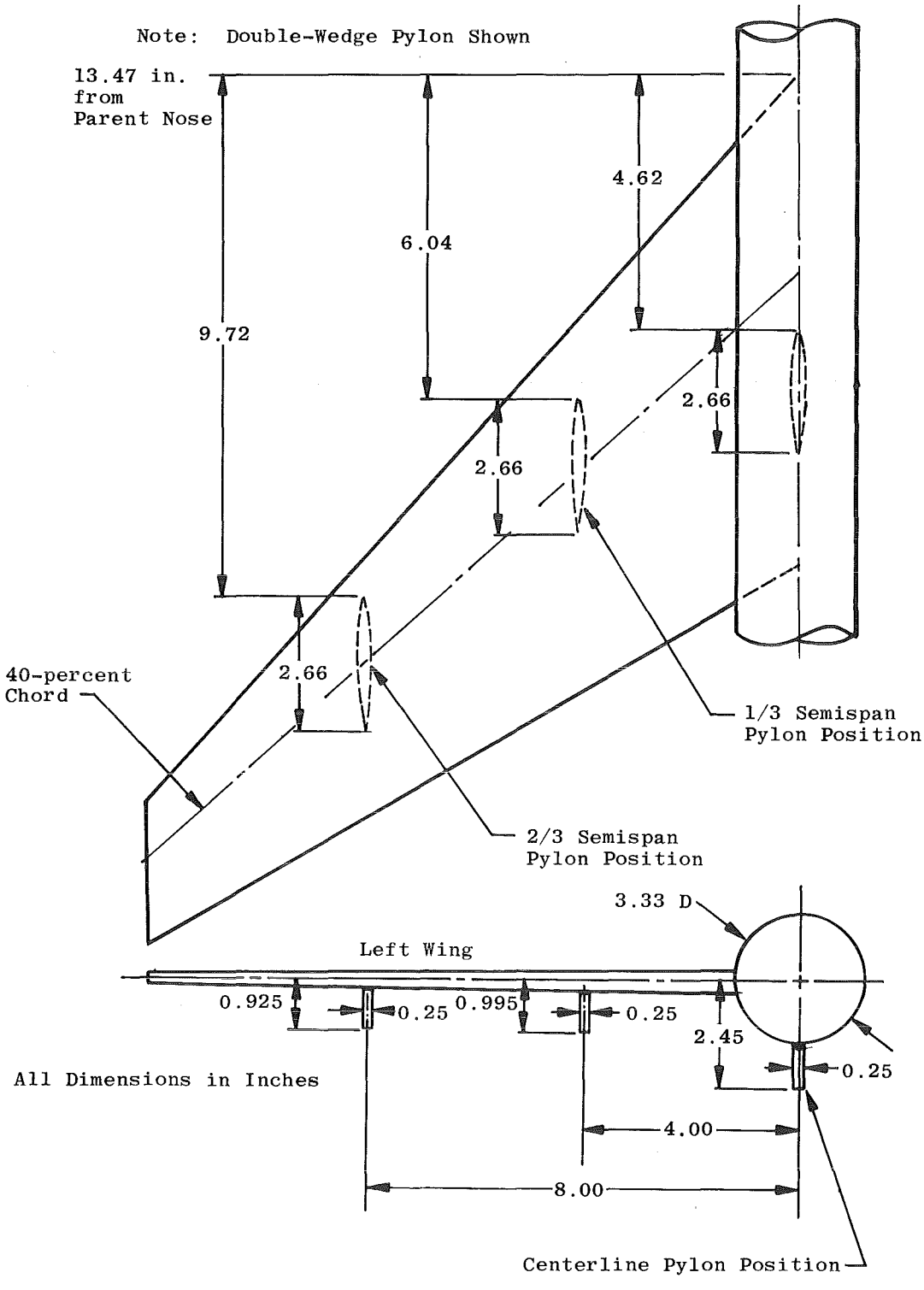

Figure 9. Pylon locations on parent aircraft.

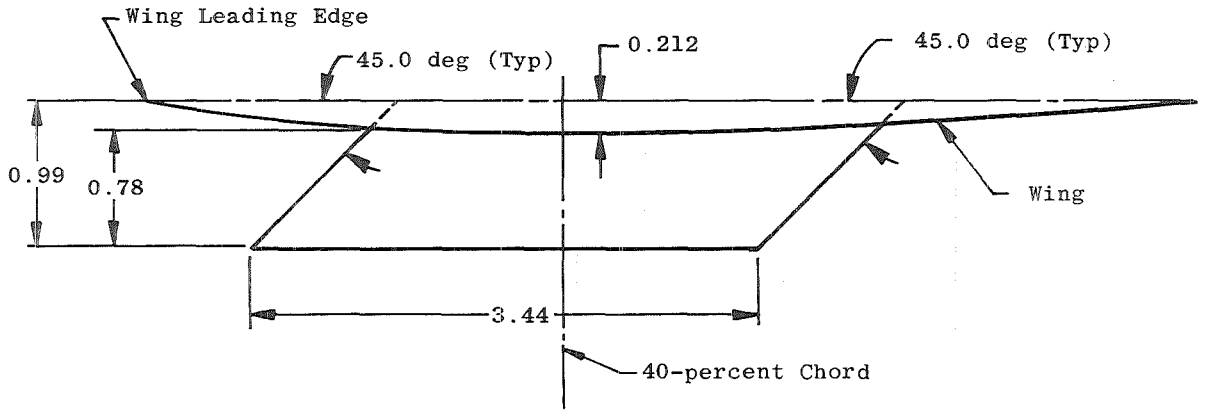

1/3 Semispan Pylon

All Dimensions in Inches

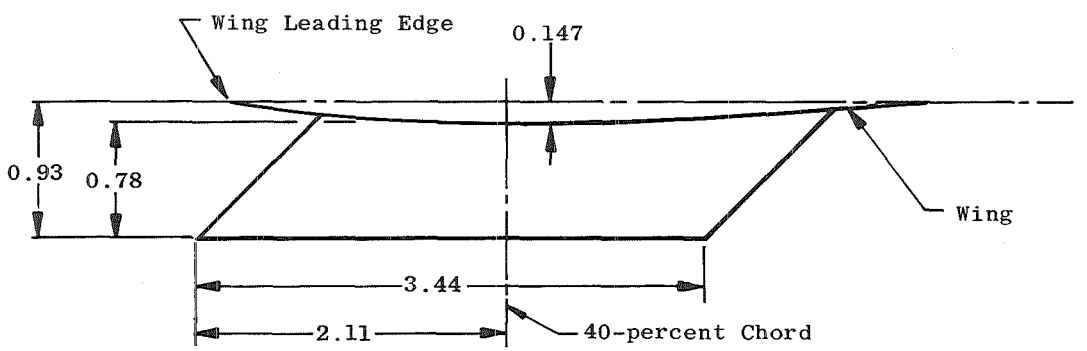

2/3 Semispan Pylon

a. Swept pylon (P3)

Figure 10. Details and dimensions of the swept pylon (P3) and double-wedge pylon (P2).

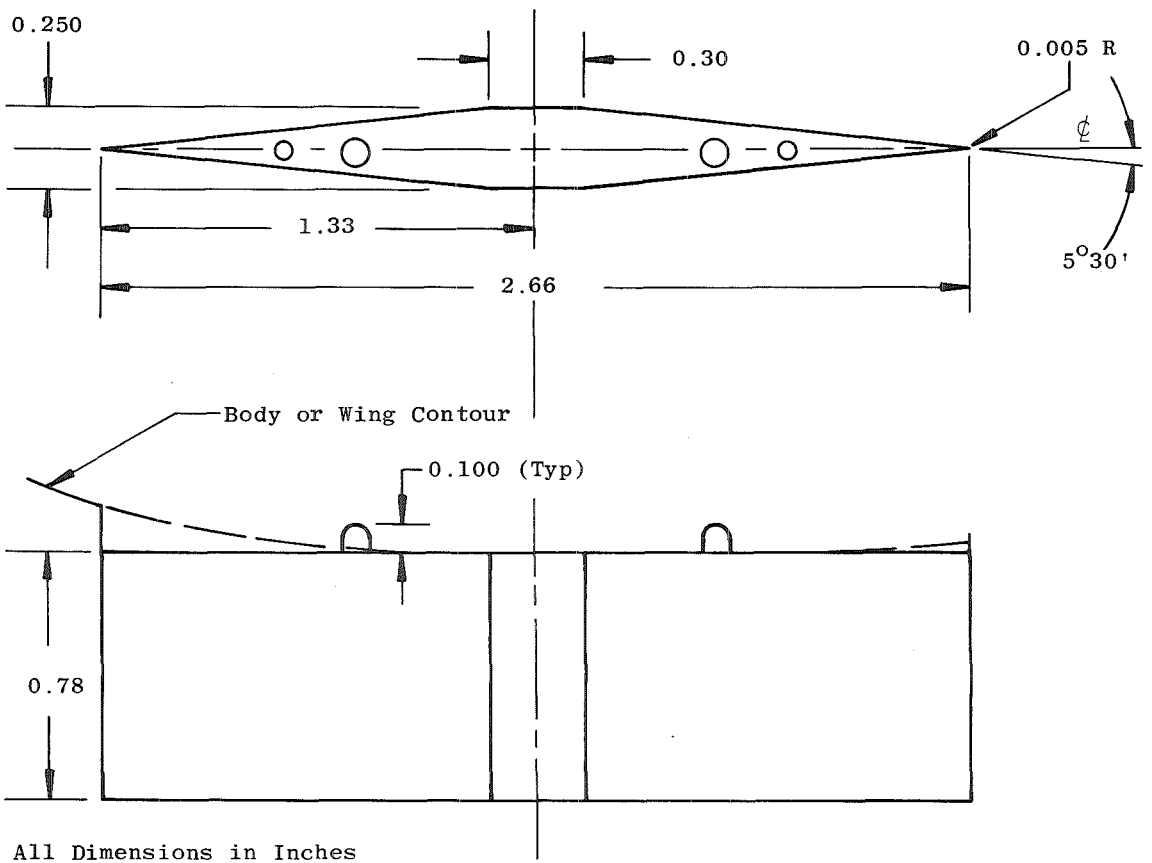

b. Double-wedge pylon (P2)
Figure 10. Concluded.

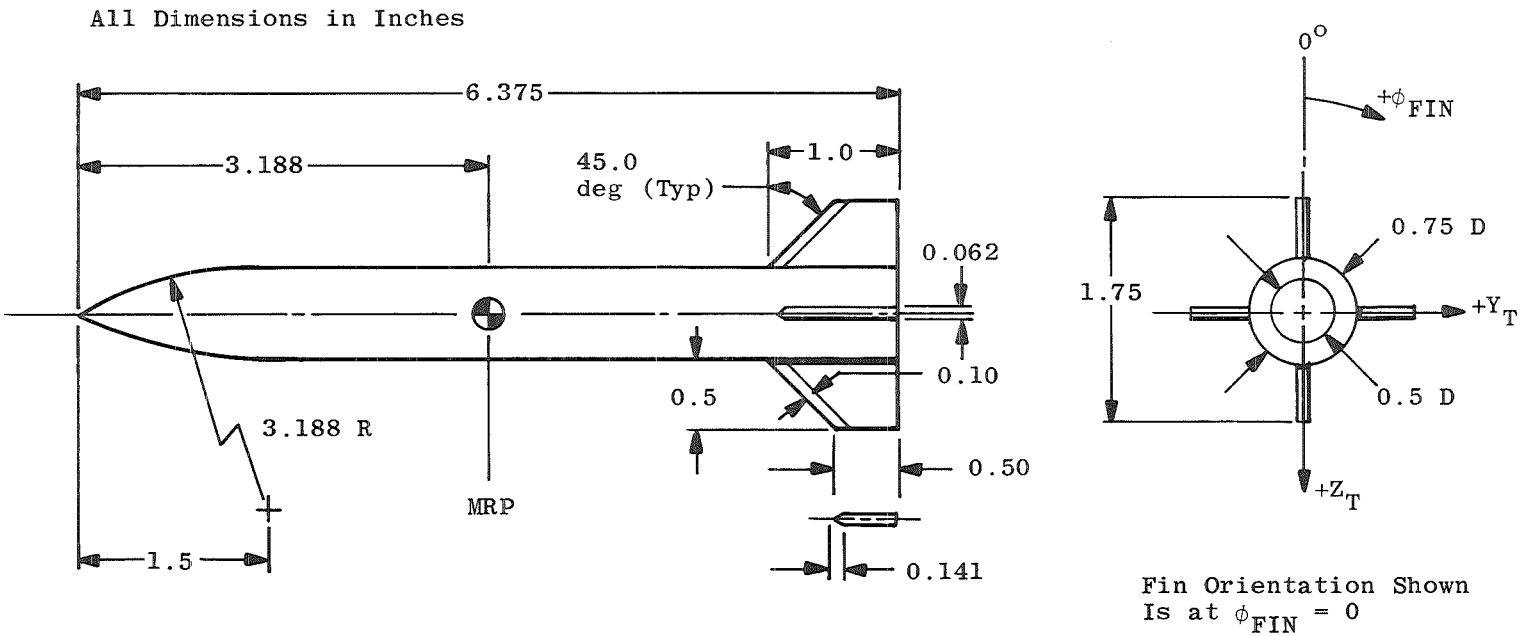

Figure 11. Store model.

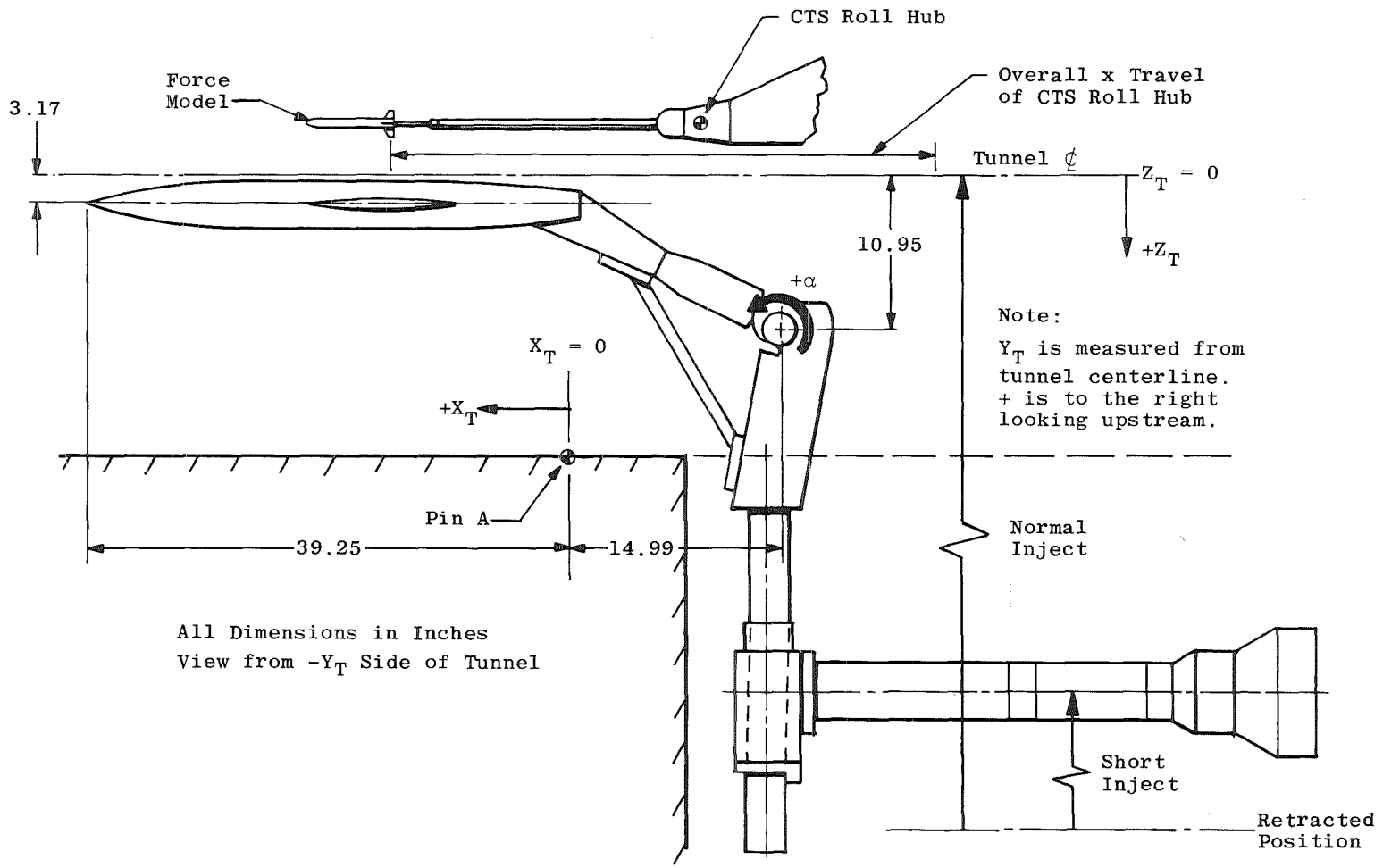

a. Sketch

Figure 12. Tunnel installation.

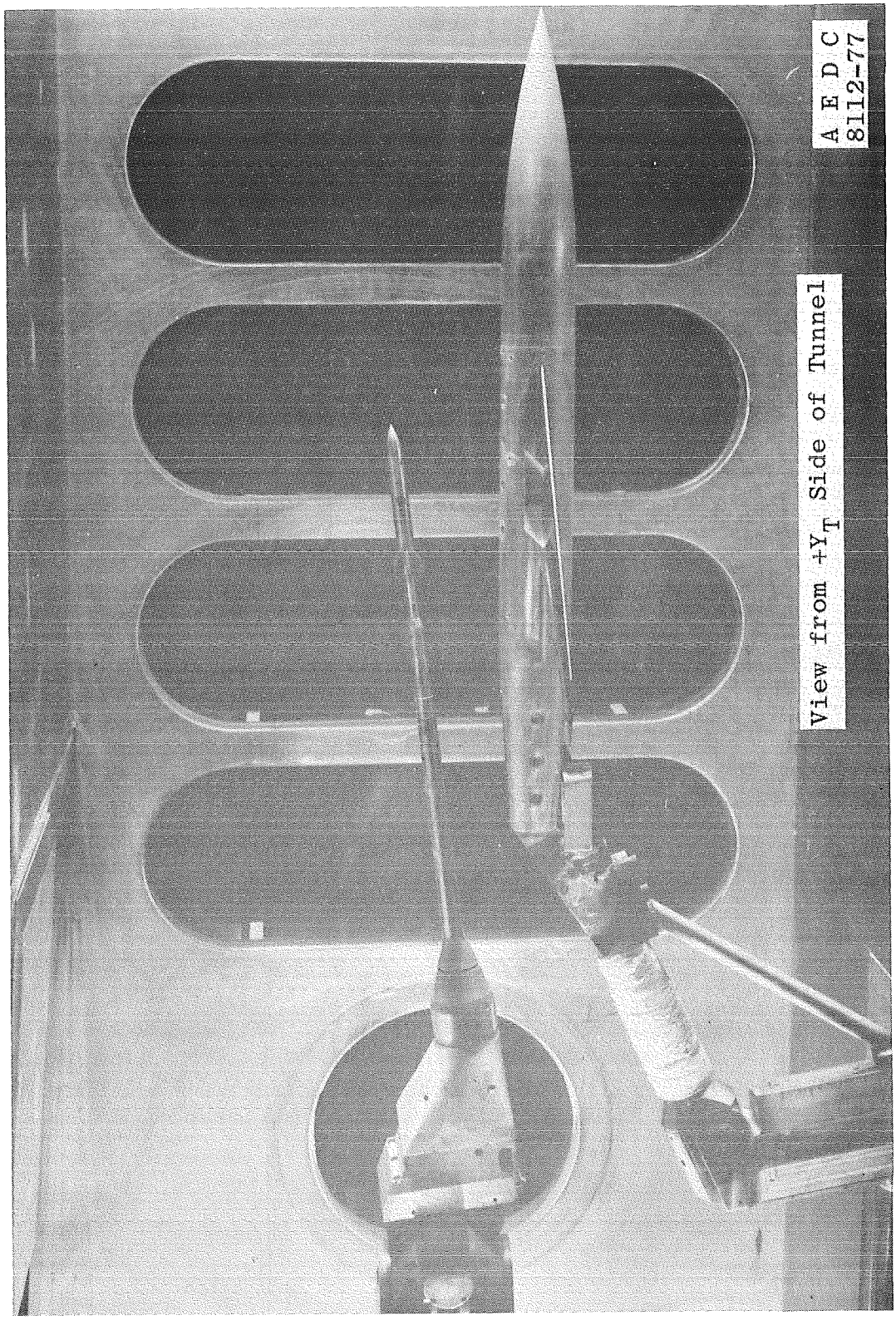

b. Photograph
Figure 12. Concluded.

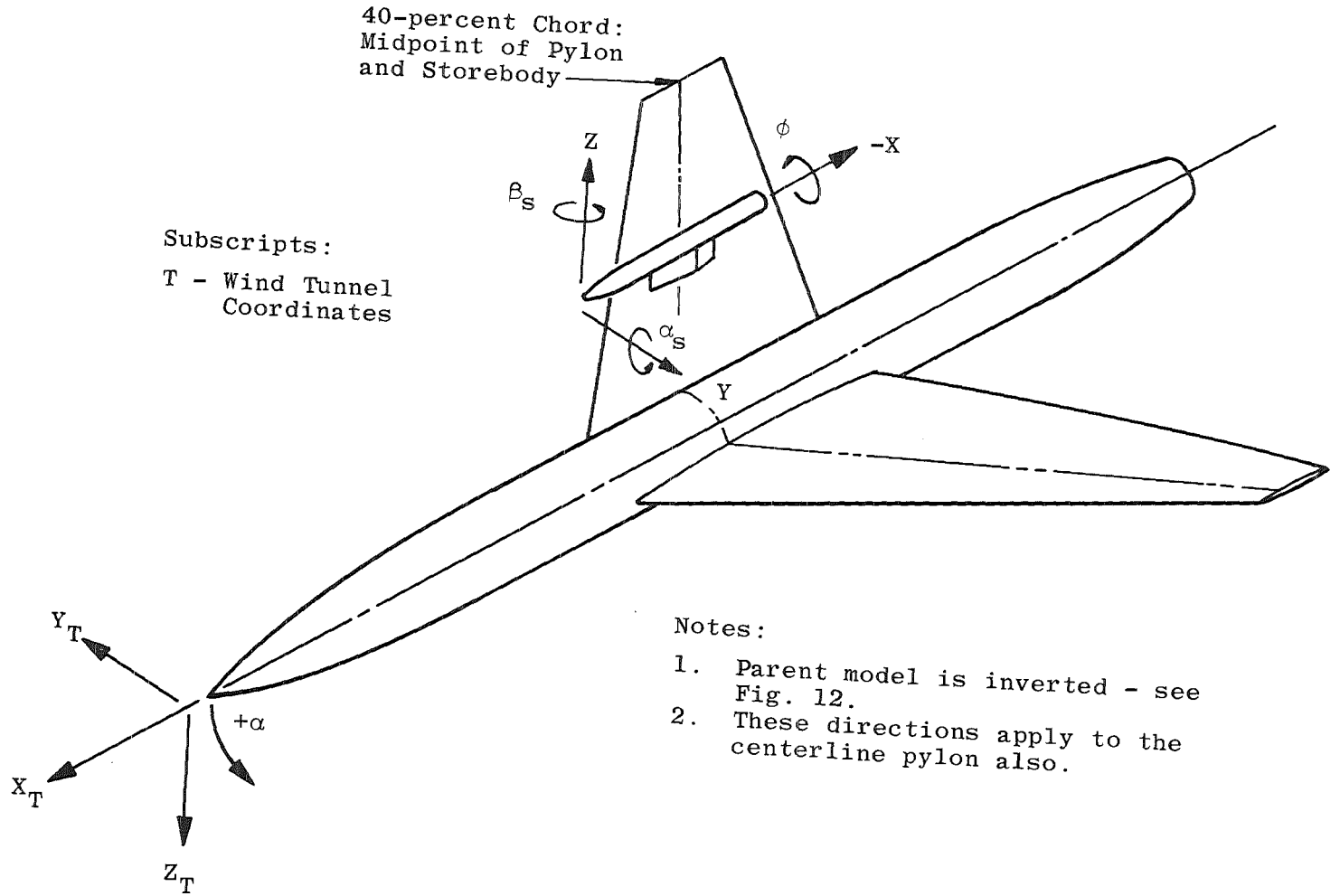

Figure 13. Coordinate systems showing positive vector directions for wind tunnel test data.

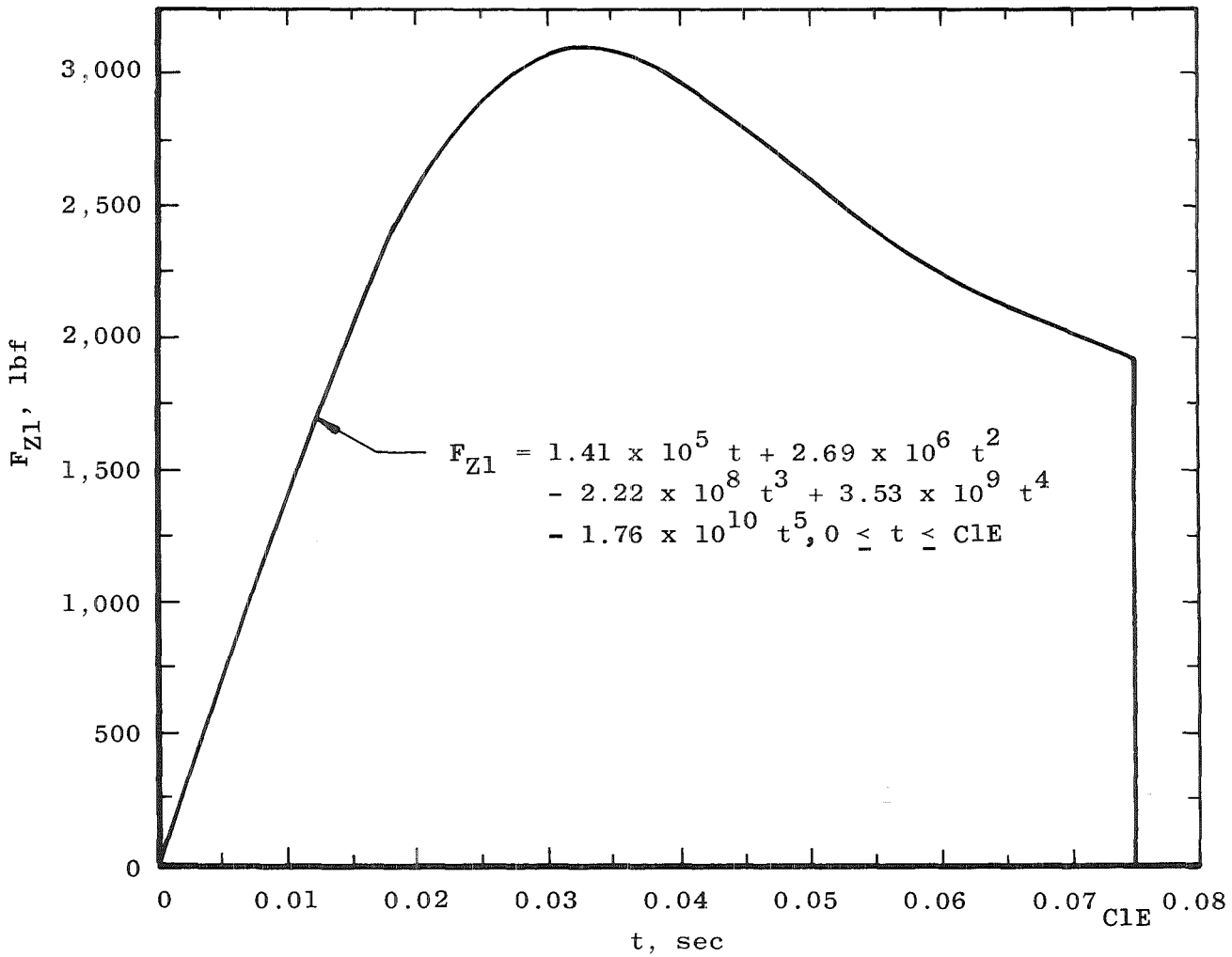

Figure 14. Simulated ejector force curve.

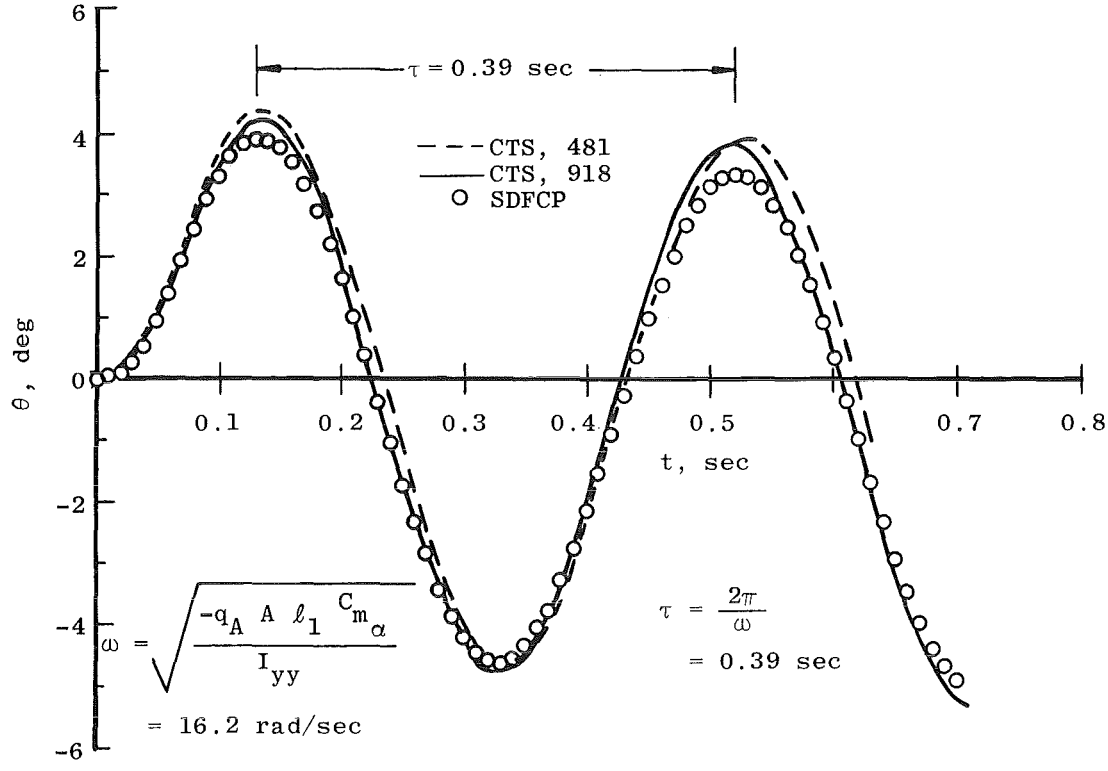

a. θ versus t

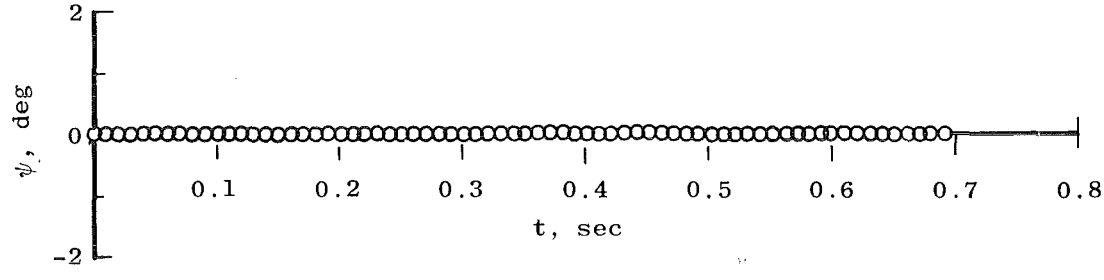

b. ψ versus t

Figure 15. Free-stream trajectory motion comparison, pitch oscillation, Data Groups No. 918 and 481.

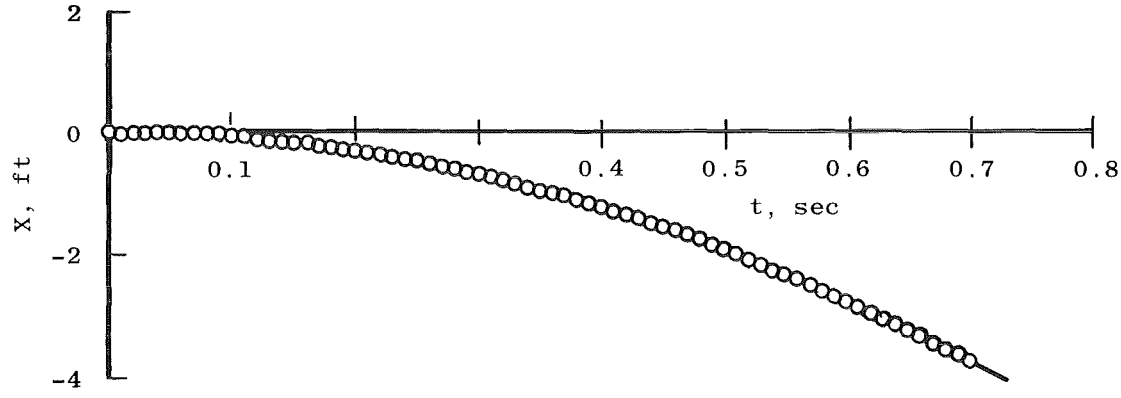

c. X versus t

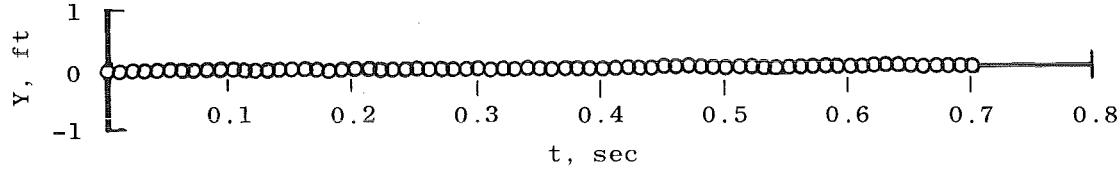

d. Y versus t

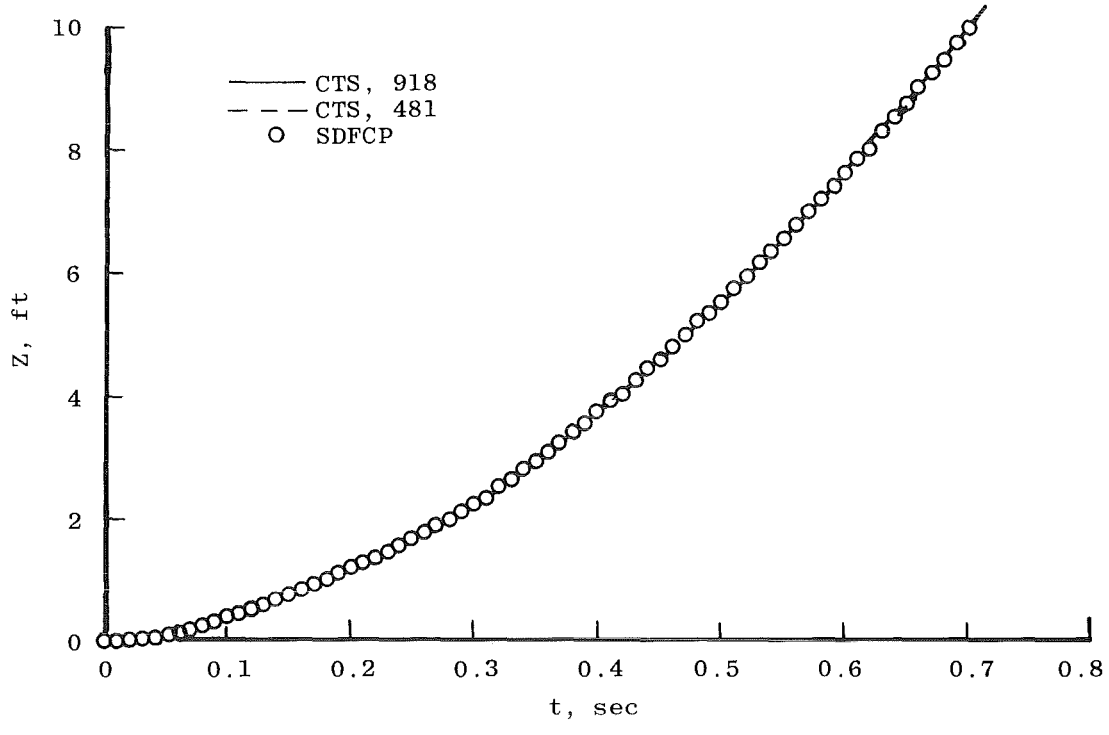

e. Z versus t

Figure 15. Concluded.

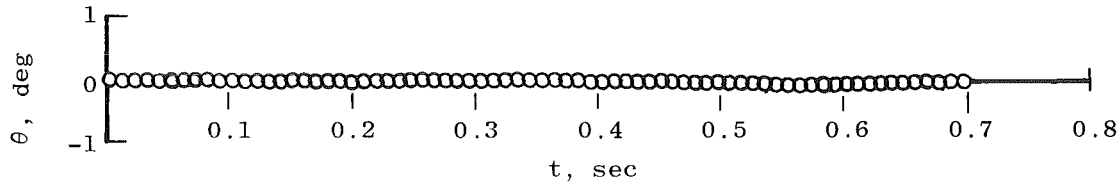

a. θ versus t

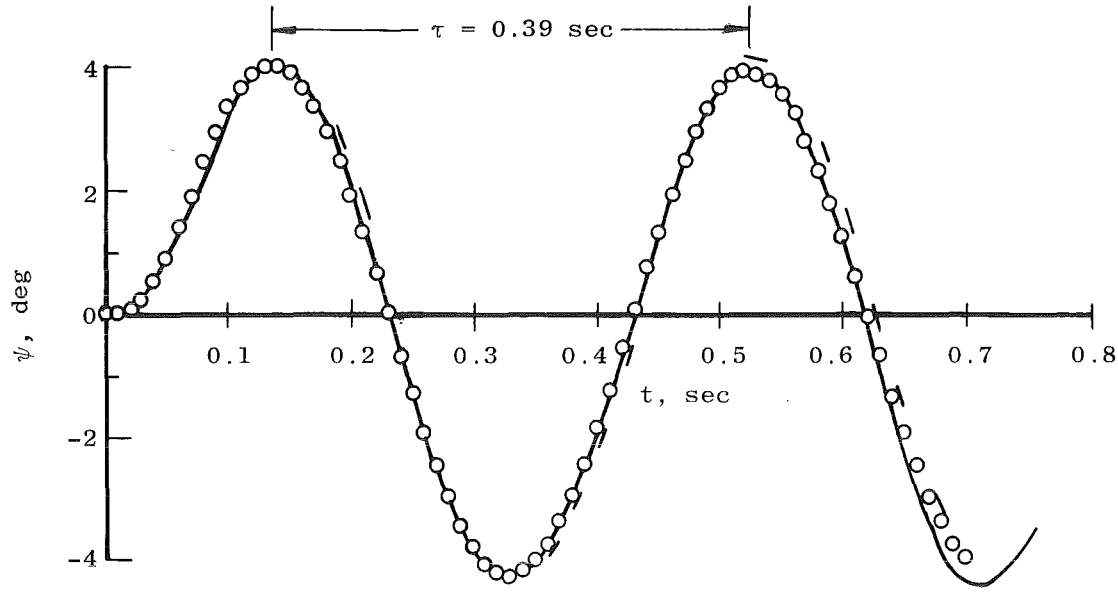

b. ψ versus t

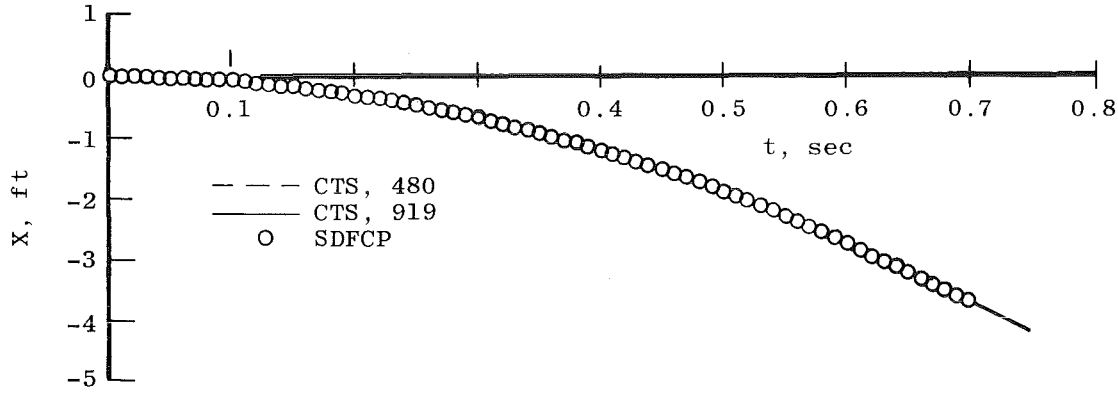

c. X versus t

Figure 16. Free-stream trajectory motion comparison, yaw oscillation, Data Group 919 and 480.

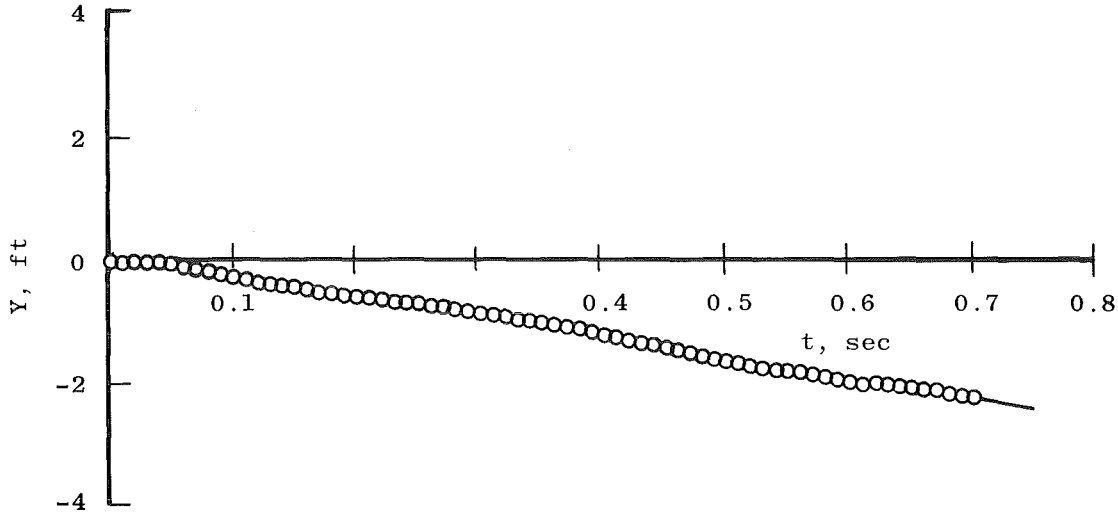

d. Y versus t

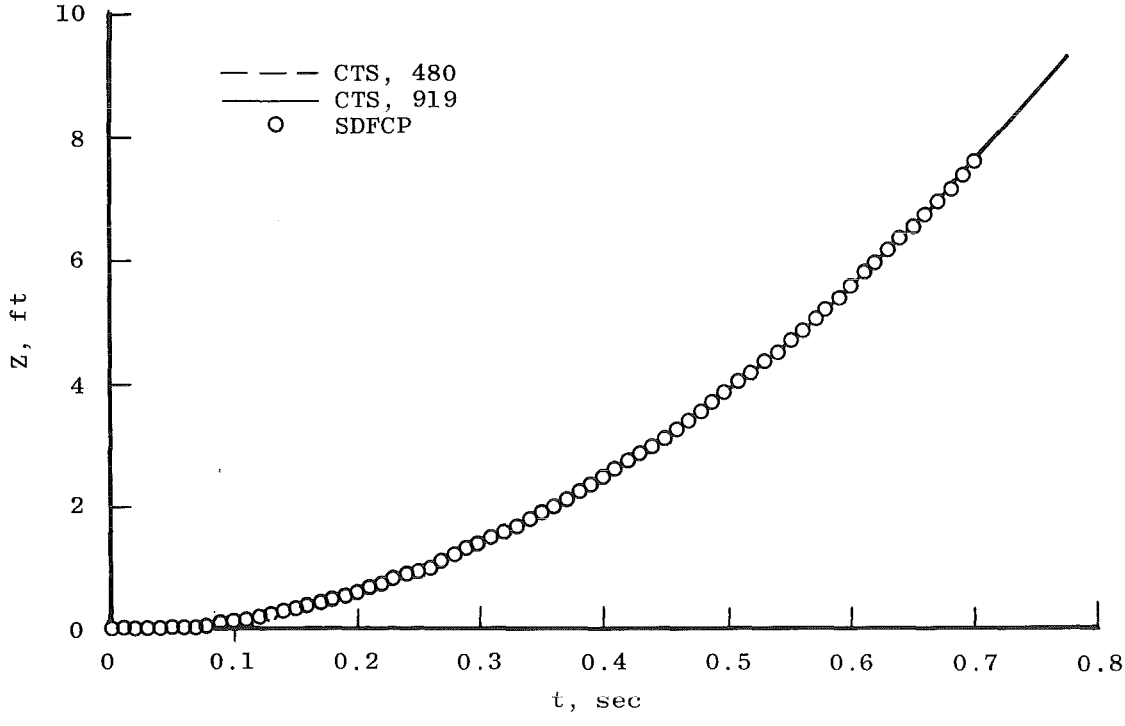

e. Z versus t

Figure 16. Concluded.

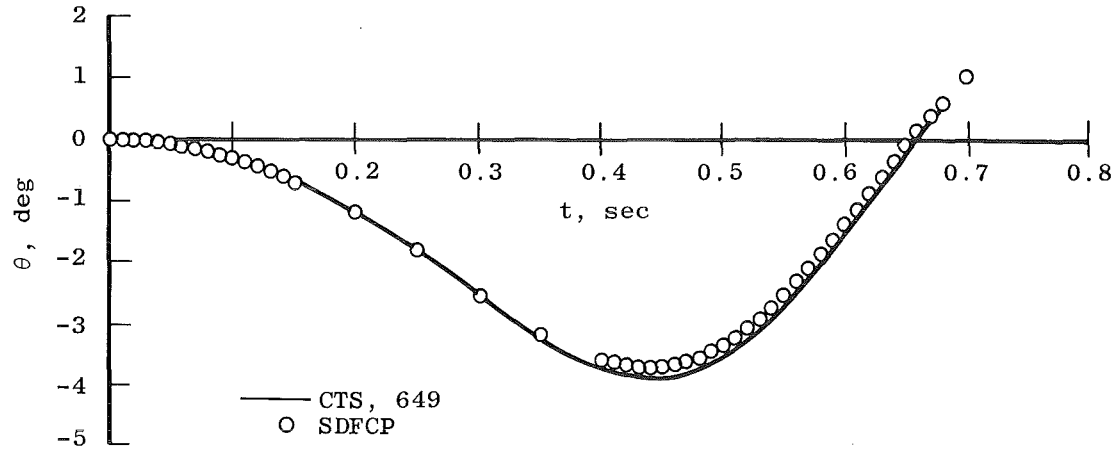

a. θ versus t

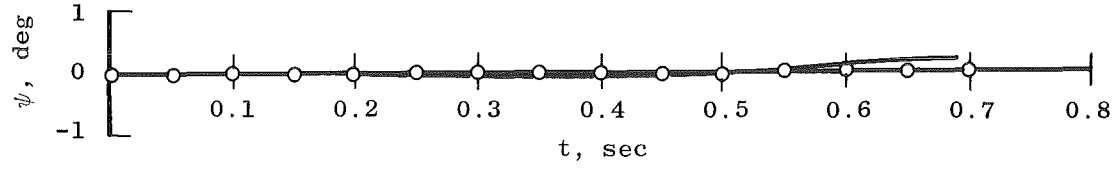

b. ψ versus t

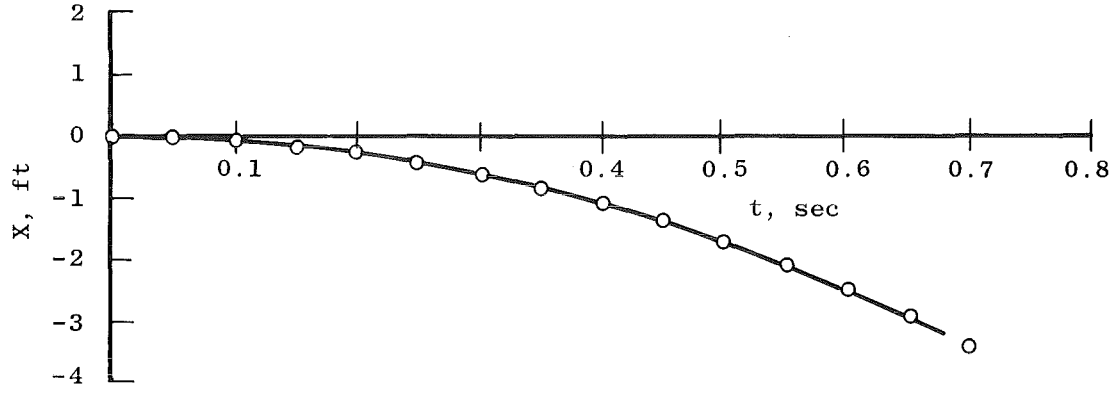

c. X versus t

Figure 17. Centerline trajectory motion comparison, Data Group 649.

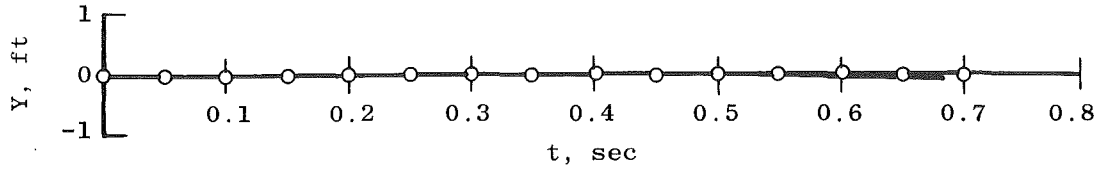

d. Y versus t

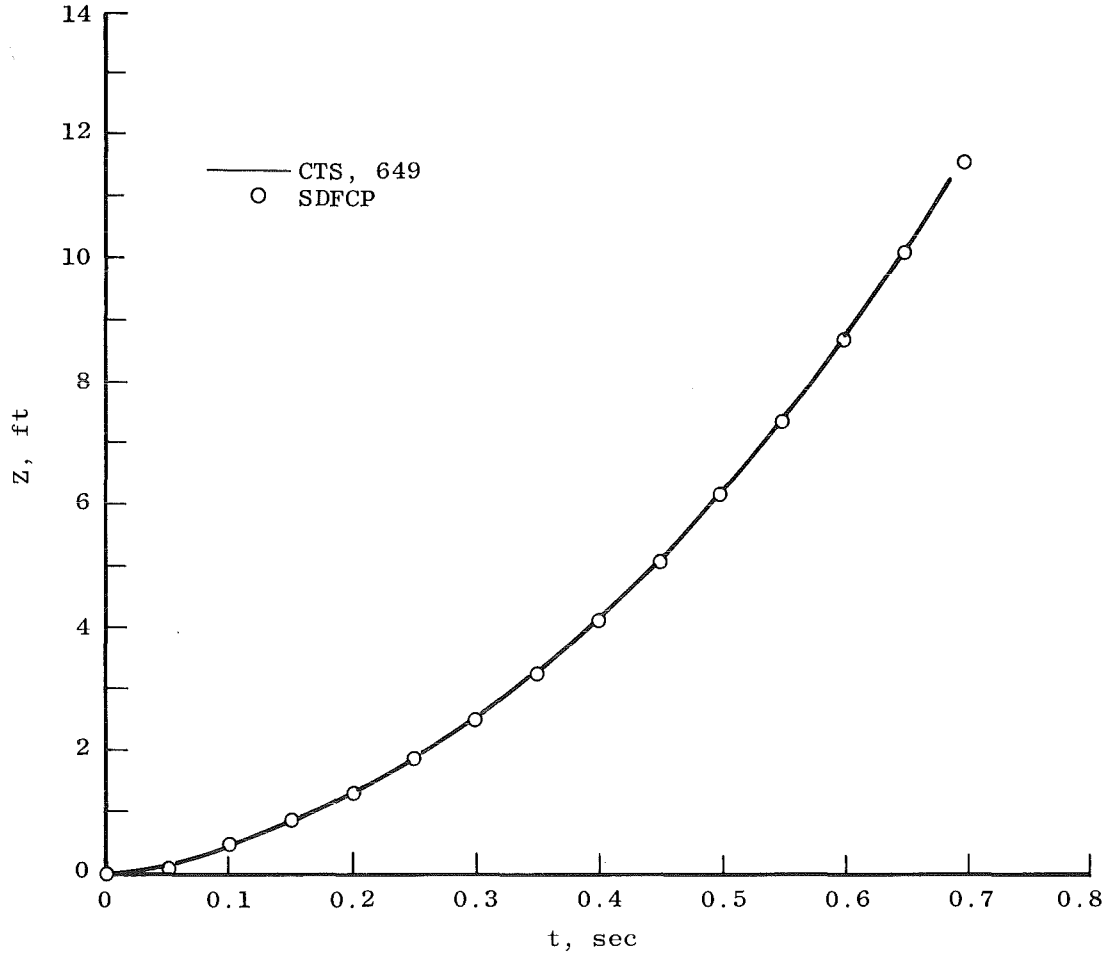

e. Z versus t

Figure 17. Concluded.

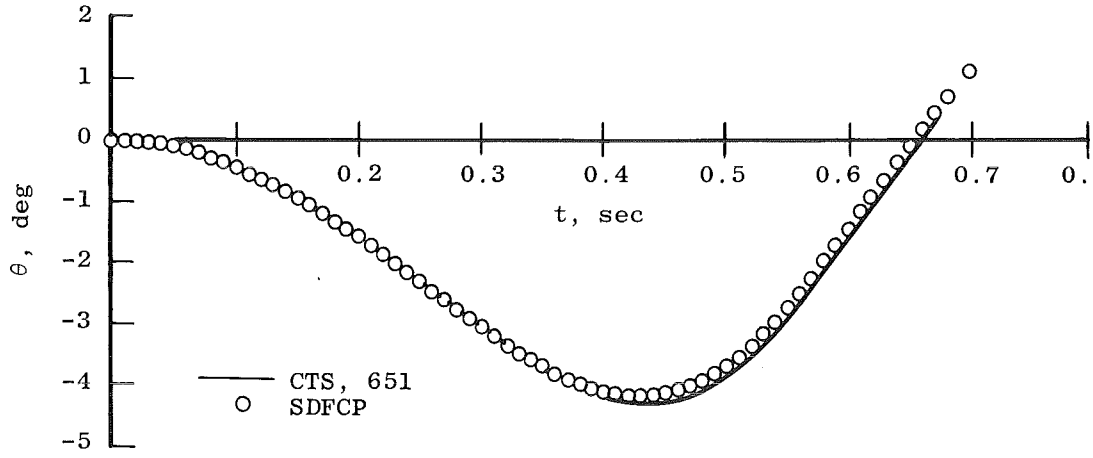

a. θ versus t

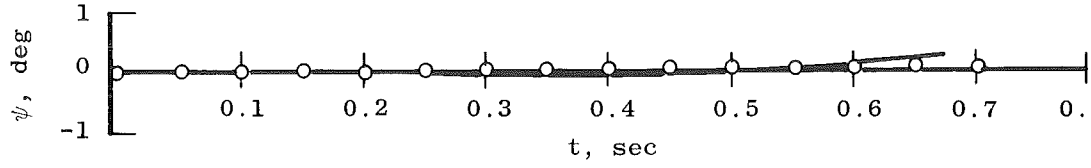

b. ψ versus t

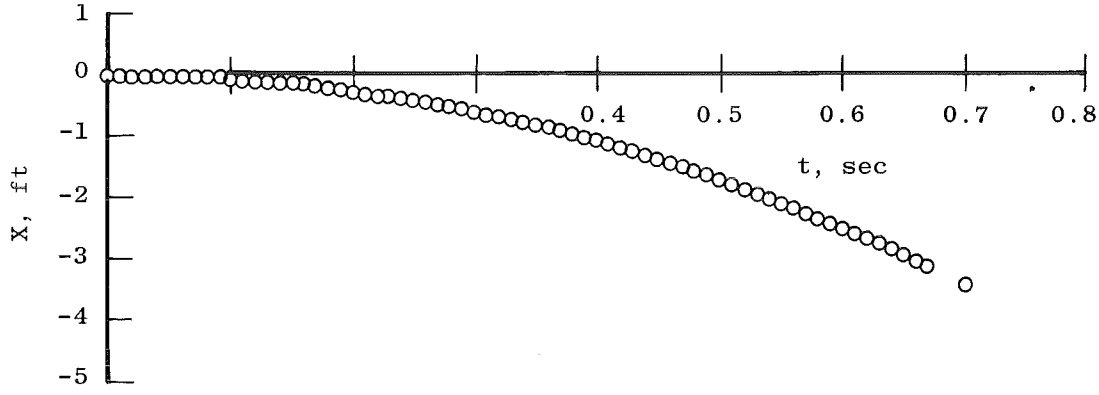

c. X versus t

Figure 18. Centerline trajectory motion comparison, Data Group 651.

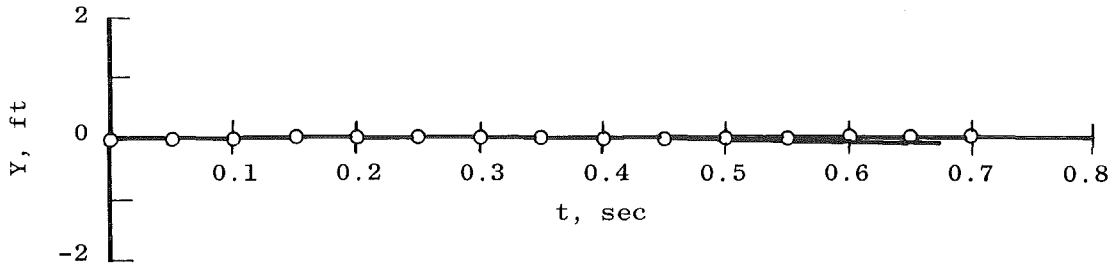

d. Y versus t

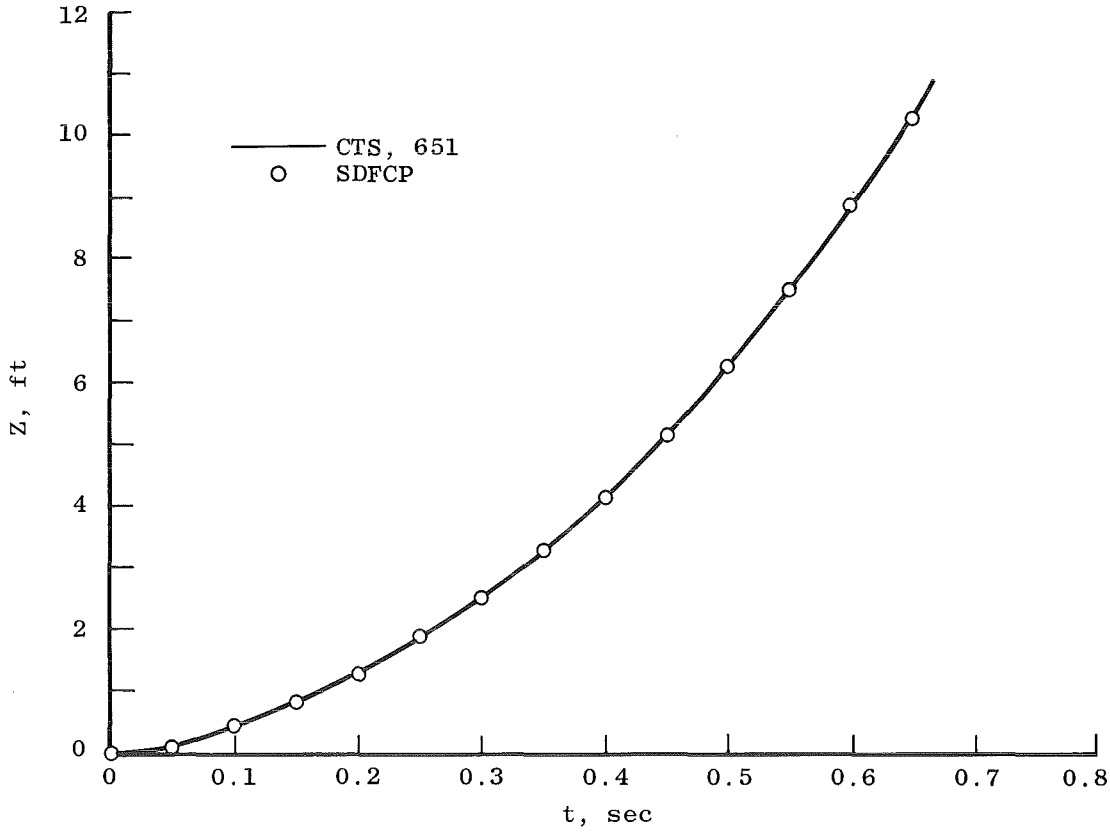

e. Z versus t

Figure 18. Concluded.

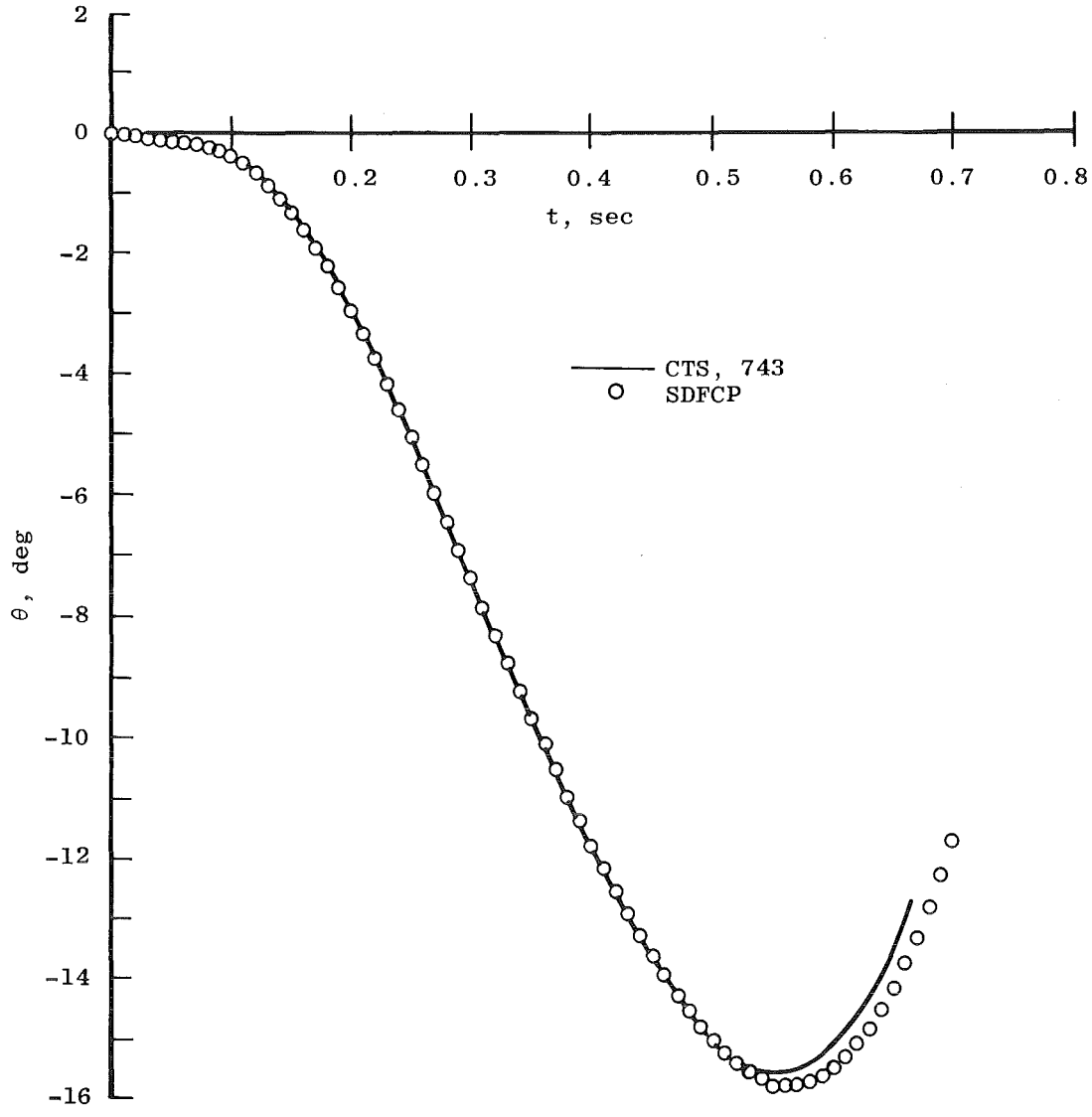

a. θ versus t

Figure 19. Wing pylon launch point trajectory motion comparison, Data Group 743.

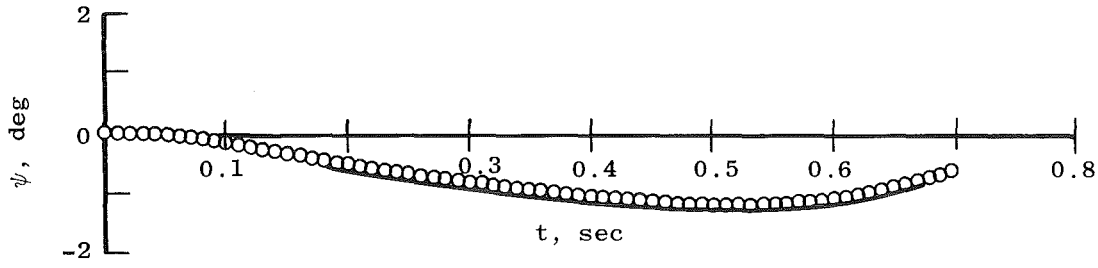

b. ψ versus t

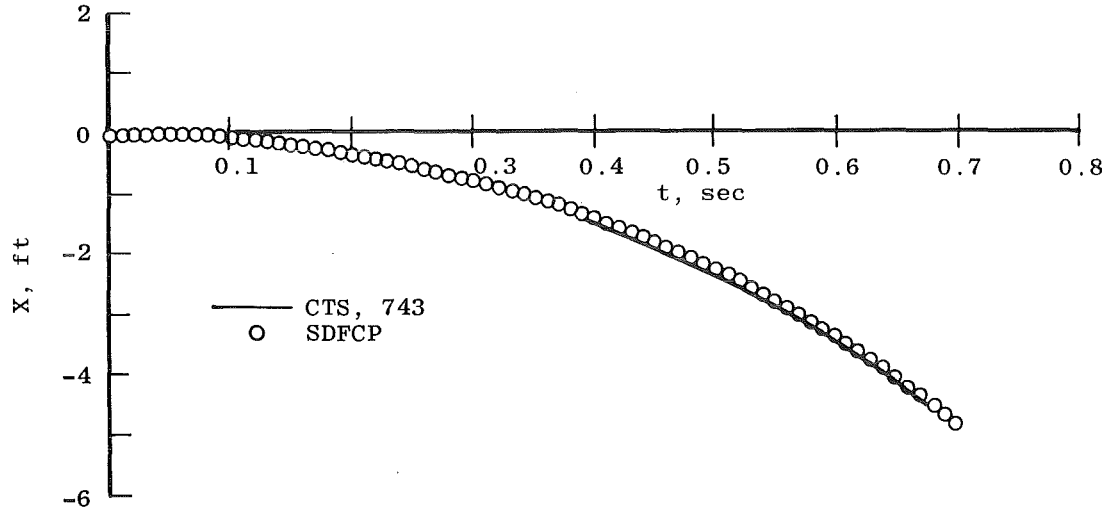

c. X versus t

Figure 19. Continued.

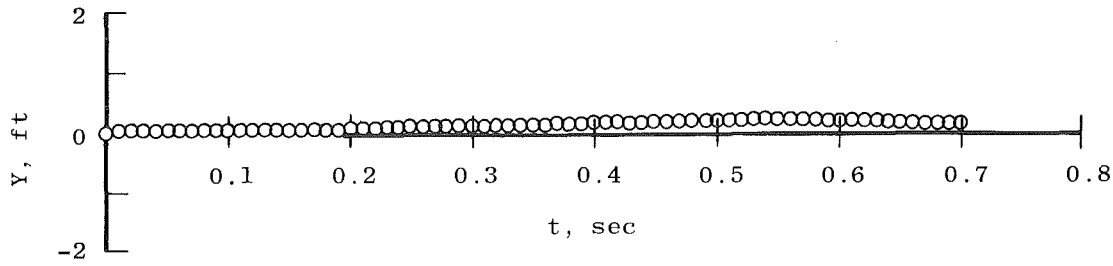

d. Y versus t

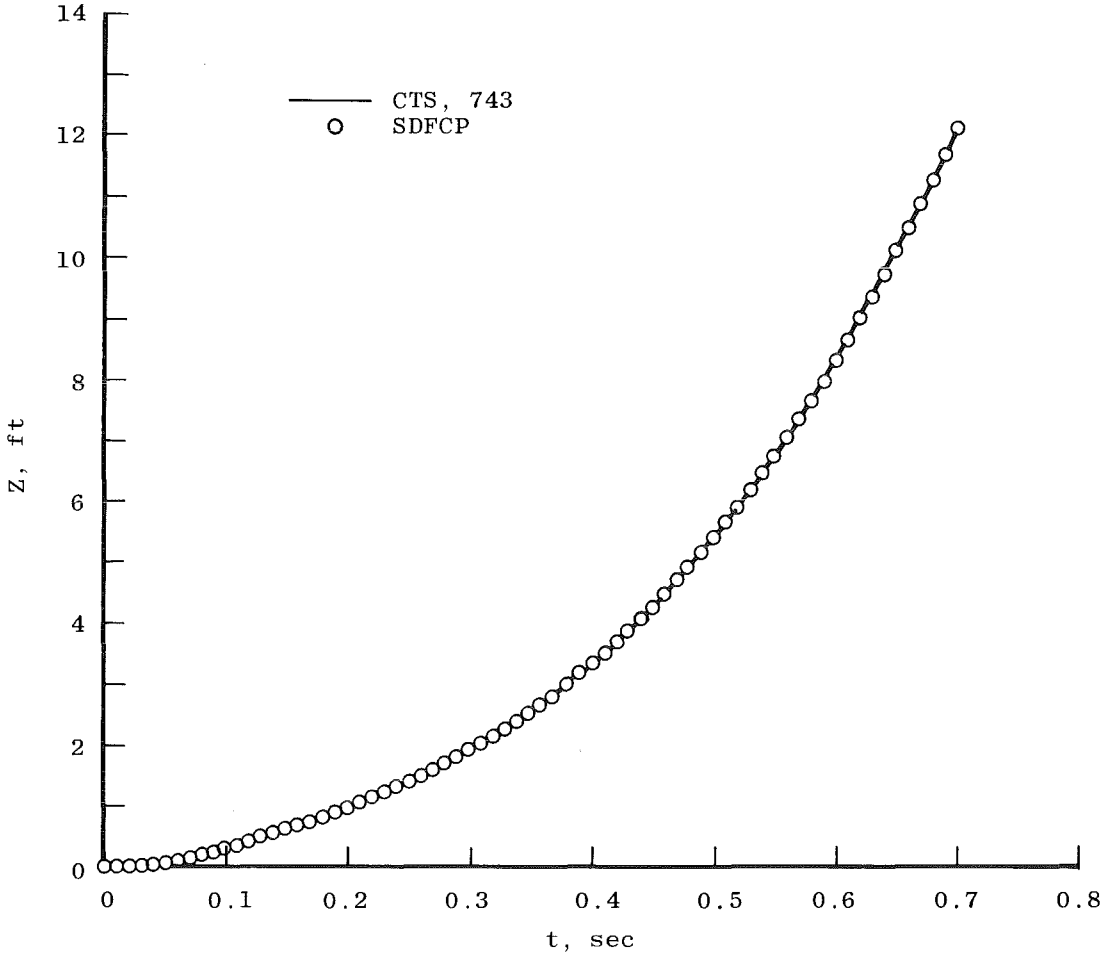

e. Z versus t

Figure 19. Concluded.

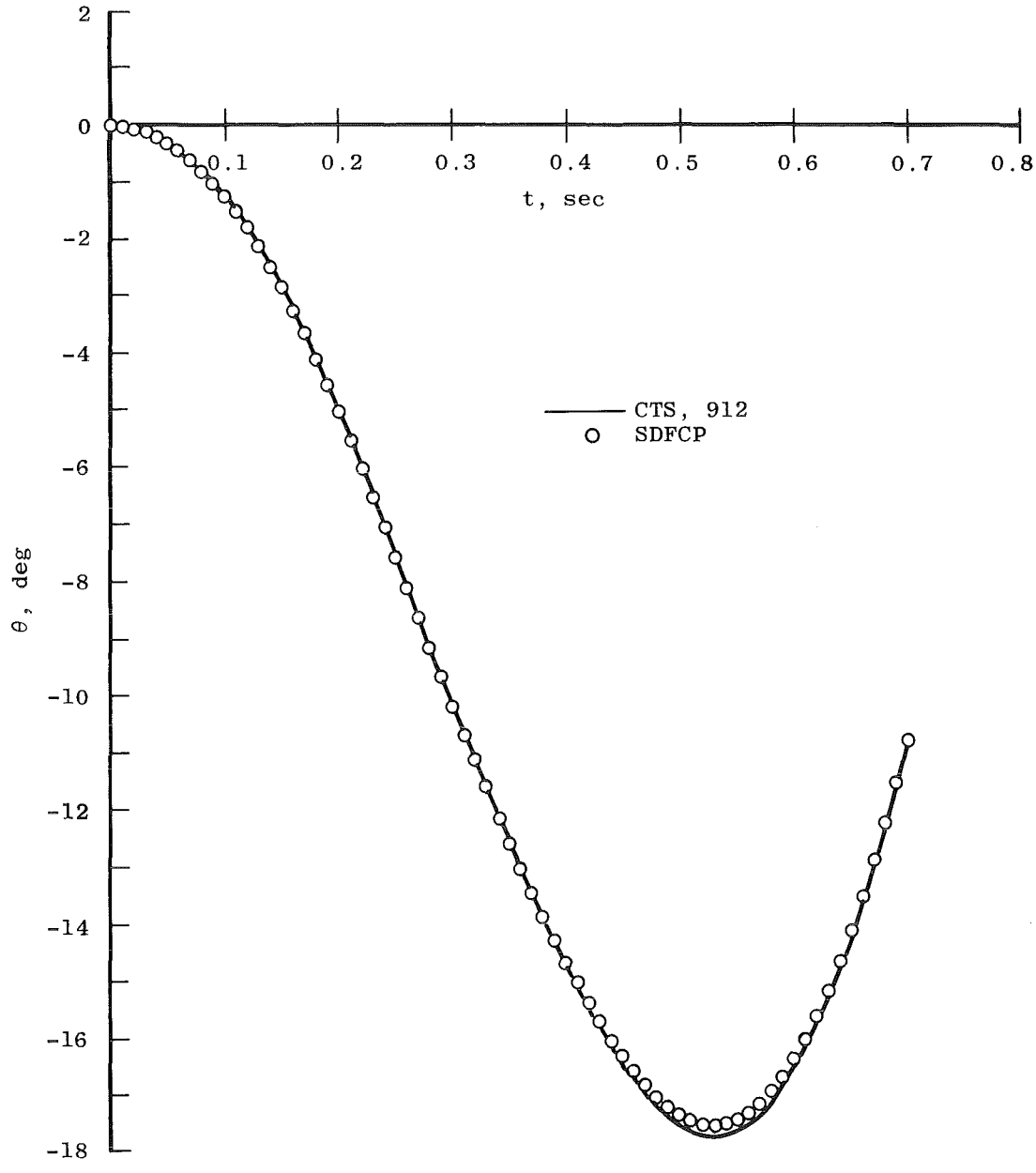

a. θ versus t

Figure 20. Wing pylon launch point trajectory motion comparison, Data Group 912.

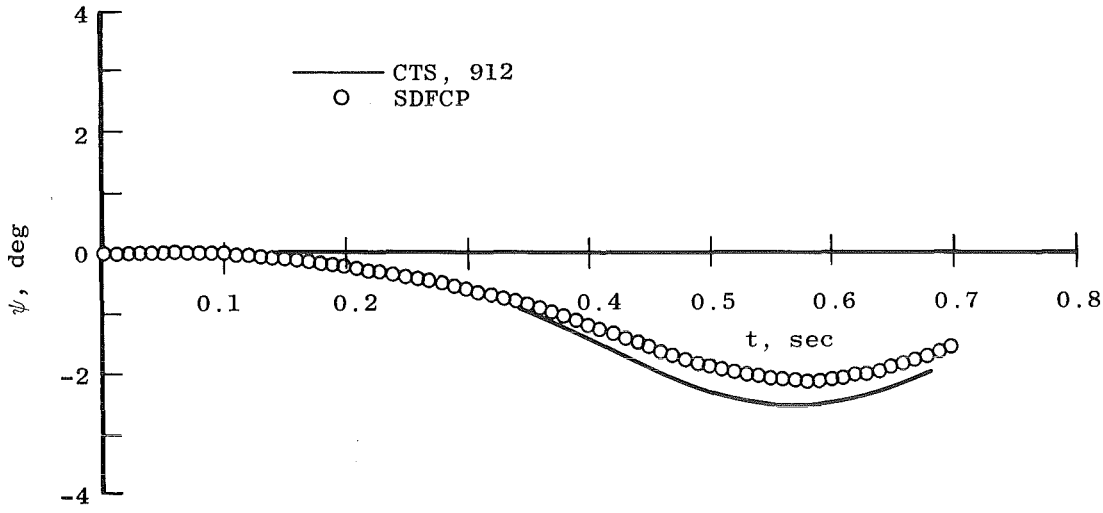

b. ψ versus t

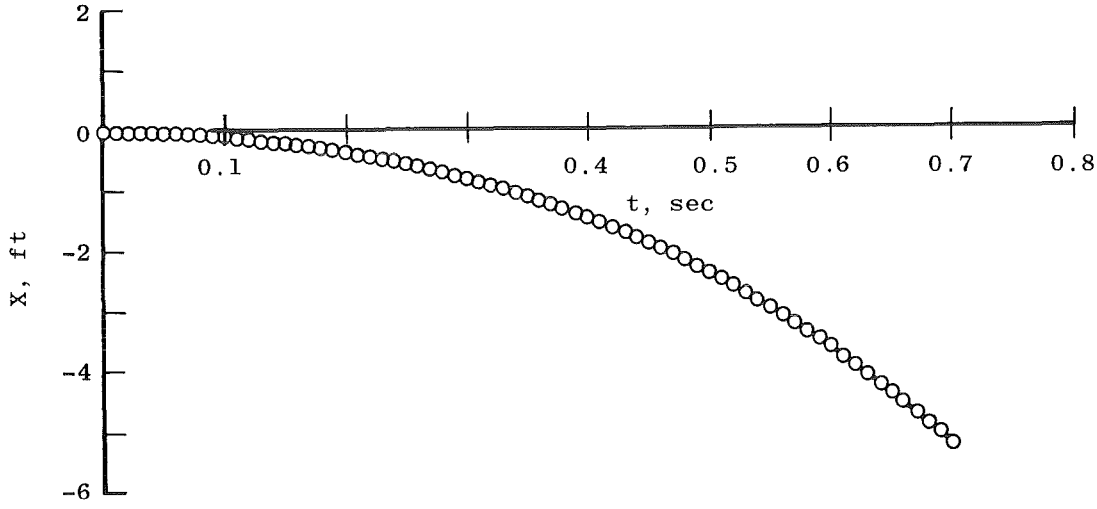

c. X versus t

Figure 20. Continued.

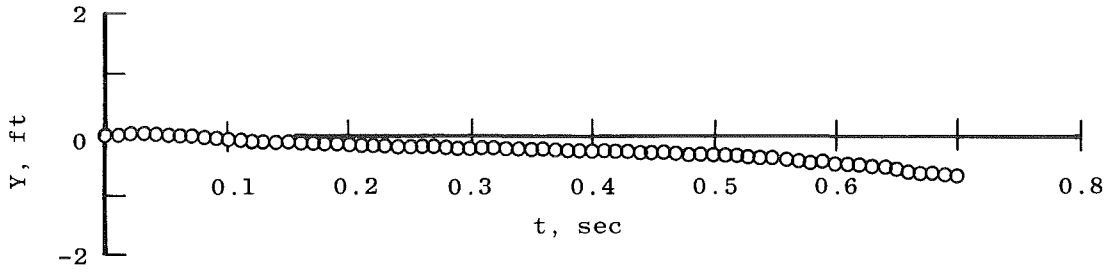

d. Y versus t

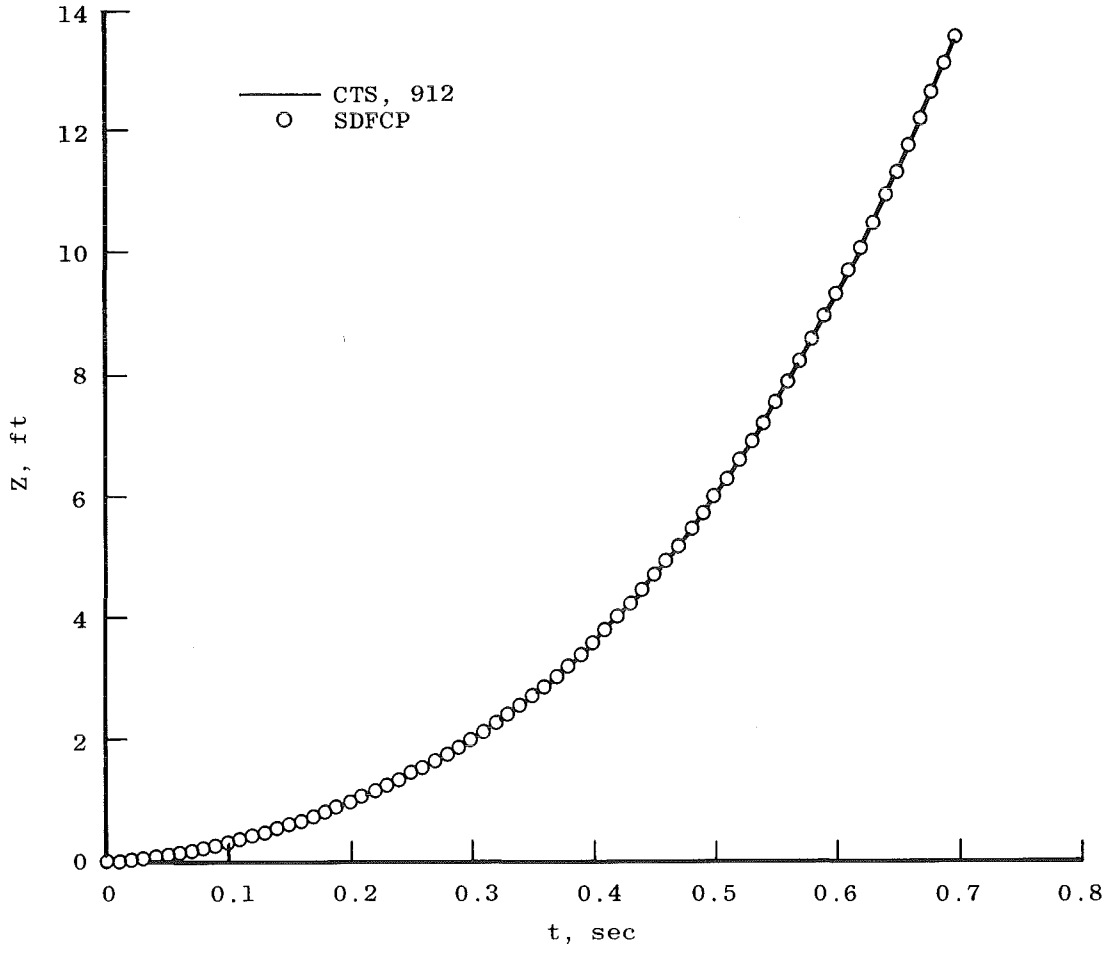

e. Z versus t

Figure 20. Concluded.

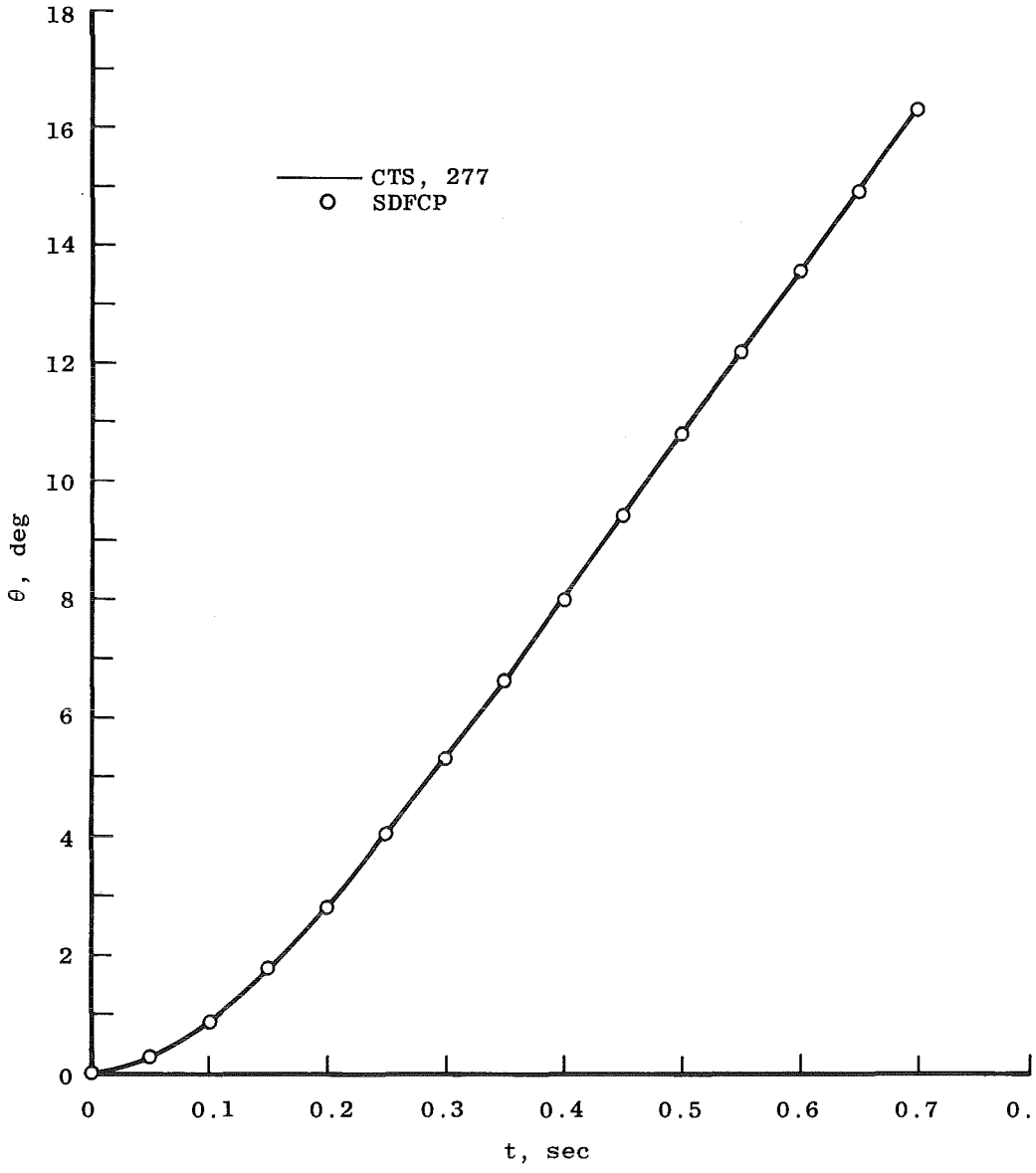

a. θ versus t

Figure 21. Asymmetric store trajectory, Data Group 277.

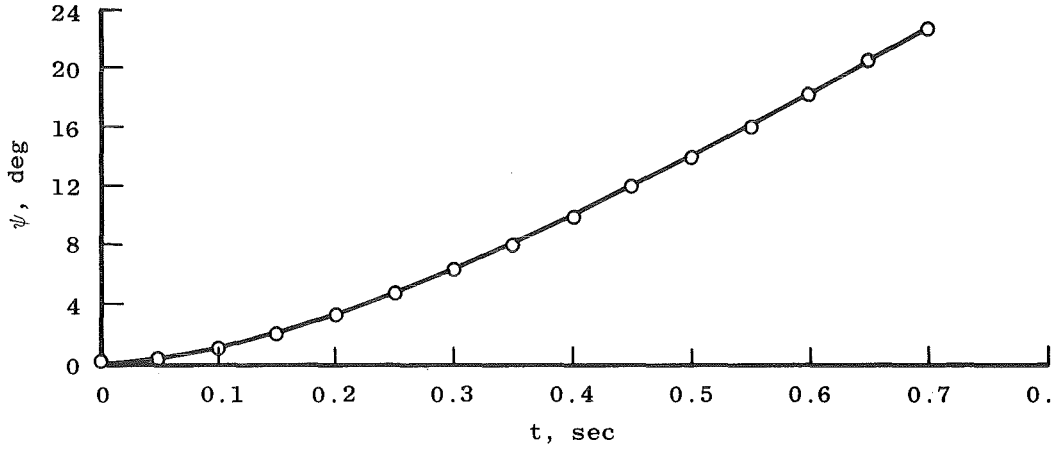

b. ψ versus t

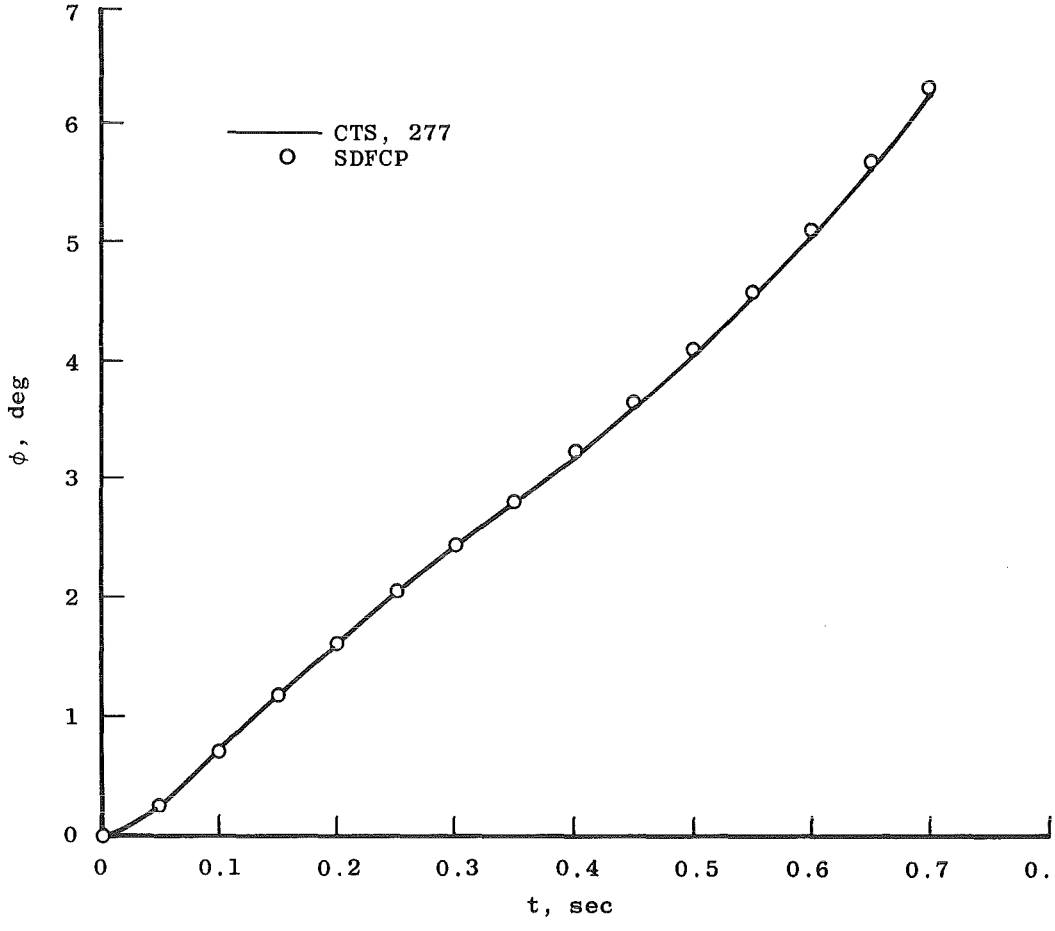

c. ϕ versus t

Figure 21. Continued.

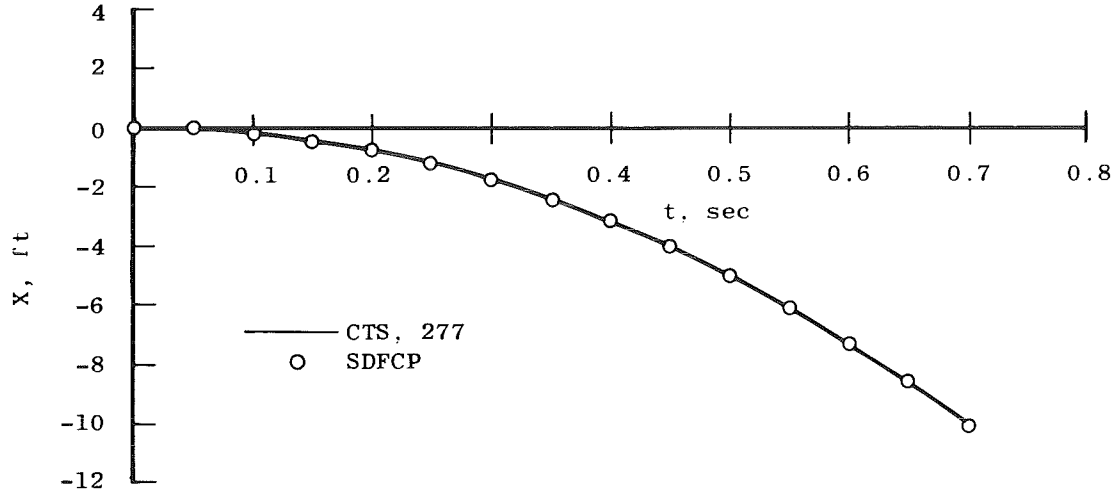

d. X versus t

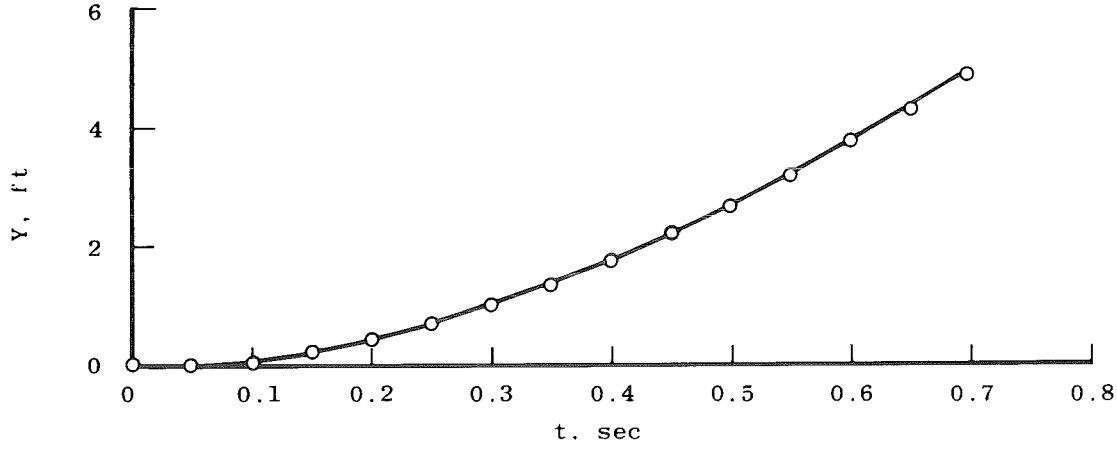

e. Y versus t

Figure 21. Continued.

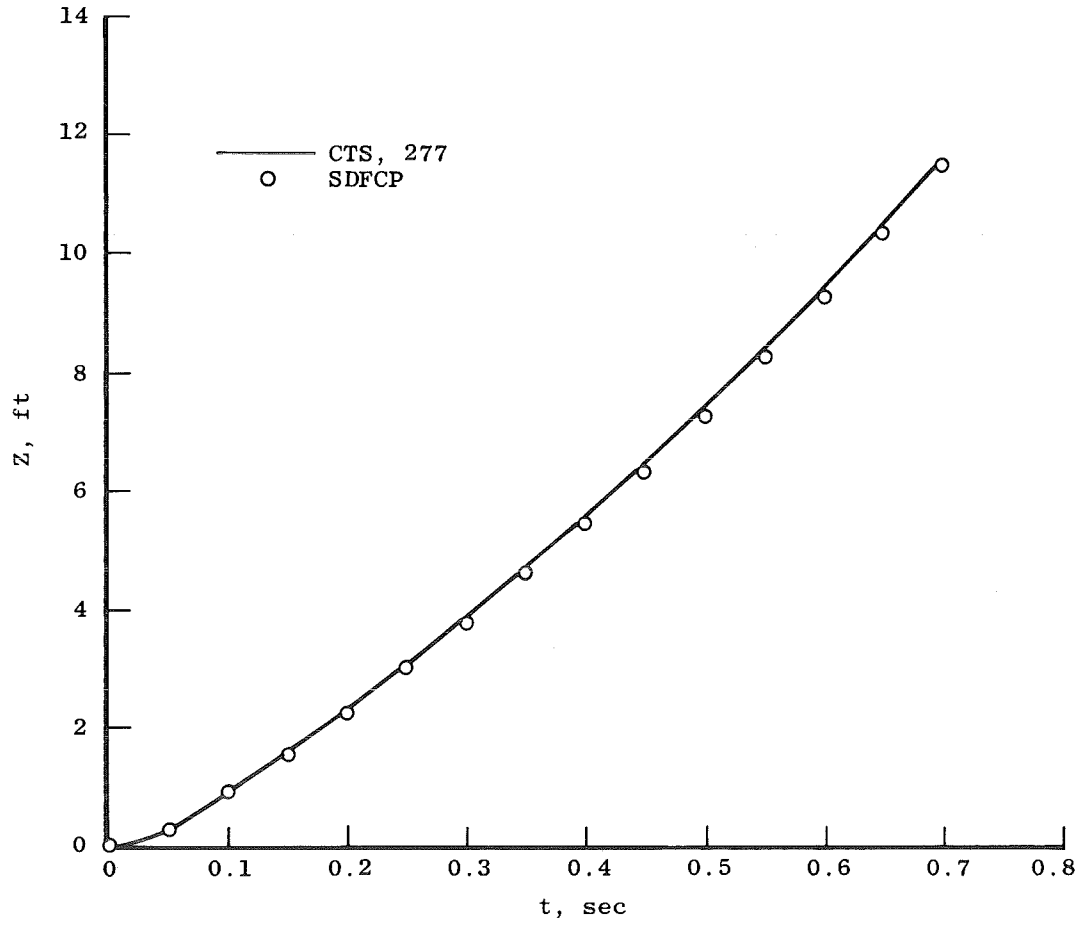

f. Z versus t
Figure 21. Concluded.

Table 1. VKF CTS Motion Capabilities

Motion	Range		Maximum Rate of Travel**
	Tunnel A	Tunnels B and C	
Axial	40 in.	40 in.	1 in./sec
Vertical	-13 to 17 in.***	-13 to 17 in.***	1 in./sec
Lateral	±15 in.***	±15 in.***	2 in./sec
Pitch	±45 deg	±15 deg*	10 deg/sec
Yaw	±45 deg	±30 deg*	10 deg/sec
Roll	±180 deg	±180 deg	20 deg/sec

*Pitch and yaw are restricted in Tunnels B and C because of the constraints imposed by a water jacket used on the roll-pitch-yaw head in these tunnels.

**The rate of travel of each degree of freedom is continuously variable from zero to the rates shown.

***Measured from tunnel centerline. Positive vertical is down.

Table 2. VKF CTS Drive System Accuracies

Motion	Drive System Accuracy
X_c	±0.005 in.
Z_c	±0.005 in.
α_c	±0.05 deg
ψ_c*	±0.05 deg
ϕ_{cB}	±0.20 deg
η_c*	±0.03 deg

*The yaw angles, ψ_c and η_c, are used to obtain both the total yaw angle (ψ) and lateral displacement (Y).

Table 3. VKF CTS Load Capacity

Load Component	Magnitude	Maximum Allowable Load Location
Pitching Moment	±2200 in.-lb	Sting Attachment Point
Yawing Moment	±725 in.-lb	Sting Attachment Point
Rolling Moment	±100 in.-lb	Roll Axis
Normal Force*	300 lb	7.25 in. Forward of Sting Attachment Point
Side Force*	100 lb	7.25 in. Forward of Sting Attachment Point
Axial Force	100 lb	Along Roll Axis

*These maximum loads will increase or decrease as the model center of pressure moves aft or forward, respectively. Balance capacity may further decrease the allowable loads.

Table 4. AFFDL/Nielsen Test Summaries
a. Force and Moment Grid Data

1. Free-Stream (ϕ = 0)

X_T	Y_T	Z_T	α_s	$-\beta_s$
17.0, 15.5, 14.0, 12.5, 11.0, 9.5, 8.0	-1.5	A	0	0
↓	0	↓	↓	↓
	1.5			
	3.0			
	6.0			
17.0	0	0	B	
17.0	↓	3.0	B	↓
17.0		0	0	P
17.0		3.0	0	P

2. Centerline Pylon (ϕ = 0)

X	Y	Z	α_s	$-\beta_s$
0, -1, -2, -3, -4, -5	-2, -1, 0, 1, 2	D	0	0
↓	-2, -1, 0, 1, 2	D	0	5
	-2, -1, 0, 1, 2	D	0	-5
	1, -1	N	-2.5	0
	↓	N	-2.5	2
		N	-2.5	-2
		R	-5	0
		↓	-5	2
			-5	-2
	0		-2.5	0
	↓		-2.5	2
			-2.5	-2
			-5	0
			-5	2
			-5	-2

3. 1/3 Semispan Pylon (ϕ = 0)

X	Y	Z	α_s	$-\beta_s$
0, -1, -2, -3, -4, -5	-2, -1, 0, 1, 2	F	0	0
↓	0	↓	↓	5
	0			-5
	-1, -2			5
	-1, -2	↓		-5
	1, 2	K		5
	1, 2	K	↓	-5
	-1, 0, 1	J	-7.5	0
	↓	J	-7.5	-2
		J	-7.5	2
		S	-15	0
		S	-15	-2
		S	-15	-2

Table 4. Continued
a. Concluded

Z Schedules

	0.05	0.10	0.25	0.50	0.75	1.00	1.25	1.50	1.75	2.00	2.25	2.50	2.75	3.00	3.25	3.50	3.75	4.00	4.25	4.50	4.75	5.00	5.25	5.50	5.75	6.00	7.00	8.00	9.00
D	X	X	X	X	X	X	X	X	—	X	—	X	—	X	—	X	—	X	—	X	—	X	—	—	—	X	X	—	—
E	—	X	X	X	X	X	X	X	—	X	—	X	—	X	—	X	—	X	—	X	—	X	—	—	—	X	X	—	—
F	X	X	X	X	X	X	X	X	—	X	—	X	—	X	—	X	—	X	—	X	—	X	—	—	—	X	X	X	—
G	X	X	X	X	X	X	X	X	—	X	—	X	—	X	—	X	—	X	—	X	—	X	—	—	—	X	X	X	X
H	—	X	X	X	X	—	—	—	—	—	—	—	—	—	—	—	—	—	—	—	—	—	—	—	—	—	—	—	—
I	—	—	X	X	X	X	—	—	—	—	—	—	—	—	—	—	—	—	—	—	—	—	—	—	—	—	—	—	—
J	—	—	X	X	X	X	X	X	—	X	—	X	—	X	—	X	—	X	—	X	—	X	—	—	—	X	X	X	—
K	—	—	—	—	X	X	X	X	—	X	—	X	—	X	—	X	—	X	—	X	—	X	—	—	—	X	X	X	—
M	—	X	X	X	X	X	X	X	—	X	—	X	—	X	—	X	—	X	—	X	—	X	—	—	—	—	—	—	—
N	X	X	X	X	X	X	X	X	—	X	—	X	—	X	—	X	—	X	—	X	—	X	—	—	—	—	—	—	—
R	—	—	X	X	X	X	X	X	—	X	—	X	—	X	—	X	—	X	—	X	—	X	—	—	—	—	—	—	—
S	—	—	—	X	X	X	X	X	—	X	—	X	—	X	—	X	—	X	—	X	—	X	—	—	—	X	X	X	—

Free-Stream Z_T Schedules

	3.0	1.5	0	-1.5	-3.0	-4.5	-6.0	-7.5
A	X	X	X	X	X	X	X	X

α_s,-β_s Schedules

	-15.0	-12.5	-10.0	-7.5	-5.0	-3.0	-2.5	-2.0	-1.0	0	1.0	2.0	2.5	3.0	5.0	7.5	10.0	12.5	15.0
B	X	X	X	X	X	X	—	X	X	X	X	X	—	X	X	X	X	X	X
C	—	—	—	X	X	X	—	X	X	X	X	X	—	X	X	X	—	—	—
P	—	—	—	X	X	X	—	X	X	X	X	X	—	X	X	X	X	—	—

Table 4. Concluded
b. Trajectory Data

	Trajectory Variables
1. Free-Stream	1,2,3,5
2. ℄ Pylon	2,6
3. 1/3 Semispan Pylon	1,2,4,5

Trajectory Variable Code

1. With and without ejector force
2. Ejector force axial position and angle
3. With and without translation in the tunnel
4. Integration interval and prediction interval
5. Moments of inertia
6. With and without plunge

Table 5. AEDC/DOT Test Summaries

a. Force and Moment Grid Data

1.	Free Stream	Re_∞: 5.0×10^6 and 3.8×10^6
		α_s: -15.0 to 15.0
		β_s: -15.0 to 15.0
		$X_T = Y_T = Z_T = 0$
		$\phi = 0$
2.	1/3 Semispan Pylon	α_s: 0, -7.5, -15.0
		$-\beta_s$: 0, -1.0, -2.0, -5.0
		X: 0, -0.03, -0.15, -0.5, -1.0
		Y: 0.55, 0, -0.25, -0.45, -1.0, -1.45
		Z: 0.1 to 9.3 in 0.25 increments
		$\phi = 0$

b. Trajectory Data

		Variables
1.	Free Stream	Moments of Inertia and Coefficient Tolerances
2.	℄ Pylon	Ejector Force Location
3.	1/3 Semispan Pylon*	Store Mass, Ejector Force Location, Ejector Force Angle, and Moments of Inertia

*Some were 6-DOF motion; others were not allowed to roll.

Table 6. Launch Point and Ejection Characteristics for Active CTS Trajectories

Group No. (First Entry)	Group No. (Second Entry)	Launch Point	Ejector Force Employed (Fig. 14)	X_1, ft	ω_m, deg
918	481	Free-stream	Yes	-0.5	0
919	480	Free-stream	Yes	-0.5	90.0
649	~	Fuselage Pylon	Yes	0	0
651	~	Fuselage Pylon	Yes	0.2	0
743	~	Wing Pylon	Yes	-1.5	0
912	~	Wing Pylon	Yes	-0.5	20.0

Table 7. Full-Scale Store Characteristics for Active CTS Trajectories

Group No. (First Entry)	Group No. (Second Entry)	A, ft	$\ell_1 = \ell_2 = \ell_3$, ft	$\bar{m}$, slugs	I_{xx}, slug-ft^2	I_{yy}, slug-ft^2	I_{zz}, slug-ft^2
918	481	1.228	1.25	40.0	20.00	70.00	70,000.00
919	480	↓	↓	↓	↓	70,000.00	70.00
649	~					700.00	700.00
651	~					↓	↓
743	~						
912	~						

NOTE: The products of inertia (I_{xy}, I_{zx}, and I_{yz}) were zero for these trajectories.

Table 8. Initial Conditions for Active CTS Trajectories

M_∞	= 1.63
U_A	= 1553.5 ft/sec (nominal)
ρ_A	= 0.005963 lbf-sec^2/ft^4 (nominal)
q_A	= 719.5 lbf/ft^2 (nominal)
H	= 39,700 ft (nominal)
γ_s	= 0 deg
σ_s	= 0 deg
θ	= 0 deg
ψ	= 0 deg
p	= 0 rad/sec
q	= 0 rad/sec
r	= 0 rad/sec

Table 9. Store Characteristics, Aerodynamic Input, and Initial Conditions for Passive CTS Trajectory

$\bar{m}$ = 15.025 slugs

I_{xx} = 25.29 slugs-ft^2

I_{yy} = 246.60 slugs-ft

I_{zz} = 237.00 slugs-ft^2

I_{xy} = 10.00 slugs-ft^2

I_{xz} = 20.00 slugs-ft^2

I_{yz} = 30.00 slugs-ft^2

$\ell_1 = \ell_2 = \ell_3$ = 2.21 ft

A = 3.83 ft^2

C_{N_o} = 0.1000 = constant

C_{m_o} = 0.1000 = constant

C_{A_o} = 0.1635 = constant

U_A = 892.89 ft/sec

ρ_A = 0.002309 lbf-sec^2/ft^4

q_A = 920.50 lbf/ft^2

p = 0 rad/sec

q = 0 rad/sec

r = 0 rad/sec

X_1 = 0 ft

F_{Z1} = 3,000.00 lb ($0 \leq t \leq 0.06$ sec)

= 3,000.00 to 0 lb ($0.06 \leq t \leq 0.065$ sec)

= 0 ($t \geq 0.065$ sec)

NOTE: 1. All initial angular orientations were zero.

NOMENCLATURE

A	Full-scale store vehicle reference area used for converting aerodynamic coefficients as measured by the balance to full-scale forces and moments, ft^2
A_b	Store model base area, $in.^2$
A_m	Parent and store model reference area for aerodynamic coefficients as measured by the balance, $in.^2$
a_x, a_y, a_z	Parent-vehicle simulated acceleration along the tunnel axes, ft/sec^2
a_0-a_5, b_0-b_5	Coefficients of polynominal curve fit of simulated full-scale store vehicle thrust, lbf, lbf/sec ..., lbf/sec^5
C1B,C2B	Polynominal break points for full-scale store vehicle simulation for forward and aft ejectors, respectively, sec or ft
C1E,C2E	Forward and aft ejector force cutoff times, respectively, for full-scale store vehicle ejector force simulation, sec or ft
C_A	Forebody axial-force coefficient, $C_{A_t} - C_{A_b}$
C_{A_b}	Base axial-force coefficient determined from the base pressure, $-(p_b - p_\infty) \cdot A_b/(q_\infty \cdot A_m)$
C_{A_t}	Total axial-force coefficient as measured by the balance, total axial force/$q_\infty \cdot A_m$
C_ℓ	Rolling-moment coefficient as measured by the balance, rolling moment/$q_\infty \cdot A_m \cdot \ell_{3_m}$
$C_{\ell_p}, C_{m_q}, C_{n_r}$	Damping coefficients in roll, pitch, and yaw, respectively, rad^{-1}
C_m	Pitching-moment coefficient as measured by the balance, pitching moment/$q_\infty \cdot A_m \cdot \ell_{1_m}$
C_{m_α}	Slope of pitching-moment coefficient versus angle of attack for store model in the free stream, rad^{-1}

C_N	Normal-force coefficient as measured by the balance, normal force/$q_\infty \cdot A_m$
$C_{N_o}, C_{m_o}, C_{Y_o}, C_{n_o}, C_{\ell_o}, C_{A_o}$	Arbitrary constant aerodynamic coefficients that can be input into the trajectory program
$C_{N_T}, C_{m_T}, C_{Y_T}, C_{n_T}, C_{\ell_T}, C_{A_T}$,	Tolerance band on predicted aerodynamic coefficients
C_n	Yawing-moment coefficient as measured by the balance, yawing moment/$q_\infty \cdot A_m \cdot \ell_{2_m}$
C_Y	Side-force coefficient as measured by the balance, side force/$q_\infty \cdot A_m$
c_0-c_5, d_0-d_5	Coefficients of polynomial curve fit of simulated full-scale store vehicle forward ejector force, lbf, lbf/sec ..., lbf/sec^5 or lbf, lbf/ft,..., lbf/ft^5
cg	Center of gravity
e_0-e_5, f_0-f_5	Coefficients of polynomial curve fit of simulated full-scale store vehicle aft ejector force, lbf, lbf/sec,...,lbf/sec^5 or lbf, lbf/ft,..., lbf/ft^5
F_{T_x}	Simulated full-scale store vehicle thrust force, lbf
F_{Z1}, F_{Z2}	Forward and aft simulated full-scale store vehicle ejector forces, lbf
H	Parent-vehicle initial pressure altitude being simulated, ft
I_{xx}, I_{yy}, I_{zz}	Full-scale store vehicle mass moments of inertia about body-fixed axes, slugs-ft^2
I_{xy}, I_{yz}, I_{xz}	Full-scale store vehicle cross product mass moments of inertia in the body-fixed axis system, slugs-ft^2
$K_{\ell_p}, K_{m_q}, K_{n_r}$	Full-scale store vehicle jet damping constants for moments about the body-fixed axes, roll, pitch, and yaw, respectively, ft lbf sec/rad

ℓ_1, ℓ_2, ℓ_3	Full-scale store vehicle reference lengths used for converting aerodynamic coefficients as measured by the balance to full-scale forces and moments, ft
$\ell_{1\,m}, \ell_{2\,m}, \ell_{3\,m}$	Parent and store model reference lengths for aerodynamic coefficients as measured by the balance, in.
$\ell_{4\,m}$	Reference length used in length Reynolds number, in.
ℓ_m	Store model length, in.
MRP	Store model moment reference point, must coincide with full-scale store vehicle cg
M_∞	Tunnel free-stream Mach number, also parent-vehicle simulated Mach number
$\overline{m}$	Full-scale store vehicle mass, slugs
p,q,r	Full-scale store vehicle angular velocities about the body-fixed axes, X_B, Y_B, and Z_B, respectively, rad/sec
p_b	Store model average base pressure, psia
p_o, q_o, r_o	Full-scale store vehicle angular velocities at the postlaunch position about the body-fixed axes, X_B, Y_B, and Z_B, respectively, rad/sec
p_t	Tunnel stilling chamber pressure, psia
$\dot{p}$	Full-scale store vehicle angular acceleration about the body-fixed X_B axis, rad/sec^2
p_∞	Tunnel free-stream static pressure, psia
q_A	Dynamic pressure that the full-scale store vehicle experiences at the simulated altitude, lbf/ft^2
q_∞	Tunnel free-stream dynamic pressure, psi

$Re_\infty \times 10^{-6}$	Tunnel free-stream unit Reynolds number, ft^{-1}
r_1-r_{10}	CTS sting geometry radius arm constants, in.
T2	Polynomial break point for full-scale store vehicle thrust simulation, sec
T3	Cutoff time for full-scale store vehicle thrust simulation, sec
TD	Ignition delay time for full-scale store vehicle thrust simulation, sec
T_t	Tunnel stilling chamber temperature, °R
t	Actual simulated flight time, sec
t_L	Full-scale store vehicle falls this time before the thrust simulation begins, sec
t_o	Postlaunch trajectory time offset, sec
t_t	Full-scale store vehicle thrust simulation burn time, sec
U_A	Velocity of the parent vehicle at the altitude being simulated, ft/sec
U_R	Full-scale store vehicle total velocity, ft/sec
u_o, v_o, w_o	Full-scale store vehicle translation velocities at the postlaunch position along the body-fixed axes X_B, Y_B, and Z_B, respectively, ft/sec
V_∞	Tunnel free-stream velocity, ft/sec
X,Y,Z	Parent-vehicle flight axis system which is fixed to and moves with the parent vehicle, ft
X_B, Y_B, Z_B	Body-fixed axis system which is fixed to and moves with the store vehicle, ft

$X_c, Z_c, \eta_c,$ ψ_c, a_c, ϕ_{cB}	CTS six-degree-of-freedom variable drives, axial, vertical, aft yaw, forward yaw, pitch and roll, respectively, in. and deg
X_1, X_2	Distance from cg to line of action of forward and aft ejector forces, respectively, from full-scale store vehicle ejector force simulation, measured along X_B axis and positive if force acts forward of cg, ft
$X_{I_o}, Y_{I_o}, Z_{I_o}$	Full-scale store vehicle position at postlaunch measured from the launch point, ft
X_T, Y_T, Z_T	Tunnel fixed axes, in.
X_w, Y_w	Parent-model airfoil coordinates, in.
x,y,z	Earth-fixed inertial axes used in the SDFCP, ft
Z_L	Full-scale store vehicle falls this distance before the thrust simulation begins, ft
a	Parent-model angle of attack, deg
$a_{pc}, \theta_c, \phi_{cA}$	CTS fixed angles, deg
a_s	Full-scale store vehicle angle of attack, deg
β_s	Full-scale store vehicle sideslip angle, deg
γ_c	Parent-vehicle simulated climb angle, positive for climb, negative for dive, deg
γ_s	Flight path angle with respect to the X_T-Y_T plane for the full-scale store vehicle, deg
ΔT_p	Prediction interval used in solution of full-scale store vehicle equations of motion, sec
Δt	Integration time step, sec

$\nu_{I_o}, \eta_{I_o}, \omega_{I_o}$	Full-scale store vehicle attitude at the postlaunch position, deg
ρ_A	Atmospheric density at the parent-vehicle simulated altitude, slugs/ft^3
ΣM_X	Sum of the full-scale aerodynamic rolling moment and any other exterior source that causes a roll torque on the full-scale store vehicle, ft-lbf
σ	Standard deviation, the square root of the mean-squared deviation from the mean of a variable
σ_s	Flight path angle with respect to the X_T-Z_T plane for the full-scale store vehicle, deg
τ	Oscillation period for the free-stream trajectories shown in Figs. 15 and 16, sec
ϕ_{AC}	Parent-vehicle simulated bank angle, positive is clockwise looking upstream, deg
ϕ_{FIN}	Store model fin orientation, deg
ψ, θ, ϕ	Full-scale store vehicle attitude in Euler angles referenced to the tunnel axes, X_T, Y_T, Z_T, deg
ω	Natural frequency for the free-stream trajectories shown in Fig. 15, rad/sec
ω_m	Angle of the simulated ejector force in the store Y_B-Z_B plane for the full-scale store vehicle, positive is clockwise looking upstream, deg

MODEL NOMENCLATURE

N1	Nose
B2	Body
P2,P3	Pylons

W	Wing
SCOC	Ogive-cylinder store with cruciform fin arrangement